SYNTHESIS, ANALYSIS AND DESIGN OF A NOVEL MECHANISM FOR THE TRAILING EDGE OF A MORPHING WING

A THESIS SUBMITTED TO
THE GRADUATE SCHOOL OF NATURAL AND APPLIED SCIENCES
OF
MIDDLE EAST TECHNICAL UNIVERSITY

BY

HARUN LEVENT ŞAHİN

IN PARTIAL FULFILLMENT OF THE REQUIREMENTS
FOR
THE DEGREE OF MASTER OF SCIENCE
IN
AEROSPACE ENGINEERING

AUGUST 2018

Approval of the thesis:

SYNTHESIS, ANALYSIS AND DESIGN OF A NOVEL MECHANISM FOR THE TRAILING EDGE OF A MORPHING WING

submitted by **HARUN LEVENT ŞAHİN** in partial fulfillment of the requirements for the degree of **Master of Science in Aerospace Engineering Department, Middle East Technical University** by,

Prof. Dr. Halil Kalıpçılar
Dean, Graduate School of **Natural and Applied Sciences** _____

Prof. Dr. Ozan Tekinalp
Head of Department, **Aerospace Engineering** _____

Prof. Dr. Yavuz Yaman
Supervisor, **Aerospace Engineering Dept., METU** _____

Examining Committee Members:

Assoc. Prof. Dr. Melin Şahin
Aerospace Engineering Dept., METU _____

Prof. Dr. Yavuz Yaman
Aerospace Engineering Dept., METU _____

Assoc. Prof. Dr. Ercan Gürses
Aerospace Engineering Dept., METU _____

Assoc. Prof. Dr. Ergin Tönük
Mechanical Engineering Dept., METU _____

Asst. Prof. Dr. Durmuş Sinan Körpe
Aeronautical Engineering Dept., University of Turkish Aeronautical Association _____

Date: **27.08.2018**

I hereby declare that all information in this document has been obtained and presented in accordance with academic rules and ethical conduct. I also declare that, as required by these rules and conduct, I have fully cited and referenced all material and results that are not original to this work.

Name, Last name: HARUN LEVENT ŞAHİN

Signature :

ABSTRACT

SYNTHESIS, ANALYSIS AND DESIGN OF A NOVEL MECHANISM FOR THE TRAILING EDGE OF A MORPHING WING

Şahin, Harun Levent
MSc, Department of Aerospace Engineering
Supervisor: Prof. Dr. Yavuz Yaman

August 2018, 130 pages

In this thesis, synthesis, analysis and design of a novel scissor-structural mechanism (SSM) with a four-bar (FB) linkage for the trailing edge of a morphing wing has been presented. The SSM, which is deployable, is created via combination of various scissor-like elements (SLEs). In order to provide mobility requirements, a FB linkage is assembled to the proposed SSM. The FB linkage is synthesized and optimized in order to give the structure required torque with a complete rotation. The SSM is designed with a novel kinematic synthesis concept in order to follow the airfoil camber with minimum design error. In this concept, various types of SLEs are assembled together to provide the desired airfoil geometries. The types (translational, polar), the number of SLEs, their orientations with respect to centerline of the airfoil and their distribution frequencies over the chord length are the design parameters, which allow designers to achieve all the possible geometric shapes. The combination rule is optimized in order to satisfy desired airfoil shapes with minimum design error as possible. Moreover, the position, velocity and acceleration analyses of the SSM have also been conducted. In order to prove aerodynamic efficiency of newly created airfoil geometries and obtain pressure distribution over the airfoil, 2D aerodynamic analyses have been done with the package program XFOIL. The flow characteristics used for the analysis are determined by the flight envelope of a generic UAV. Obtained pressure

distribution is applied as the lumped force on the joints. By assigning the approximate link masses and mass centers, the dynamic force analysis of the mechanism has also been performed in order to estimate the required torque to drive the synthesized SSM.

Keywords: Morphing Wings, Kinematic Synthesis, Scissor-Structural Mechanisms, Scissor-Like Elements, Dynamic Analysis

ÖZ

BÜYÜK ORANDA ŞEKİL DEĞİŞTİREBİLEN BİR UÇAK KANADININ FİRAR KENARI İÇİN ETKİN BİR MEKANİZMANIN OLUŞTURULMASI, İNCELENMESİ VE TASARIMI

Şahin, Harun Levent
Yüksek Lisans, Havacılık ve Uzay Mühendisliği Bölümü
Tez Yöneticisi: Prof. Dr. Yavuz Yaman

Ağustos 2018, 130 sayfa

Bu tezde, büyük oranda şekil değiştirebilen bir uçak kanadının firar kenarı için bir dört-çubuk (DÇ) mekanizması ile birlikte etkin bir makas-yapısal mekanizmanın (MYM) oluşturulması, incelenmesi ve tasarımı sunulmuştur. Dağıtılabilir olan makas-yapısal mekanizma, çeşitli makas-benzer elemanların (MBE) birleştirilmesi ile yaratılmıştır. Devinimlik gereksinimlerini sağlamak için önerilen MYM'ye bir DÇ mekanizması eklenmiştir. DÇ mekanizması, tam bir dönüş ile yapıya gerekli tork vermek için oluşturulur ve eniyilenir. MYM, kanat kamburunu asgari tasarım hatasıyla takip edebilmek için etkin bir kinematik oluşturma anlayışıyla tasarlanmıştır. Bu anlayışta, istenilen kanat kesit geometrilerini sağlamak için çeşitli MBE türleri bir araya getirilmiştir. Türler (dönüşümsel, kutupsal), MBE'lerin sayısı, kanat kesidi eksenine göre yönelimleri ve veter uzunluğu üzerindeki dağılım sıklıkları, tasarımcıların tüm olası geometrik şekilleri elde etmelerini sağlayan tasarım değişkenleridir. İstenilen kanat kesit şekillerini mümkün olduğunca asgari tasarım hatasıyla karşılamak için birleştirme kuralı eniyilenmiştir. Ayrıca, MYM'nin yer değiştirme, hız ve ivme incelemeleri de yapılmıştır. Yeni oluşturulan kanat kesit geometrilerinin aerodinamik verimliliğini kanıtlamak ve kanat kesidi üzerindeki basınç dağılımını elde etmek için XFOIL paket programı ile 2B aerodinamik

incelemeler de yapılmıştır. İncelemeler için kullanılan akış özellikleri, genel bir İHA'nın uçuş zarfı için belirlenmiştir. Elde edilen basınç dağılımı, eklemler üzerinde toplanmış kuvvet olarak uygulanmıştır. Biyel kütle ve kütle merkezlerini yaklaşık olarak atayarak, oluşturulmuş MYM'yi tahrik etmek için gereken torku tahmin etmek için mekanizmanın dinamik kuvvet incelenmesi de gerçekleştirilmiştir.

Keywords: Büyük Oranda Şekil Değiştirebilen Kanatlar, Kinematik Oluşturma, Makas-Yapısal Mekanizmalar, Makas-Biçimli Elemanlar, Dinamik İnceleme

Annem'e

ACKNOWLEDGMENTS

The author wishes to express his deepest gratitude to his supervisor Dr. Yavuz Yaman for his guidance, advice, criticism, encouragements and insight throughout the research. I am also grateful to Dr. Gürses, Dr. Körpe Dr. Şahin and Dr. Tönük who served in my thesis defense committee. Their comments and suggestions improved my thesis further to this final state.

Teşekkür'ün bu bölümüne Türkçe devam ediyorum.

Öncelikle eğitim hayatım boyunca desteğini benden hiç esirgemeyen, sevgisiyle, saygısıyla, varlığıyla bana güç veren canım kardeşim Mert Şahin'e sonsuz gönül borcumu belirtmek istiyorum. Ayrıca her daim arkamda duran ve bana destek olan tüm akrabalarıma da teşekürlerimi iletiyorum.

Bölümde çalıştığım zamanlarda beni hiç yalnız bırakmayan ve destekleriyle bu tezin tamamlanmasına yardımda bulunan Burak, Emre, Ezgi, Metehan, Tuğba, Kenan, Arda, Özgür Y., Hazal, Zeynep, Özgür H., Süleyman, Ali Tevfik, Özcan, Yunus, Pınar, Berk, Engin, Derya, Tansu ve RÜZGEM ekibi Özgün, Oğuz, S. Onur, Ahmet ve Onur'a sonsuz teşekkürlerimi ifade etmek istiyorum.

Adını yazmadığım diğer tüm sevgili arkadaşlarıma da çok teşekkür ediyorum.

Ve son olarak, beni büyüten, eğiten ve bu günlere hazırlayan, yaşamı boyunca sevgisini hiç ama hiç eksik etmeyen, ne yazık ki iki yıl önce yitirdiğim, canım annem, Perihan Şahin'i bu satırlar vasıtasıyla bir kez daha anmak istiyorum. Bu tezi anneme adıyorum.

TABLE OF CONTENTS

LIST OF TABLES

TABLES

LIST OF FIGURES

FIGURES

LIST OF SYMBOLS

SYMBOLS

A_0, A_1, B_0, B_1: Joint locations of FB linkage

$\{a_j\}_1^4$: Link lengths of FB linkage

ψ: Crank (input) angle

θ: Coupler angle

ϕ: Follower (output) angle

$\{p_j\}_1^3$: Freudenstein parameters

λ: Total number of multiply separated prescribed positions

W, Z, W^*, Z^*: Dyad link lengths

α: Rotation of Z

β: Rotation of W

m, m^*: Ground pivots (center points)

k, k^*: Moving pivots (circle points)

$\{\vec{R}_{P_j}\}_2^\lambda$: Position vectors of multiply separated prescribed positions

δ: Coupler displacement

μ: Transmission angle

N: Total number of SLEs

$C_j, D_j, E_j, C_{j+1}, E_{j+1}$: Joint locations of jth SLE

$\{l_j\}_1^N, \{l'_j\}_1^N$: Section lengths of SLEs

$\{k_j\}_1^N, \{k'_j\}_1^N$: Lengths factors of SLEs

$\{t_j\}_1^N$,: Thicknesses of SLEs

$\{\varphi_j\}_1^N$: Angles between links of SLEs

$\{w_j\}_1^N, \{h_j\}_1^N$: Foldability vector parameters of SLEs

$\{\theta_j\}_1^N$: Orientation angles of SLEs

$\{\gamma_j\}_1^N, \{\gamma'_j\}_1^N$: Orientations of sections of SLEs about global coordinates

$\{\dot{\gamma}_j\}_1^N, \{\dot{\gamma}'_j\}_1^N$: Angular velocities of sections of SLEs

$\{\ddot{\gamma}_j\}_1^N, \{\ddot{\gamma}'_j\}_1^N$: Angular accelerations of sections of SLEs

G_j, G'_j: Mass center locations of links of jth SLE

$l_{g_j}, l_{g'_j}, \delta_j, \delta'_j$: Mass center vectors and angle of mass center vectors from the joint C_j of jth SLE

$\vec{g}_{D_j}, \eta_{D_j}, \vec{g}_{C_{j+1}}, \eta_{C_{j+1}}, \vec{g}_{E_{j+1}}, \eta_{E_{j+1}}$: Mass center vectors and angle of mass center vectors from the other joints of jth SLE

$\vec{F}_{C_j}, \vec{F}_{D_j}, \vec{F}_{C_{j+1}}, \vec{F}_{E_{j+1}}$: Internal forces acting on jth SLE

$\vec{F}_{G_j}, \vec{F}_{G'_j}, \vec{T}_{G_j}, \vec{T}_{G'_j}$: Inertial forces and moment acting on forces of jth SLE

C_p, C_l, C_d : Pressure, lift, drag coefficients

LIST OF ABBREVIATIONS

ABBREVIATIONS

AoA: Angle-of Attack

CHANGE: Combined morphing assessment software using flight envelope data and mission based morphing wing prototype development

DARPA: The Defense Advanced Research Projects Agency

DLR: The German Aerospace Center

DOF: Degree-of Freedom

FB: Four-Bar

MAV: Micro Air Vehicle

METU: Middle East Technical University

MSPP: Multiply Separated Prescribed Positions

PZT: Lead Zirconate Titanate (Piezoelectric Ceramic Material)

RPM: Repeat per Minute

SLE: Scissor-Like Element

SMA: Smart Memory Alloy

SSM: Scissor-Structural Mechanism

UAV: Unmanned Aerial Vehicle

CHAPTER 1

INTRODUCTION

1.1 Motivation of the Thesis

Starting from the invention of aircraft and the first controlled flight by Wright brothers, designers imagine and endeavor to create birds-like aerial vehicles with the belief and inspiration of the fact that evolution shaped birds to make them more effective and productive. Although today's aircraft shows high performance than flying species in many aspects; most of aerial vehicles are not optimal yet due to their design and lack of technology. However, latest advances in material science, actuation mechanism, structural and manufacturing technologies lead designers to think out such an aircraft, which has the ability to change its shape to adapt itself different intended flight conditions. Since the wings are the main and the most important parts of an aircraft, which produce the required lift force and carry the important elements such as engines and control surfaces; those major changes should be made in the wings. Hence, this newly emerged research area named "Morphing Aerial Vehicles" refers mostly morphing of the aircraft wings.

Morphing wings, require integration of several sciences. Although overcoming such a multi-disciplinary challenge is very difficult, researchers work on specific research areas in order to develop new technologies, which makes the morphing wing more feasible. Therefore, in this thesis, more than a general aspect, kinematic synthesis of actuation mechanism, which morph the trailing edge of an aircraft wing is investigated. In order to answer the question of "What is the appropriate method to morph the wing profile?", this thesis claims and presents that "Deployable mechanisms are best fit for that purpose due to their advantageous properties".

This thesis is devoted to the kinematic synthesis and analysis of scissor-structural mechanisms which consist of several type of scissor-like elements. Scissor-structural mechanisms are the type of deployable structures, which are used mostly for large morphological manipulation of structures in architecture. Concentrated on that philosophy, the same structures are attempted to applied to solve related engineering problems. For morphing wings, which require large alteration of the skin and the body, usage of SSM can be a powerful solution.

1.2 Outline of the Thesis

This thesis consists of six chapters.

Chapter 2 presents the literature review of morphing wing concept. Starting with the question of "What is morphing wing?", definition of morphing, its purpose and philosophy behind of its design are explained. Then, classification of the morphing wing with brief explanations are done. After, historical background of morphing wing with related patents and research studies are investigated to get inspired and from those works. The chapter ends with benefits and drawbacks of morphing technologies with the explanation of multi-disciplinary challenge of it.

Chapter 3 focus on the kinematic synthesis and analysis of planar FB linkages, because design of machines highly depends on proper synthesis of used mechanism. First of all, analytical methodologies of kinematic synthesis are explained which are divided into three categories: function generation, motion generation and path generation. Furthermore, defects in kinematic synthesis are discussed. This chapter also discusses mechanism selection criteria and algorithms. In order to select the appropriate mechanism(s) from the solution set, two conditions are checked which are: whether they are suitable for feasible transmission angle criteria and whether they are Grashof type mechanism or not. Lastly, the algorithm gives the mechanism which has the shortest perimeter. This chapter ends with kinematic analysis of the FB linkages.

Chapter 4 deals with the kinematic synthesis and analysis of the SSMs. Inspired by the idea brought forward in the field of architecture; in aeronautical and space sciences, researchers study and use deployable structures to provide large geometrical changes.

SSMs are the type of deployable structures which are formed by SLEs. First of all, typology of SLEs are discussed. Moreover, analytical relations which gives kinematic properties of the SSMs are derived. After, design procedure of SSMs is briefly explained. This chapter ends with dynamic force analysis of SSMs.

Chapter 5 is devoted to the results obtained from the developed algorithm. With the developed computer-routine, several linkages which include single FB and SSM are presented and compared with each other in terms of mean design error. Moreover, effect of proposed SSMs on the wing skin are investigated which includes both required amount of elongation of the wing skin material and the aerodynamic performance of the wing surface formed. This chapter ends with kinematic analysis and dynamic force analysis of the proposed SSMs respectively.

Chapter 6 summarizes the achievements of the research, makes suggestions for future work and concludes the dissertation.

1.3 Limitations of the Thesis

In this thesis, the study is limited to kinematic synthesis and analysis of SSMs for the trailing edge of an aircraft wing. Although geometric properties of the mechanism are well-investigated and such a mechanism can have many other applications, the developed method is only presented to design such a mechanism to camber/decamber and chord morphing of an aircraft wing.

Throughout the thesis, all parts of the mechanism are considered as rigid. Moreover, the aircraft skin is assumed to perform desired shape changes. With those two conditions, designed mechanism provide given tasks with minimum possible design error. However, any comprehensive study which consider the weight of the structure to answer the question “Whether used system is feasible or not” is not done in details.

In terms of aerodynamics, the resulting loading cases are limited to 1 g aerodynamic loading. Hence, the behavior of the control surface under higher load cases are not considered in the thesis.

During the design of the trailing edge of the aircraft, the necessary electrical equipment of servo actuators such as cabling, battery selection and placement of these equipment are also not considered.

CHAPTER 2

LITERATURE REVIEW

In this chapter, the literature review of the study is presented briefly. After an introduction, the terminology of morphing and morphing wing concept are explained. Then classification of morphing wing is expressed. The historical background of the morphing wing, contributions related with this topic are mentioned. Finally, the multi-disciplinary nature of morphing wing is explained with benefits and limitations of the morphing wing.

2.1 Introduction

Nature is the main source of inspiration and imagination for humankind due to its grace, complexity, beauty, mystery and also has the ability to solve complex engineering problems. Starting from the early ages, smart people have solved basic problems that they were faced with by direct mimic of the nature. Most of the primitive inventions that are used in daily life can be counted as example to that reality.

After starting to build more complex machines, nature motivated human to fly like birds by expanding his imagination further. When such desire is combined with human mind and hardworking, first aircraft has been succeeded to be developed [1]. The curiosity and inspiration behind how birds achieve to fly in the air are never stopped and designers continue to compare their crude aircraft with nature. Due to biological evolution, flying species have gained simplicity, elegance and efficiency; however, airplanes today look quite different from birds in many aspects [1].

Hovering (Kingfisher) [2]

Soaring (Bald Eagle) [3]

Gliding (Mallard Duck) [4]

Flapping (Hummingbird) [5]

Figure 2.1: Adaptation of birds' wings against different flight actions

The nature teaches human with birds that the flight action can vary according to different atmospheric conditions and desired flight paths as hovering, gliding, soaring and flapping. Birds accomplish those flight actions as seen from Figure 2.1, listed above, by altering their wings rapidly into various forms, even in complex urban environments. As a result, researcher put the differences between aircraft and birds through experiments and direct comparison, then they conclude that aircraft are much rigid and have inflexible bodies unlike natural fliers. Therefore, researches had a common sense that aircraft can achieve greater efficiency if they can behave like birds; in other words, aircraft should change the shape of their wings in flight robustly for efficient cruise and aggressive maneuvers. Morphing technology allows aircraft to use a wide range of wing configurations for particular flight tasks, so that the weak appearance of the aircraft will be reduced to a certain stage.

2.2 What is "Morphing Wing"?

From the Wright brothers, man has gone through several structural changes to increase the efficiency of aircraft. For example, the very first aircraft, "The Wrigth Flyer" accomplished that by enabling the control of the wing twist with the help of a cable driven system. Much of those structural changes have been considered for aircraft wings, on which the principal control elements of aircraft are located. Most of modern aircraft use conventional control surfaces. Those control surfaces can be categorized as primary (ailerons, rudder, elevator) and secondary (flaps, slats, spoilers) control surfaces. The main purpose of the control surfaces is to change the geometry of the wing and allow the aircraft to fly at a range of flight conditions. The adaptation of an aircraft to various flight conditions is generally related with the lift generated by their wings. Due to the fact that secondary control surfaces are known also as high-lift devices, design of changeable secondary control surfaces leads aircraft to fly at a range of flight conditions.

Need of extra lift and existence of control surfaces apparently create a huge complexity. However, in the nature, insects and birds perform difficult missions by adapting their wing in a smooth but rapid manner without any complexity. Henceforth, performance of high-lift devices and control surfaces are not optimal since such a complex design does not provide a smooth transition which is poor in terms of aerodynamic efficiency. For example, if one considers flaps or ailerons, lack of smoothness of camber in the chord-wise direction due to hinge line causes a sudden change in the pressure distribution. This fact is usually associated with a drag penalty, little loss in lift generated and the possibility of separation [6], [7].

In the Cambridge Dictionary, the verb "morph" is defined as "to gradually change, or change someone or something, from one thing to another" [8]. In the field of aeronautics, morphing or "shape morphing" is identified commonly as changing the aircraft geometry in certain, futuristic and unconventional manner in order to increase the vehicle's performance. There is a general agreement that the conventional hinged control surfaces or high-lift devices generally cannot be considered as morphing. Aircraft morphing, especially "wing morphing", provide the possibility of obtaining

an adaptive wing structure which offer radical shape changes to produce optimum performance over an aircraft's nominal operational envelope [9] even expand its operating envelope [10].

2.3 Classification of "Wing Morphing"

Studies related with morphing wing are classified in terms of dimensions that are affected. There are three generally accepted major groups for morphing aircraft concepts: planform alternation, airfoil adjustment and out-of-plane transformation [11]. In the category of planform alternation, the aircraft wing is aimed to be manipulated in terms of span change, chord-length change and sweep-angle change. In the airfoil adjustment category, resizing the thickness and changing the camber rate of the airfoil is the main idea. In out-of-plane transformation, which is the least studied category due to its less insignificance, the span-wise and chord-wise bending with wing twisting are intended.

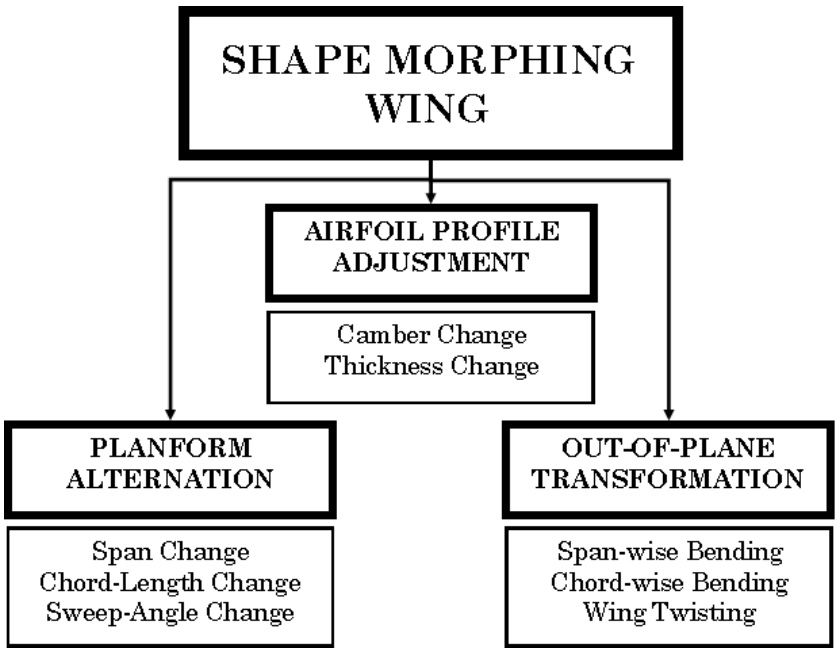

Figure 2.2: Classification of Wing Morphing

2.3.1 Airfoil Profile Adjustment

It is proven that the camber of an airfoil has a significant impact on the aerodynamic forces generated under fluid flow [12], [13]. Therefore, the most effective way to control the forces and moments that occur on aircraft wings is to change the camber of the airfoil [14]. For that reason, the airfoil profile adjustment, and more specifically "camber morphing", is the dominant research topic in the morphing wing applications when compared to the wing planform alternation and out-of-plane transformation. The method of actuation mechanism of camber morphing varies due to the size of the aircraft [1].

The most common actuation method is "conventional (lumped) actuators". In the method of the lumped actuation, conventional actuators are selected which are servo- and ultrasonic motors, and pneumatic and hydraulic devices which are supported by rigid machine elements or moving parts. It is observed that the conventional methods are used generally in order to morph fixed-wing aircrafts; whereas, they may be rarely used for chord morphing of blades of rotary-wing aircrafts.

Second most popular actuation method is smart material actuators (SMAs), which are used in rotorcraft blades and unmanned aerial vehicles (UAVs). Implementation of SMAs within the structural elements have the advantages over conventional actuation mechanisms in terms of weight, reliability and maintenance; however, the possibility of generating large geometrical shapes is decreasing as the size of the aircraft increases.

The third actuation method for inducing camber morphing is piezoelectric ceramic materials (PZTs), which are used mostly in small UAVs, and micro air vehicles (MAVs). PZTs, which has typical characteristics of high frequency, high load, and low strain, are proven to counteract aeroelastic and vibration effects in addition to camber morphing [15]. Deformations produced by PZTs are also too small compared with conventional mechanisms.

For all applications and actuation methods, the importance of the skin is usually overlooked because the proposed concepts usually deal with 2D aerodynamic

configurations. This could be one reason why there are a significant number of wind tunnel evaluations, however only a few flight test.

2.3.2 Wing Planform Alternation

In the type of wing planform alternation, three parameters are aimed to be modified which are span, chord, and sweep. Any change in span and sweep can affect the wing aspect ratio (AR), which is a critical parameter that changes the lift-to-drag ratio $\left(\frac{L}{D}\right)$. If the aspect ratio of the wing increases, both range and endurance will increase [16]. Change in aspect ratio is a very important parameter for the design of the aircraft wing since it has both aerodynamic and dynamic impact by affecting the lift curve slope $\left(C_{L_\alpha}\right)$ forces and the inertia of the aircraft.

In the wing planform alternation, span and sweep morphing are studied especially for military UAV applications. Chord morphing or variable chord wing, which has limited investigations, is studied for helicopter rotor blades and also UAVs mostly. Chord morphing is the least studied wing planform alternation type, because it requires large challenges but provides small benefits. In other words, manipulating chord length requires a lot of structural difficulty; for example, how to move the spars or how to stretch the skin are still unanswered questions [1].

2.3.3 Wing Out-of-Plane Transformation

The parameters that affect the aircraft wing out-of-plane transformation are: twist angle, dihedral/gull angle, and angle-of-attack (AoA) through span-wise bending. Those three parameters can be manipulated either individually or in combination. Out-of-plane morphing of the aircraft wing is accepted as the least common type of morphing solution except wing twist.

Although out-of-plane transformation is the oldest type of the shape morphing, wing twist morphing was ignored due to aeroelastic concerns for many years. However, advances in composite aerospace materials have made twist morphing possible today. It is investigated by several research studies that twist morphing can produce a significant impact on the aerodynamic behavior of a lifting surface without the need

of large platform modifications; however, those applications usually require complex and heavy actuation mechanisms. Furthermore, twist morphing can serve multiple tasks simultaneously, such as alleviate gust and maneuver load; increase the lift coefficient; and replace conventional control surfaces.

The most recent studies have focused on continuous geometric morphing of the wing (root to tip) to generate improved outcomes; however, this requires complex and heavy mechanisms coupled with flexible skins.

2.4 Historical Background of the Morphing Wing

Interestingly, the very first idea of morphing wing emerged even with the invention of first controlled/ powered flight by Wrigth brothers, due to the twisting wing feature of the Flyer [17]. What enabled Wright brothers to warp the wing is the wing material of the Flyer which is fabric; however, the technique used in that days abandoned, since metals became the primary material for airplanes.

Over the years, large companies were established in civil aviation. These companies helped the technology to progress rapidly. The morphing wing also took its own share from such a progression. Therefore, in the 20^{th} century, several concepts (especially related with airfoil adjustments) have been patented. However, improvements in materials science, forced researchers to create new concepts.

2.4.1 Patents

Starting from the invention of the aircraft, several patent applications have been proposed by inventors, commonly in the name of large aircraft companies, concerning the camber/ decamber ability of the aircraft wing and control surfaces. In Figure 2.3 and Figure 2.4 some of those patents proposed between 1920-1981 are shown. It is clearly seen from the patents that, in the early 20th century, most of the inventors/companies were focused on a design of a full wing-section, mostly a structural-mechanism, in which designers intended to replace conventional rib structure. For that purpose, regarding a flexible or discrete wing skin, those inventors proposed several limited solutions for the trailing edge of the wing. Inventors of that

era often called their inventions as “airplane wing” since they were trying to figure an optimum solution for the wing construction.

However, in the late 20th century, with the entrance of the large companies into the industry, as a need of mass production, construction of wing gained its commonly accepted, structurally feasible shape. Then common interest turned to design a seamless control surface which is aimed give a required camber to the whole aircraft wing. Inventors/companies tried to do their best to design much more complex mechanisms to give camber both manipulating leading and trailing edge the wing. Commonly they declared their inventions as “airfoil” because in those patents inventors/companies have an attitude to replace the aircraft wing ribs with a suitable mechanism which brings the aircraft wing a variable camber characteristic.

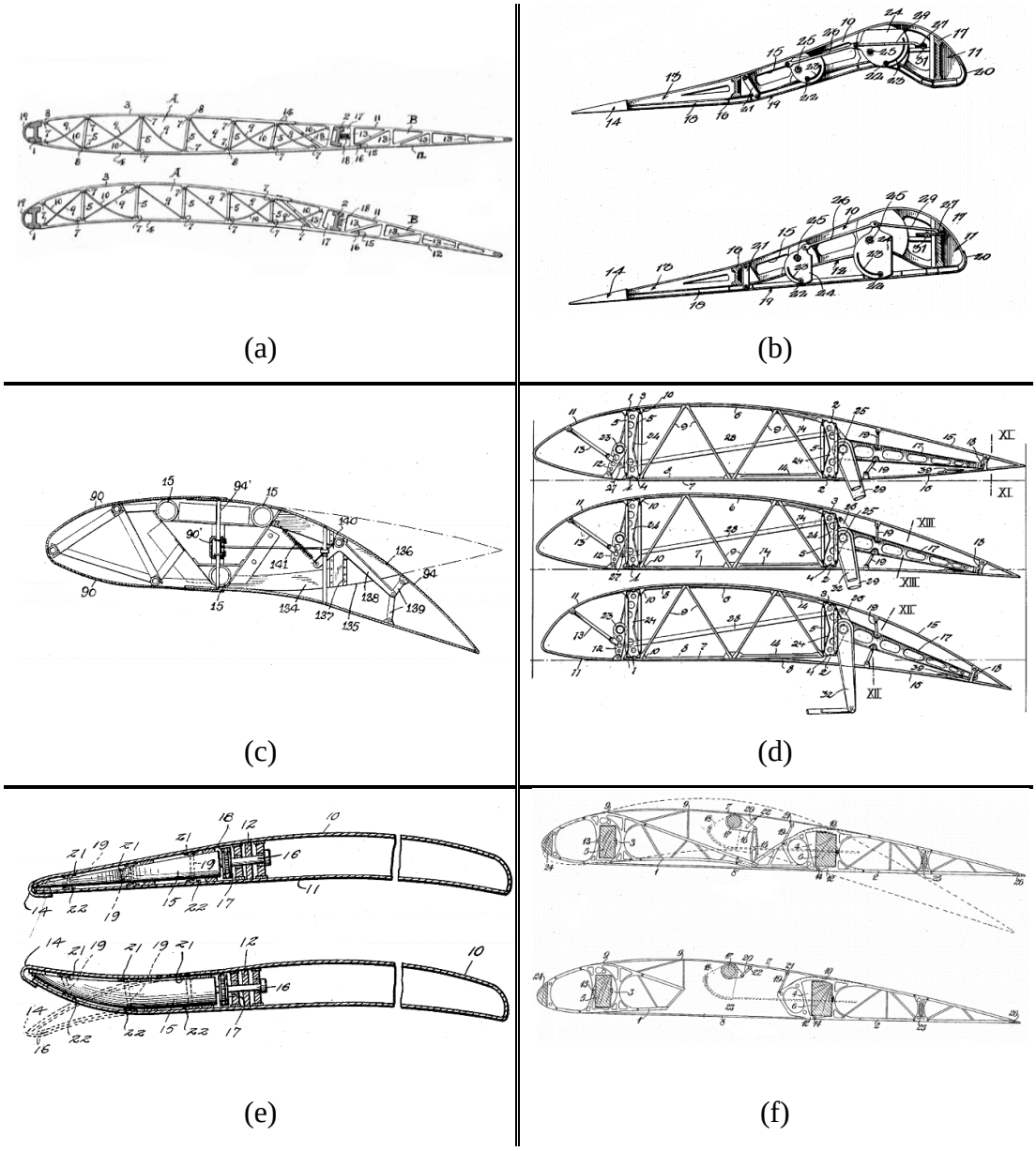

Figure 2.3: (a) Variable-camber Rib for Aeroplane-wings [18] (1920), (b) Aeroplane Wing Construction [19] (1922), (c) Aeroplane Control [20], [21] (1929), (d) Aerofoil [22] (1930), (e) Airplane Appliance [23] (1931), (f) Construction of Flexible Aeroplane Wings Having a Variable Profile [24] (1932)

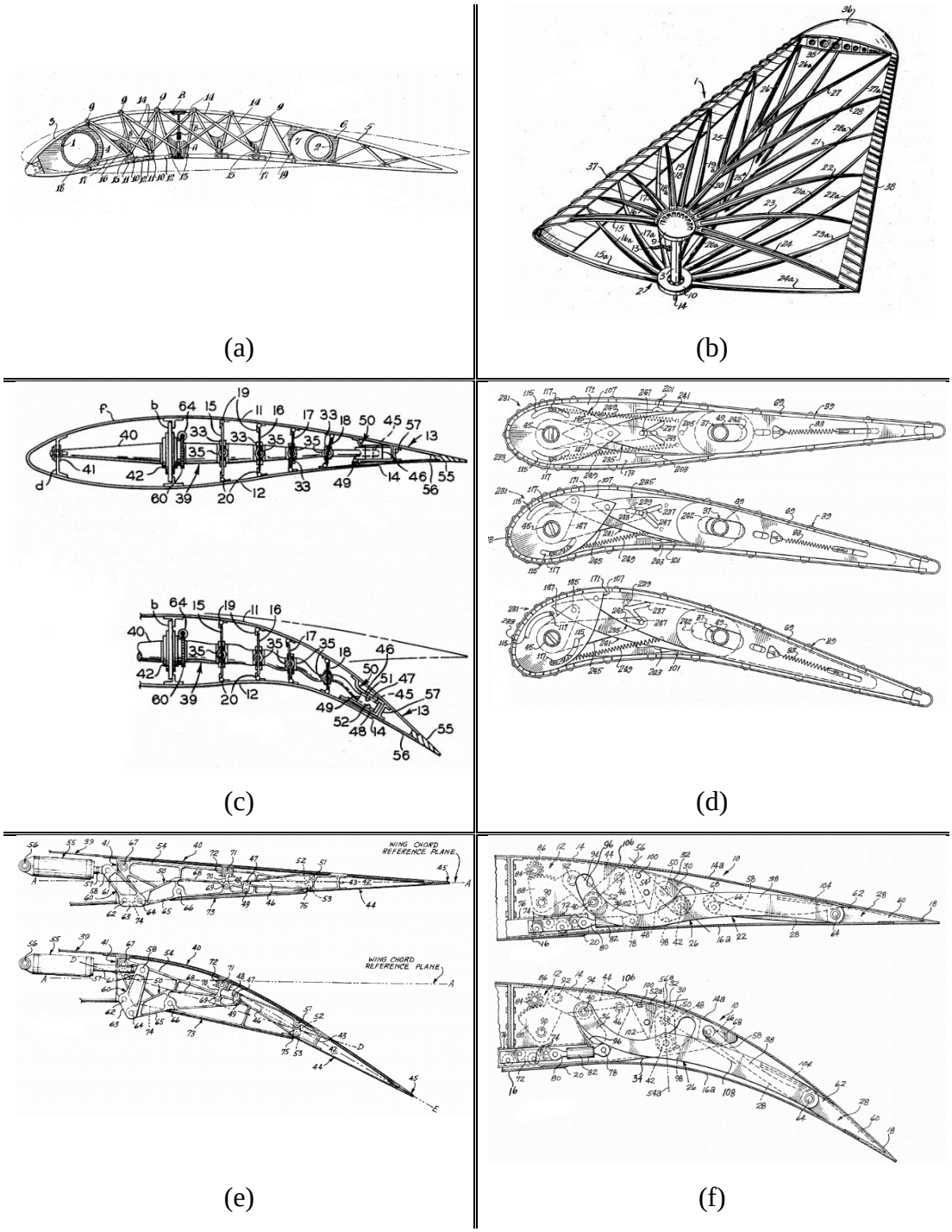

Figure 2.4: (a) Airfoil [25] (1935) , (b) Variable Camber Wing [26] (1946), (c) Variable-camber Airfoil [27] (1963), (d) Variable Camber Airfoil [28] (1967), (e) Variable-camber Airfoil [29] (1977), (f) Variable Camber Trailing Edge for Airfoil [30] (1978)

2.4.2 Research Studies

In addition to the patents proposed, researches continue to find out alternative solutions for camber morphing. In Figure 2.5 and Figure 2.6 some of those research studies are shown. As seen from those studies, a wide range of solutions were found in terms of actuation method. Some of studies also include aerodynamic analysis of surfaces formed by those solutions. Although there is not a consensus on the best actuation mechanism, most of the solutions asserted the replacement of rib structure with moving parts.

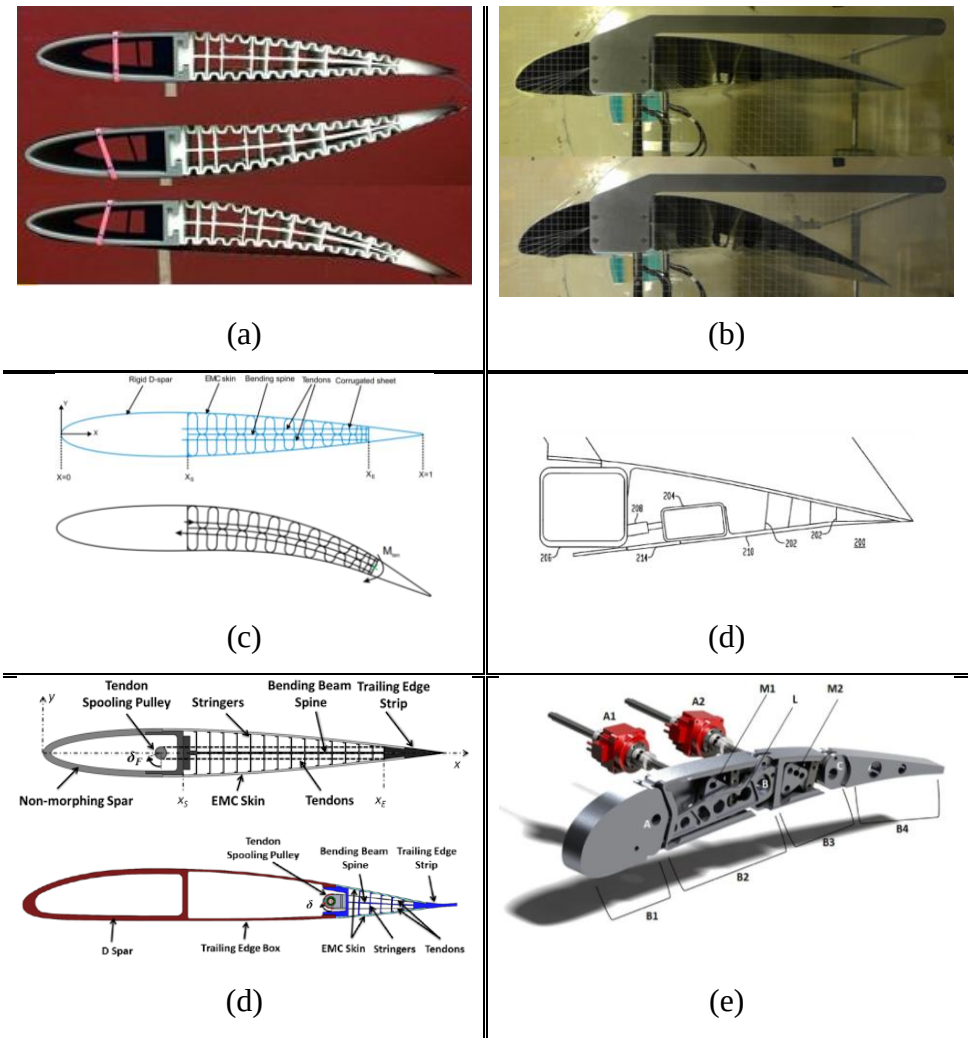

Figure 2.5: (a) Smart Morphing Wing [31], (b) Variable Camber Morphing Wing [32], (c) Morphing Wing Composed of Double Corrugated Structure [33], (d) FlexFoil^{TM} [34], (e) Fish Bone Active Camber Morphing Airfoil [35],(f) Smart Rib [36]

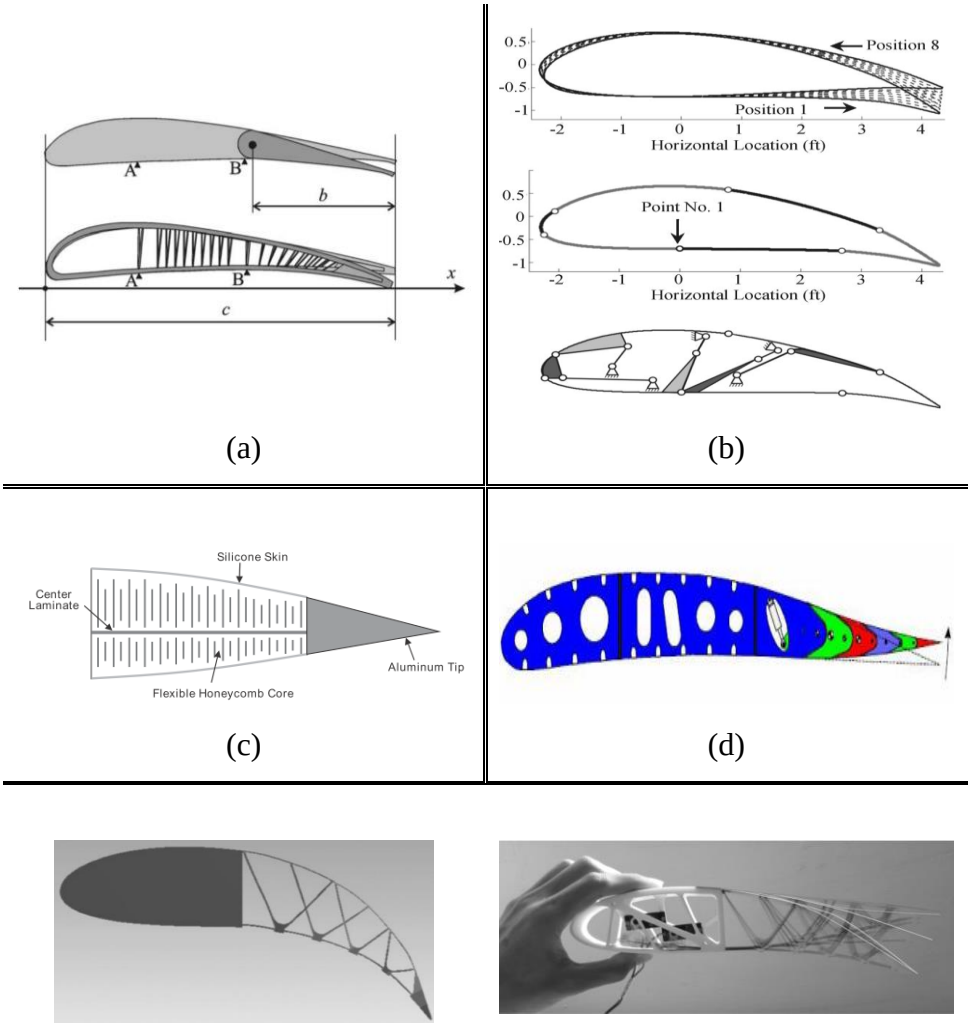

Figure 2.6: (a) Adaptive Belt-Rib Airfoil [37], (b) Planar, Shape-Changing Rigid-Body Mechanisms for Morphing Aircraft Wings [38], (c) DARPA Smart Wing [39], (d) DLR Finger Concept [40], (e) Morphing Carbon Fiber Composite Aerofoil Concept [41]

2.5 Multidisciplinary Challenge

In order to design an aircraft, one should consider efficient togetherness of many different disciplines. Therefore, it can be said that, an entire morphing wing project should also be investigated and proven in terms of its feasibility with all micro, macro structural and fluidic approaches [42]. Figure 2.7 shows the multidisciplinary nature of the morphing wing research:

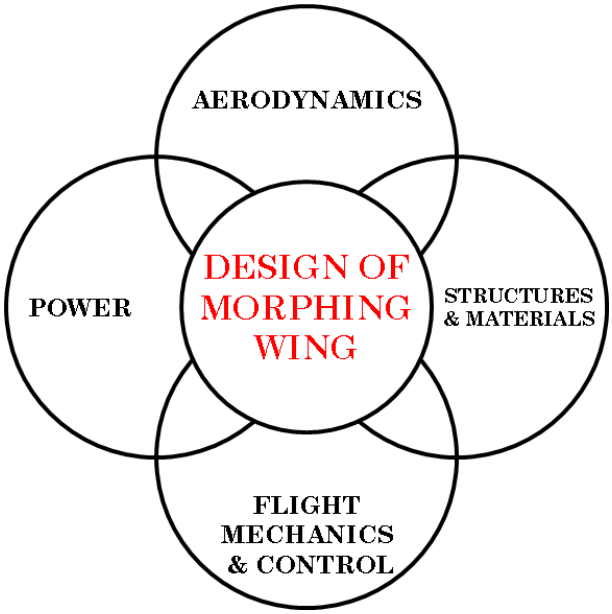

Figure 2.7: Multidisciplinary Nature of Morphing Wing Research [42]

Design of a fully morphed aircraft wing requires consideration of several branches. First of all, aerodynamic shapes created by aircraft wing determine the aerodynamic and inertial characteristics of an aircraft wing, which is crucial for flight performance. Flight mechanics and aerodynamics may be thought of as the disciplines in which the morphing target shapes can be determined. In order to create such aerodynamic shapes, the aircraft wing should be ensured that it has the correct materials, sensible designed structure and actuation mechanism that morph the designed structure. The function of the structural system is to provide and maintain the desired deflection while carrying the external air loads. Providing the shape change implies large deflection and low stiffness while maintaining the intended shape and carrying the loads implies high stiffness and small deformation. Therefore, design of structural system is the most problematic period. The engines or power plants are another factor that should be considered, because most of the commercial aircrafts carry their engines, which generate thrust and supply power for other systems, on their wings. The design of a morphing aircraft will require even greater interdisciplinary considerations. Morphing adds a degree of dynamism to the function of the aircraft and thus results in changing parameters across all disciplines. Aerodynamic and structural analyses will need to be

performed simultaneously, as there is a closed-loop effect between aerodynamic forces and structural displacements, and combined with overall aircraft performance studies, as considered by [37], [42]–[46].

2.6 Benefits of Morphing

As mentioned before, conventional control surfaces are the incomplete/outmoded forms of the morphing wing. From the very beginning, designers imagine fully-morphed aircraft wings; however, due to lack of technology, they invented and used simplification of the ultimate idea. The conventional control surfaces are evinced inventions of that ultimate idea. If the imagination of fully-morphed aircraft is realized; it is obvious that such aircraft have wings which offer significant potential benefits over conventional rigid wings. These benefits can be examined under four headings:

First and the most important of all is that morphing wing will produce optimum aerodynamic performance over an aircraft's nominal operational envelope [9] and can also expand its operating envelope [10]. This performance benefit comes out and adds a multirole capacity to the aircraft due to radical changes in the wing shape. These benefits come out because morphing gives resizing capability to design parameters such as planform area in terms of span length, chord length, sweep angle and aspect ratio, twist angle, dihedral/anhedral angle, AoA, airfoil thickness, even with wing location on the fuselage and taper ratio.

Secondly, replacing conventional surfaces with morphing surfaces improve the fight control and maneuverability [47], [48]. Morphing wings increase control surface effectiveness and the maximum load factor for the same wing-root bending moment by shifting the load distribution inboard by replacing conventional control surfaces with smooth and continuous control surfaces.

Thirdly, it is obvious that morphing wing technology reduces drag, affect thrust generated in a positive way; as a result, the flight range increases. Morphing wings optimize aerodynamic efficiency over the operating range of lift coefficient (C_L) values by varying airfoil section properties: in particular, by making use of variable camber by leading and trailing edge deflection devices. Moreover drag coefficient

(C_D) is reduced by eliminating gaps and discontinuities in wing shape created by conventional control surfaces by replacing them with smoothly varying gapless control surfaces and actuation mechanisms of conventional control surfaces that protrude outside the wing contour by using internally actuated control surfaces. With the introduction of morphing wing, it is also possible to reduce weight by replacing conventional heavy systems with light new systems and by tailoring shape to allow load manipulation/alleviation [49]–[52].

Lastly, the use of morphing technology, reduces vibration and gives the opportunity to control flutter in order to improve comfort, safety and reduce fatigue. Since turbulent flow created by gaps and discontinuities in wing shape created by conventional control surfaces are reduced and with the morphing wing local flow can be controlled by making small adjustments to the wing surface, the problem of flutter can be eliminated pretty well.

Morphing may also lead operational costs to reduce by significant fuel savings [53] and eliminating the requirement of multiple different single-role aircraft by using a single multirole aircraft. Furthermore, maintenance costs can be reduced by reducing wear and the number of parts by eliminating moving parts by using technologies such as compliant mechanisms.

2.7 Discussion and Conclusion

In Chapter 2 the literature review of morphing wing concept is presented. The term "morph" is defined, "morphing wing" concept is clarified and its purpose and philosophy behind of its design are explained. Then, classification of the morphing wing with brief explanations are done. Historical background of morphing wing with related patents and research studies are presented, which show that morphing of the trailing edge of an aircraft wing is still hot topic and there is no a well-accepted solution for that problem. In the end of the chapter, benefits of morphing technologies are described in detail.

CHAPTER 3

KINEMATIC SYNTHESIS AND ANALYSIS OF PLANAR FOUR-BAR MECHANISMS

This chapter is devoted to the kinematic synthesis of the planar four-bar (FB) mechanisms. After an introduction, the synthesis tasks are explained in detail. After brief explanation of defects in mechanism synthesis, mechanism selection criteria and algorithm are given. The chapter ends with kinematic analysis of the FB linkages.

3.1 Introduction

Designing a mechanical system requires passing through a set of stages. Simply, one can distinguish engineering design process into three phases. The very first phase is the “conceptual design” in which design purpose, requirements and specifications, are determined roughly. In the conceptual design, basic questions related to size, weight, cost, working principle, configuration and performance are answered. In the second phase which is “preliminary design”, more broad investigations are made. Preliminary design requires more quantitative answers and an iterative progression; therefore, all major engineering branches play an important role. The last stage named “detailed design” deals with largely material selection, manufacturing methods, cost and maintenance. In the detailed design stage, all parts are examined one by one, the first production begins and the first preliminary prototype is manufactured at the end.

The field of kinetic and kinematics is very important for these three design phases for structural and mechanistic issues. The field of kinetics deals with the forces on system in motion; whereas, kinematics is the study of motion without regard to forces. A machine typically contains mechanisms that transform power to some desirable forces and motion. Kinematic synthesis determines the shape, size and the number of the

mechanical elements that form the mechanism. As seen from the Figure 3.1, kinematic synthesis has three categories which are type synthesis; number synthesis; and dimensional synthesis. In the phase of "type synthesis", the type of the mechanism and its mechanical components are determined. The second phase, "number synthesis", refers to the determination of degree-of-freedom (DOF) and the number of links and joints required. The last step of the kinematic synthesis is the "dimensional synthesis", in which dimensions and angles are determined that affect the motion characteristics of the mechanism [54] – [59].

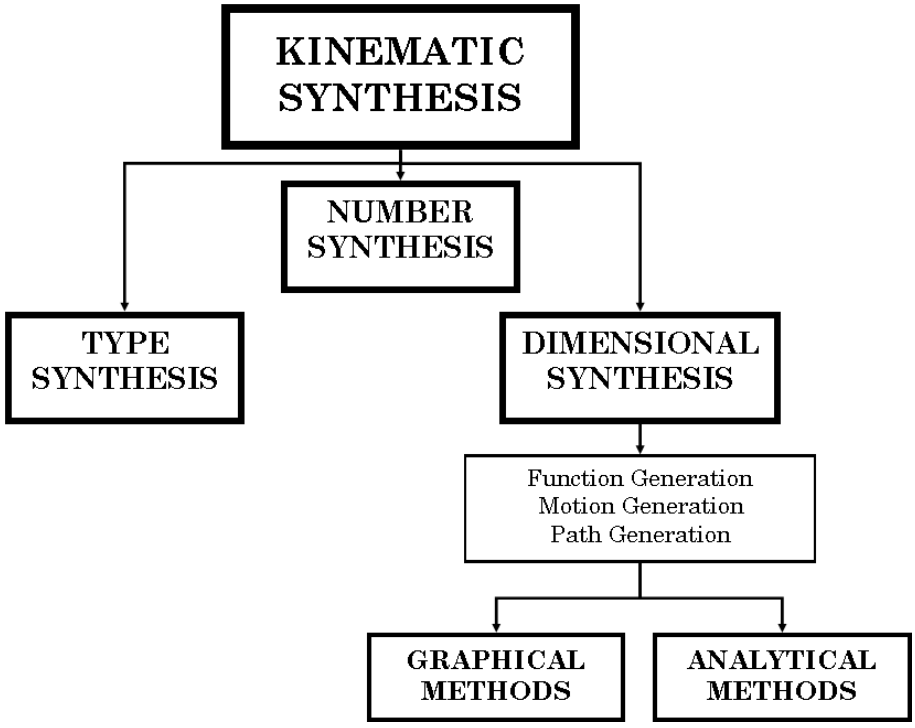

Figure 3.1: Phases of Kinematic Synthesis

3.2 Synthesis Tasks

Dimensional synthesis of FB linkages can be divided into three sub-classes.

3.2.1 Function Generation

In some planar FB applications, the rotation of the output link may be constrained to do a function, which is a common problem faced with in mechanical design [60]. In other words, rotation of the input link, which is called *crank*, and the rotation of the

output link (a.k.a. *follower*) may be correlated. To solve such problems, Freudenstein was formulated the classical problem of planar FB function generators algebraically, in which rotations of output links are prescribed and correlated with the rotations of the crank [61].

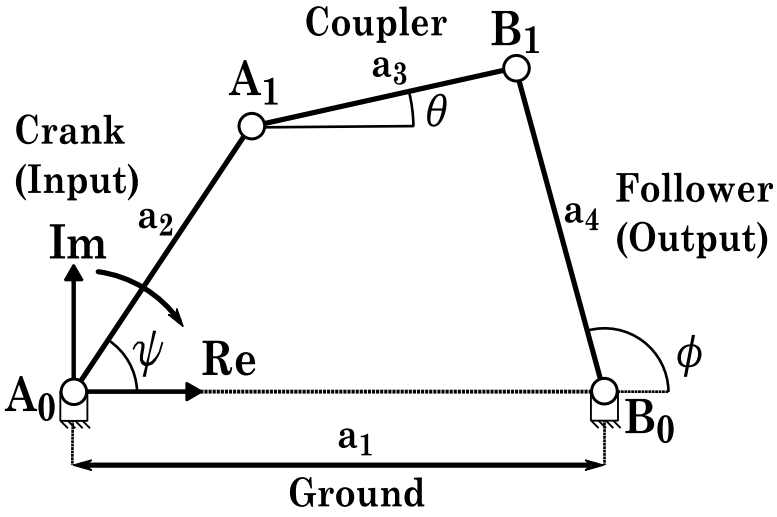

Figure 3.2: Planar Four-Bar Linkage

In Figure 3.2, a planar FB linkage is shown. Generally, a FB linkage have four revolute joints. In Figure 3.2, ψ denotes the *input angl*e of the crank, ϕ the *output angle*, θ is the *coupler angle*. The $\{a_j\}_1^4$ are the link lengths of the ground, crank, coupler and follower respectively. The loop closure equation can be written as:

$$\overrightarrow{A_0A_1} + \overrightarrow{A_1B_1} = \overrightarrow{A_0B_0} + \overrightarrow{B_0B_1} \tag{3.1}$$

Equation (3.1) can be re-written by using complex notation as:

$$a_2e^{i\psi} + a_3e^{i\theta} = a_1 + a_4e^{i\phi} \tag{3.2}$$

In complex plane, it is also possible to write another loop closure equation which corresponds to the mirror image of the mechanism with respect to real-axis. By using the conjugate property of the complex numbers, below relation can be obtained:

$$a_2 e^{-i\psi} + a_3 e^{-i\theta} = a_1 + a_4 e^{-i\phi} \tag{3.3}$$

Multiplying equations (3.2) and (3.3), then using the identity of $\cos(x) = \frac{(e^{ix}+e^{-ix})}{2}$ gives:

$$a_3^2 = a_1^2 + a_2^2 + a_4^2 + 2a_1 a_4 \cos(\phi) - 2a_1 a_2 \cos(\psi) - 2a_2 a_4 \cos(\phi - \psi) \tag{3.4}$$

Equation (3.4) is a scalar relationship which correlates the input angle to output angle. Freudenstein proposes to work with linkage ratios by selecting a linkage (i.e. ground) unity. By dividing equation (3.4) by term $2a_2 a_4$, one can obtain well-known *Freudenstein equation* which relates input and output angles in a compact form. Once these have done, below definition of Freudenstein parameters arises as:

$$p_1 \equiv \frac{a_1^2 + a_2^2 - a_3^2 + a_4^2}{2a_2 a_4}, p_2 \equiv \frac{a_1}{a_2}, p_3 \equiv \frac{a_1}{a_4} \tag{3.5}$$

Hence, the Freudenstein equation in its homogeneous form becomes:

$$F(\psi, \phi) = p_1 + p_2 \cos(\phi) - p_3 \cos(\psi) - \cos(\phi - \psi) = 0 \tag{3.6}$$

In function generation synthesis task, since the input and output angles are prescribed, for $\{\psi_j, \phi_j\}_1^\lambda$ below equation system can be constructed which is:

$$[S]\{p\} = \{b\} \tag{3.7}$$

where λ denotes number of multiply separated prescribed positions (MSPP). For example, in order to synthesize function generators, one should set input-output angle set where the total number of known angle set, λ, which determines the total number of linear equations. The matrix $[S]$ and vectors $\{p\}, \{b\}$ of equation (3.7) can be defined as:

$$[S] \equiv \begin{bmatrix} 1 & \cos(\phi_1) & -\cos(\psi_1) \\ 1 & \cos(\phi_2) & -\cos(\psi_2) \\ \vdots & \vdots & \vdots \\ 1 & \cos(\phi_\lambda) & -\cos(\psi_\lambda) \end{bmatrix}, \{p\} \equiv \begin{Bmatrix} p_1 \\ p_2 \\ p_3 \end{Bmatrix}, \{b\} \equiv \begin{Bmatrix} \cos(\phi_1 - \psi_1) \\ \cos(\phi_2 - \psi_2) \\ \vdots \\ \cos(\phi_\lambda - \psi_\lambda) \end{Bmatrix} \quad (3.8)$$

The solution procedure of equation (3.7) can be divided into three case according to the value of the parameter λ.

If $\lambda < 3$, the number of equations are less than the number of unknowns; in other words, there exists infinitely many solutions. In such a case, to overcome the difficulty arises, one can choose one set of more input and output angles arbitrarily and compute alternatives to select the mechanism which best fits with the desired function.

If $\lambda = 3$, the number of equations are equal to the number of unknowns. In this case, the system of equations gives only one unique solution for Freudenstein parameters ($\{p_j\}_1^3$), unless the matrix $[S]$ is not singular.

If $\lambda > 3$, the number of equations exceeds the number of unknowns; thus, any type of numerical approach gives an approximate solution; although, there exists an exact solution in some cases. To overcome such problems, *approximate synthesis* of planar FB mechanisms is extensively studied [62]–[64], which is beyond the scope of this thesis. However, for large number of multiply separated positions, *least-square approximation* can be used [64].

In the field of kinematic synthesis, two types of error definition are used commonly. The first type error is the "design error" and the second one is "structural error" [65]. Design error related with error residual accumulated through optimization and structural error is the difference between desired and actual condition. For approximate synthesis of function generators, error vector can be defined as:

$$\{e\} \equiv \{b\} - [S]\{p\} \quad (3.9)$$

and design error can be calculated through taking the RMS value of the error vector as:

$$e_d = \sqrt{\frac{1}{\lambda}\sum_{1}^{\lambda} e_j^2} \tag{3.10}$$

Then equation (3.7) takes the form to compute the Freudenstein parameters:

$$\{p_0\} = [S]^I\{b\} \tag{3.11}$$

Equation (3.11) is the least-square approximation of the given overdetermined system of linear equations, where $[S]^I$ is "Moore-Penrose" generalized inverse of the matrix $[S]$:

$$[S]^I = ([S][S]^T)^{-1}[S]^T \tag{3.12}$$

Calculating the least-square approximation $\{p_0\}$ form equation (3.11) directly is not advisable, especially for $\lambda > 1000$. However, in this dissertation, λ is selected as order of 10.

Below table describes an algorithm for the synthesis of function generators:

Table 3.1: Algorithm for Synthesis of Function Generators

Algorithm 3.1-Synthesis of Function Generators

use $\{\psi_j, \phi_j\}_1^{\lambda}$

If $\lambda = 2$

Loop in i **until** N_i **and** j **until** N_j

$[p(i,j)] \leftarrow [S(i,j)]^{-1}[b(i,j)]$

$a_1 \leftarrow 1.0,\ a_2(i,j) \leftarrow a_1/p_2(i,j),\ a_4(i,j) \leftarrow a_1/p_3(i,j)$

$a_3(i,j) \leftarrow \sqrt{a_1^2 + a_2(i,j)^2 + a_4(i,j)^2 - 2p_1(i,j)a_2(i,j)a_4(i,j)}$

End Loop

Else $\lambda = 3$

$\{p\} \leftarrow [S]^{-1}\{b\}$

$a_1 \leftarrow 1.0,\ a_2 \leftarrow a_1/p_2,\ a_4 \leftarrow a_1/p_3$

$a_3 \leftarrow \sqrt{a_1^2 + a_2^2 + a_4^2 - 2p_1a_2a_4}$

Else $\lambda \geq 3$

$\{p_0\} \leftarrow (([S][S]^T)^{-1}[S]^T)\{b\}$

$\{e_0\} \leftarrow \{b\} - [S]\{p_0\}$

$\{e_{d_0}\} \leftarrow \sqrt{\frac{1}{N_{MSP}}}\|\{e_0\}\|$

$a_1 \leftarrow 1.0,\ a_2 \leftarrow a_1/p_{0_2},\ a_4 \leftarrow a_1/p_{0_3}$

$a_3 \leftarrow \sqrt{a_1^2 + a_2^2 + a_4^2 - 2p_{0_1}a_2a_4}$

End If

3.2.2 Motion Generation

In the problem of motion generation, a.k.a. rigid-body guidance, a set of MSPP of a rigid body is given and aimed to be visited in the prescribed order. This problem has been raised up by Ludwig Burmester for planar FB linkages [66]. In the literature, there are many works related with the theory and formulation of the problem. The most common and accepted solution procedure is based on dyadic approach. Erdman and Sandor laid the foundation of dyad synthesis of planar FB linkages which is mostly used in this dissertation [57]. Tesar [67]–[69] developed MSPP synthesis in coplanar motion for three and four positions and Polat [70] derived necessary equations using the dyadic approach. Demir [71], Martin [72] and Erener [73] applied this formulation in AutoCAD, Mathcad and CATIA environment respectively.

A dyad is defined as two-line vector pairs which are coupled to two other links. This term does not just belong to the planar linkages; however, in the planar linkages there are only four types of dyads arises which are RR (revolute-revolute), RP (revolute-prismatic), PR (prismatic-revolute), PP (prismatic-prismatic). Any planar FB linkage can be depicted as two RR dyads, each of which satisfies the prescribed motion independently and forms a single, 1-DOF mechanism. In dyadic approach, the formulation gives the synthesis of a single dyad (i.e. RR); therefore, with the synthesis of another dyad and combination of these two dyads just form a planar FB mechanism. The dyads for a planar FB mechanism are illustrated in Figure 3.3.

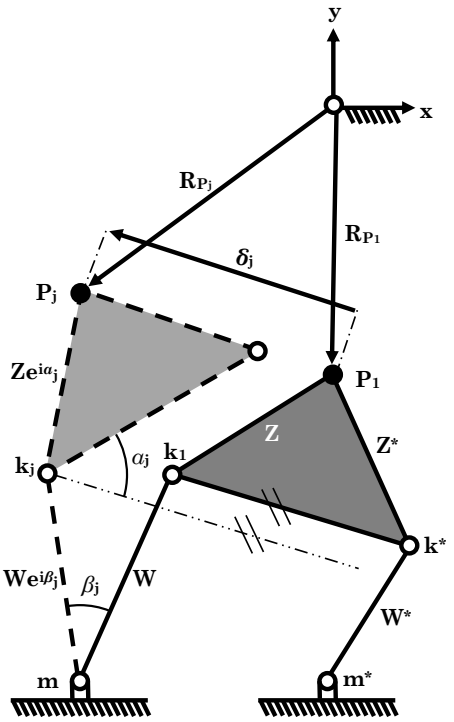

Figure 3.3: Dyadic Representation of a Planar Four-Bar Linkage

In the Figure 3.3, W and Z represent the first of two dyads (left-side) of the planar FB mechanism and vectors W^* and Z^* represent the second of two dyads (right-side). Vectors W and W^* represent the crank and output links respectively, if the prime-mover is selected to drive the left-side dyad. The crank and output links are the type of *binary*; whereas, vectors Z and Z^* are assumed to form a common *ternary* link. Variables m, m^* are ground pivots (where the letter "m" resembles "Mittelpunkt" meaning "center point" in German), k, k^* are moving pivots (where the letter "k" resembles "Kreispunkt" meaning "circle point" in German) and P_j's represent the prescribed coupler positions which are aimed to be satisfied [57].

In the dyadic approach, the displacement of the coupler at j^{th} position can be defined as $\vec{\delta}_j \equiv \vec{R}_{P_j} - \vec{R}_{P_1}$ where $\left\{\vec{R}_{P_j}\right\}_2^{\lambda}$'s are the vectors describing known prescribed coupler points. For planar linkages, vectors can be defined as complex numbers by using Euler's identity of $e^{i\theta} = \cos(\theta) + i\sin(\theta)$. In order to obtain a coupler displacement, $\vec{\delta}_j$, the vector $\overrightarrow{W}$, which represents the crank, should make a rotation of

β_j and the vector $\vec{Z}$, which represents the coupler, should make a rotation of α_j. Therefore, considering the composed closed-loop $k-m-P_1-k_j-m$, following closed-loop equation can be written:

$$\overrightarrow{mk}+\overrightarrow{kP_1}+\overrightarrow{P_1P_j}=\overrightarrow{mk_j}+\overrightarrow{k_jP_j} \tag{3.13}$$

In the form of complex numbers:

$$\vec{W}+\vec{Z}+\vec{\delta}_j=\vec{W}e^{i\beta_j}+\vec{Z}e^{i\alpha_j} \tag{3.14}$$

$$\vec{W}\left(e^{i\beta_j}-1\right)+\vec{Z}\left(e^{i\alpha_j}-1\right)=\vec{\delta}_j \tag{3.15}$$

Note that equation (3.15) is often called the "standard form" of the dyadic representation of planar FB linkages. As shown from the equation (3.15), there is a set of equations for known poses (prescribed points, $\{P_j\}_1^\lambda$, and orientations, $\{\alpha_j\}_2^\lambda$'s, therefore , these equations can be solved for unknown crank and coupler link lengths and crank rotations $\left(W,Z,\{\beta_j\}_2^\lambda\right)$. Re-writing equation (3.15) by defining a vector. $\vec{R}\equiv-\vec{W}-\vec{Z}$ gives:

$$\vec{R}\left(1-e^{i\beta_j}\right)+\vec{Z}\left(e^{i\alpha_j}-e^{i\beta_j}\right)=\vec{\delta}_j \tag{3.16}$$

Similar with the task function generation, equation (3.16), the solution procedure of equation (3.16) can be divided into three cases. If $\lambda<5$, it is possible to freely choose or manipulate some unknown parameter(s). If $\lambda=5$, then there is no chance to select any parameters freely, the solution gives only one exact result. If $\lambda>5$, since the number of equations are higher than the number of unknowns; finding a solution is possible only by approximation methods. Table 3.2 gives a summary for the cases when the number of equations are lower than the number of unknowns ($\lambda<5$):

Table 3.2: Number of Equations, Unknowns and Free Choices according to Number of Prescribed Poses in Dyad Method

Number of prescribed poses	**Number of equations**	**Number of unknowns**	**Number of free choices**
2	2	5 (R, Z, β_2)	3
3	4	6 (R, Z, β_2, β_3)	2
4	6	7 $(R, Z, \beta_2, \beta_3, \beta_4)$	1
5	8	8 $(R, Z, \beta_2, \beta_3, \beta_4, \beta_5)$	0

Note that, equation (3.16) can only be used for finitely separated poses (i.e. positions, $\{P_j\}_1^\lambda$, and orientations, $\{\alpha_j\}_2^\lambda$). In other words, with dyadic approach, it is also possible to prescribe derivatives of the displacement of the coupler instead of its positions. For that purpose, the same equation can be manipulated to be used for infinitesimally separated positions to specify the first derivative of the coupler displacement, $\left\{\frac{d\vec{\delta}}{d\alpha}\right\}$, and the second derivative of the coupler displacement, $\left\{\frac{d^2\vec{\delta}}{d\alpha^2}\right\}$. In order to use prescribed rate of coupler displacements, equation (3.16) has to be derived with respect to the particular rotation, α_j. For motion generation synthesis, the loop closure equation for infinitesimally separated positions can be written as:

$$\vec{R}\frac{d}{d\alpha}\left(1-e^{i\beta}\right)\Big|_{\beta=\beta_j}+\vec{Z}\frac{d}{d\alpha}\left(e^{i\alpha}-e^{i\beta}\right)\Big|_{\substack{\alpha=\alpha_j\\ \beta=\beta_j}}=\frac{d}{d\alpha}\vec{\delta}_j(\alpha)\Big|_{\alpha=\alpha_j} \qquad (3.17)$$

For situations where the finitely and infinitesimally separated positions are combined, following equation can be used:

$$\vec{R}\frac{d^{j'}}{d\alpha^{j'}}\left(1-e^{i\beta}\right)\Big|_{\beta=\beta_j}+\vec{Z}\frac{d^{j'}}{d\alpha^{j'}}\left(e^{i\alpha}-e^{i\beta}\right)\Big|_{\substack{\alpha=\alpha_j\\ \beta=\beta_j}}=\frac{d^{j'}}{d\alpha^{j'}}\vec{\delta}_j(\alpha)\Big|_{\alpha=\alpha_j} \qquad (3.18)$$

where j is the index of the finitely separated positions and the j' is the index of the infinitesimally separated position corresponding to the previous finitely separated position.

With the help of above equations (3.17) and (3.18), after the rates of the coupler displacement are specified, one can determine or arbitrarily select the corresponding crank velocity and acceleration.

3.2.2.1 Three Prescribed Position Synthesis

When the number of prescribed positions (finitely separated, case p-p-p) is three, $\lambda = 3$, the equation (3.16) can be expanded as follows:

$$\begin{aligned} \vec{R}\left(1 - e^{i\beta_2}\right) + \vec{Z}\left(e^{i\alpha_2} - e^{i\beta_2}\right) &= \vec{\delta}_2 \\ \vec{R}\left(1 - e^{i\beta_3}\right) + \vec{Z}\left(e^{i\alpha_3} - e^{i\beta_3}\right) &= \vec{\delta}_3 \end{aligned} \tag{3.19}$$

Equation (3.19) is a set of complex equations in which $\vec{R}, \vec{Z}$ are complex unknown vectors and β_2, β_3 are unknown angular displacements of the crank. As described in Table 3.2, the number of equations are lower than the number of unknowns, which yields infinite number of solutions in the order of $O(\infty^2)$. Therefore, in order to solve that set of equations, *two* of unknowns should be selected arbitrarily. Since it is easier to choose angles arbitrarily compared to the link lengths, if β_2, β_3 are determined, equation set (3.19) can be solved for unknowns $\vec{R}$ and $\vec{Z}$ as follows.

$$\vec{R} = \frac{\vec{\delta}_2\left(e^{i\alpha_3} - e^{i\beta_3}\right) - \vec{\delta}_3\left(e^{i\alpha_2} - e^{i\beta_2}\right)}{(e^{i\alpha_3} - e^{i\beta_3})(1 - e^{i\beta_2}) - (e^{i\alpha_2} - e^{i\beta_2})(1 - e^{i\beta_3})} \tag{3.20}$$

$$\vec{Z} = \frac{\vec{\delta}_2\left(1 - e^{i\beta_3}\right) - \vec{\delta}_3\left(1 - e^{i\beta_2}\right)}{(e^{i\alpha_2} - e^{i\beta_2})(1 - e^{i\beta_3}) - (e^{i\alpha_3} - e^{i\beta_3})(1 - e^{i\beta_2})} \tag{3.21}$$

It is also possible to select one of the unknown vectors, $\vec{R}$ or $\vec{Z}$, as a free parameter selected arbitrarily in order to solve the equation set (3.19) for unknown angles β_2, β_3

and the unselected vector. By doing so one can obtain unique circles that shows the coordinates of the center or circle curves.

In order to prescribe infinitely separated positions, equations (3.20) and (3.21) can be re-written in a compact form as:

$$\vec{R} = \frac{\mathbb{D}_2(\mathbb{A}_3 - \mathbb{B}_3) - \mathbb{D}_3(\mathbb{A}_2 - \mathbb{B}_2)}{(\mathbb{A}_3 - \mathbb{B}_3)(\mathbb{S}_2 - \mathbb{B}_2) - (\mathbb{A}_2 - \mathbb{B}_2)(\mathbb{S}_3 - \mathbb{B}_3)} \tag{3.22}$$

$$\vec{Z} = \frac{\mathbb{D}_2(\mathbb{S}_3 - \mathbb{B}_3) - \mathbb{D}_3(\mathbb{S}_2 - \mathbb{B}_2)}{(\mathbb{A}_2 - \mathbb{B}_2)(\mathbb{S}_3 - \mathbb{B}_3) - (\mathbb{A}_3 - \mathbb{B}_3)(\mathbb{S}_2 - \mathbb{B}_2)} \tag{3.23}$$

where $\mathbb{A}_2, \mathbb{A}_3, \mathbb{B}_2, \mathbb{B}_3, \mathbb{D}_2, \mathbb{D}_3, \mathbb{S}_2, \mathbb{S}_3$ take the values which are listed in the Table 3.3 according to the corresponding synthesis task:

Table 3.3: Terms used in Dyad Loop Equations for Finitely and Infinitesimally Separated Three Positions

	p-p-p	**pp-p**	**ppp**
$\mathbb{A}_2$	$e^{i\alpha_2}$	i	i
$\mathbb{A}_3$	$e^{i\alpha_3}$	$e^{i\alpha_2}$	-1
$\mathbb{B}_2$	$e^{i\beta_2}$	$i\dot{\beta}$	$i\dot{\beta}$
$\mathbb{B}_3$	$e^{i\beta_3}$	$e^{i\beta_2}$	$\dot{\beta}^2 + i\ddot{\beta}$
$\mathbb{D}_2$	$\vec{\delta}_2$	$\frac{d\vec{\delta}}{d\alpha}$	$\frac{d\vec{\delta}}{d\alpha}$
$\mathbb{D}_3$	$\vec{\delta}_3$	$\vec{\delta}_2$	$\frac{d^2\vec{\delta}}{d\alpha^2}$
$\mathbb{S}_2$	1	0	0
$\mathbb{S}_3$	1	1	0
Selected parameters	β_2, β_3	$\dot{\beta}, \beta_2$	$\dot{\beta}, \ddot{\beta}$

where in Table 3.3, “p-p-p”, “pp-p” and “ppp” resemble *three finitely separated positions*, *two infinitesimally separated positions and one finitely separated position*, *three infinitesimally separated positions* respectively [73].

3.2.2.2 Four Prescribed Position Synthesis

When the number of prescribed positions (finitely separated, case p-p-p-p) is increased to four, $\lambda = 4$, then the dyad-loop equation (3.16) can be expanded as follows:

$$\begin{aligned}
\vec{R}\left(1 - e^{i\beta_2}\right) + \vec{Z}\left(e^{i\alpha_2} - e^{i\beta_2}\right) &= \vec{\delta}_2 \\
\vec{R}\left(1 - e^{i\beta_3}\right) + \vec{Z}\left(e^{i\alpha_3} - e^{i\beta_3}\right) &= \vec{\delta}_3 \\
\vec{R}\left(1 - e^{i\beta_4}\right) + \vec{Z}\left(e^{i\alpha_4} - e^{i\beta_4}\right) &= \vec{\delta}_4
\end{aligned} \tag{3.24}$$

Cramer’s rule can be used to solve the set of equations (3.24), in which one of the three parameters $\beta_2, \beta_3, \beta_4$ can be selected arbitrarily. Since, as seen from the Table 3.2, difference between number of equations and unknowns is one, infinite number of solutions is possible in the order of $O(\infty)$. Whichever parameter, $\beta_2, \beta_3, \beta_4$, is freely chosen; every selection will yield the same curves. If the set of equations (3.24) is solved for a range of β_2, a locus of moving point locations (circle points) and $k_1 = \vec{R}_{P_1} - \vec{Z}$ and fixed point locations (center points) $m = k_1 + \vec{R} + \vec{Z}$ can be produced.

The solution of the system exists if and only if the rank of the augmented matrix of the coefficients equals to two. Then the equation set (3.24)can be written in the form of an augmented matrix M. Since the rank of that augmented matrix is two, its determinant is zero:

$$|M| = \begin{vmatrix} 1 - e^{i\beta_2} & e^{i\alpha_2} - e^{i\beta_2} & \vec{\delta}_2 \\ 1 - e^{i\beta_3} & e^{i\alpha_3} - e^{i\beta_3} & \vec{\delta}_3 \\ 1 - e^{i\beta_4} & e^{i\alpha_4} - e^{i\beta_4} & \vec{\delta}_4 \end{vmatrix} = 0 \tag{3.25}$$

If the determinant given in equation (3.25) is expanded about its first column, the $\{\Delta_j\}_1^4$ variables are known, since they contain only known input data:

$$\Delta_1 + \Delta_2 e^{i\beta_2} + \Delta_3 e^{i\beta_3} + \Delta_4 e^{i\beta_4} = 0 \tag{3.26}$$

where

$$\Delta_1 = -\Delta_2 - \Delta_3 - \Delta_4 \tag{3.27}$$

$$\Delta_2 = \begin{vmatrix} 1 - e^{i\alpha_3} & \vec{\delta}_3 \\ 1 - e^{i\alpha_4} & \vec{\delta}_4 \end{vmatrix} \tag{3.28}$$

$$\Delta_3 = -\begin{vmatrix} 1 - e^{i\alpha_2} & \vec{\delta}_2 \\ 1 - e^{i\alpha_4} & \vec{\delta}_4 \end{vmatrix} \tag{3.29}$$

$$\Delta_4 = \begin{vmatrix} 1 - e^{i\alpha_2} & \vec{\delta}_2 \\ 1 - e^{i\alpha_3} & \vec{\delta}_3 \end{vmatrix} \tag{3.30}$$

The equation (3.26), which is also referred as the "compatibility equation", is a nonlinear equation which contains the unknown variables $\beta_2, \beta_3, \beta_4$. This compatibility equation can be solved for a range of values for one selected unknown $\beta_2, \beta_3, \beta_4$. Since it is easy to determine the first rotations of the crank, i.e. β_2, the nonlinear compatibility equation can be solved either geometrically/analytically (calculated with the given algorithm) or numerically.

In order to solve the compatibility equation (3.26) geometrically/analytically, equation (3.26) can be regarded as the loop-closure equation of a FB linkage, where Δ_1 resembles the fixed link, $\{\Delta_j\}_2^4$ and $\{\beta_j\}_2^4$ resemble movable links with corresponding link rotations from their starting positions. Then, using algorithm given in Table 3.4, unknown angles, β_3, β_4, can be found.

Table 3.4: Algorithm for Synthesis of Motion Generators with Four Finitely Separated Prescribed Positions

Algorithm 3.2- Synthesis of Motion Generators with Four Finitely Separated Prescribed Positions

use $\{\Delta_j\}_2^4, \{(\beta_2)_j\}_1^{N_j}$

Loop in j **until** N_j

$\Delta = \Delta_1 + \Delta_2 e^{i(\beta_2)_j}$

$\cos(\theta_3) \leftarrow \frac{\Delta_4^2 - \Delta_3^2 - \Delta^2}{2\Delta_3\Delta}$ where $\{\Delta_j\}_2^4 = \left|\{\Delta_j\}_2^4\right|$ and $\Delta = |\Delta|$

$\sin(\theta_3) \leftarrow \left|\sqrt{1 - \cos^2(\theta_3)}\right|$

$\theta_3 \leftarrow \text{atan2}(\sin(\theta_3), \cos(\theta_3))$ where $\sin(\theta_3) \geq 0$ and $0 \leq \theta_3 \leq \pi$

$\beta_3 \leftarrow \arg\Delta + \theta_3 - \arg\Delta_3$

$\tilde{\theta}_3 \leftarrow 2\pi - \theta_3$

$\tilde{\beta}_3 \leftarrow \arg\Delta + \tilde{\theta}_3 - \arg\Delta_3$

$\cos(\theta_4) \leftarrow \frac{\Delta_3^2 - \Delta_4^2 - \Delta^2}{2\Delta_4\Delta}$

$\sin(\theta_4) \leftarrow \left|\sqrt{1 - \cos^2(\theta_4)}\right|$

$\theta_4 \leftarrow \text{atan2}(\sin(\theta_4), \cos(\theta_4))$ where $\sin(\theta_4) \geq 0$ and $0 \leq \theta_4 \leq \pi$

$\beta_4 \leftarrow \arg\Delta - \theta_4 - \arg\Delta_4$

$\tilde{\theta}_4 \leftarrow -\theta_4$

$\tilde{\beta}_4 \leftarrow \arg\Delta + \tilde{\theta}_4 - \arg\Delta_4 + \pi$

End Loop

After determination of the other crank rotations, β_3, β_4, the set of equations formed in (3.24) can be solved either by using Cramer's rule or any other method.

It is also possible to prescribe infinitely separated positions and select related crank angular velocities or accelerations for four prescribed positions. Those formulations given in Appendix B.

3.2.3 Path Generation

Tracing continuous curves is another problem that faced with in mechanical design. In aerospace industry, design of landing gears can be counted as one of examples of path generation. While robot manipulators are powerful alternative for path generators, in repetitive applications, using a simple mechanism can be less expensive and more practical.

Thanks to the dyadic representation of planar FB linkages, the synthesis of path generators is the same with motion generation task. However, in the path generation task, since the orientation of the coupler is not important, coupler rotations, $\{\alpha_j\}_2^\lambda$, can be selected arbitrarily. Moreover, derived equations and algorithms in the motion generation section can be used by inserting related crank rotations, $\{\beta_j\}_2^\lambda$ as if they were coupler rotations. Hence, related coupler rotations can be found. After the determination of coupler rotations and construction of first dyad, RR, the second dyad can be generated through the procedure with motion generation. By doing so, desired path can be generated by knowing the corresponding crank rotations.

3.3 Defects in Mechanism Synthesis

As mentioned before, points on the Burmester curve pair resemble possible center and circle points which are used to construct the mechanism that fulfill the desired motion theoretically. However, in many cases, the constructed mechanism cannot fulfill the required task due to branch, circuit or order defects.

Branch defects occur if the mechanism does not have a single linkage assembly configuration; in other words, the mechanism has to be dissembled from a joint and the re-assembled from another joint in order to satisfy the all prescribed positions. In circuit defect, which a common defect seen in kinematic synthesis of FB linkages [58], constructed mechanism cannot achieve the prescribed motion due to lock-up or binding condition. Branch and circuit defects are similar to each other since both require disassembly of the mechanism while in branch defect, reassembly is sufficient to achieve the prescribed motion, in circuit defects it is not. Therefore, circuit defects

can be mentioned as fatal condition. If the mechanism does not visit the positions in prescribed order, there exists an order defect. In the motion generation, both branch and order defects are inherent due to theoretical formulation [74].

3.4 Mechanism Selection Criteria and Algorithms

In most of the cases, applying explained kinematic synthesis tasks for motion and path generation results in more than one exact solution without defect. In this situation, selection of the correct solution (correct joint locations to construct the mechanism) becomes a difficult job. In order to simplify that problem, Martin developed a systematic approach, in which all solutions are calculated, then those solutions are compared with each other to select the one which falls into the Grashof type, which subject to the feasible transmission angle criteria and after all which has the least perimeter [72].

3.4.1 Mobility of the Input and Output Links

In most of the machine design problems, rotation behavior of the used mechanism must be taken into account for the sake of simplicity. Therefore, in the design of planar FB mechanisms, rotatability of the crank is one of the important feature, since most of the common prime-movers supply continuous rotation.

In planar FB mechanisms, if the crank link is capable of full-rotation with respect to the ground, then this kind of mechanisms are classified as the “Grashof” type. For example, when a drive mechanism is implemented to rotate the crank link. What determines the rotation behavior of the FB linkages are Grashof condition and the inversion chosen. Grashof condition is an inequality and can be given as

$$L_{min} + L_{max} < L_a + L_b \tag{3.31}$$

where L_{min}, L_{max} resemble shortest and longest link lengths and L_a, L_b resemble the other intermediate link lengths. As mentioned, the Grashof condition is not sufficient itself to the determine the rotation characteristics of the crank, the inversion also plays a role. Although there are more complex classifications, simple Grashof type planar FB mechanisms can be classified as shown in Table 3.5:

Table 3.5: Classification of Grashof type Mechanisms

Class	Type of the mechanism	Shortest link	Relationship between link lenghts
I	Crank-rocker	Crank	$L_{min} + L_{max} < L_a + L_b$
	Double-crank	Ground	$L_{min} + L_{max} < L_a + L_b$
	Double-rocker	Coupler	$L_{min} + L_{max} < L_a + L_b$
II	Triple-rocker	Any	$L_{min} + L_{max} > L_a + L_b$
III	Change Point	Any	$L_{min} + L_{max} = L_a + L_b$

For the Class I, if the ground link adjacent to the shortest link, one can get a crank-rocker. Which means the shortest link can fully rotate and becomes crank, the other link adjacent to the ground link behaves as an output link and oscillates (rocks). When the ground link is the shortest, both links pivoted to the ground can fully rotate

For the Class II (also called as non-Grashof type), all inversions of the constructed mechanism will give the same results which is named triple-rocker, due to the fact that all links oscillates instead of full-rotation.

For the Class III, all inversions will result in the either double-cranks or crank-rockers. The name comes from the fact that all inversions have the change point, where all links become collinear and this is a kinematically indeterminate position where the linkage may move to one of the two branches depending on other conditions.

3.4.2 Transmission Angle

One of the important parameters that gives an idea about the static force transmission quality is the transmission angle suggested by Alt is the transmission angle. Formally, transmission angle can be defined as *the angle between axes of coupler and the follower links*.

The importance of transmission angle comes from the kinetostatic analysis of the mechanism. In other words, transmission angle is related with the quality of the force

transmission and can be used to determine the best design among a family of possible mechanisms.

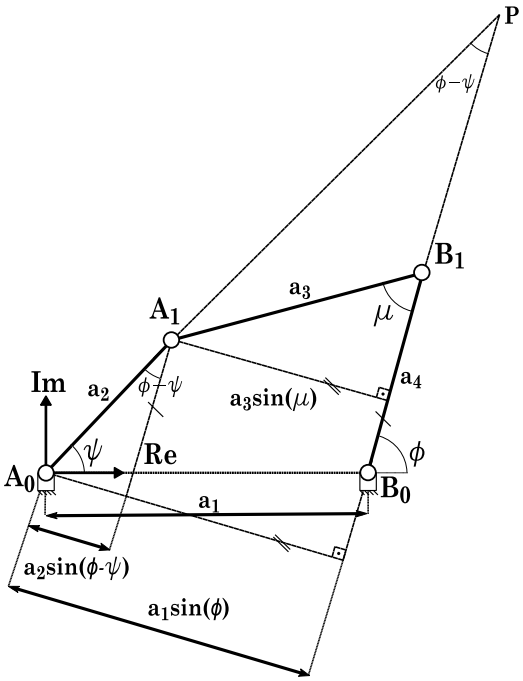

Figure 3.4: Representation of Transmission Angle

Applying cosine rule to a common planar FB linkage, $\cos(\mu)$ can be derived in terms of crank angle, ψ, as:

$$\cos(\mu) = \frac{a_3^2 + a_4^2 - a_1^2 - a_2^2 + a_1 a_2 \cos(\psi)}{2a_3 a_4} \tag{3.32}$$

Interestingly, transmission angle can be re-written in terms of Freudenstein parameters and linkage discriminant as:

$$\sin^2(\mu) = \frac{p_3^2}{p_2^2 + p_3^2 + p_2^2 p_3^2 - 2p_1 p_2 p_3} \Lambda(\psi) \tag{3.33}$$

where $\Lambda(\psi)$ is the "linkage discriminant", which is a parabola in $\cos(\psi)$ and not only linkage but also posture dependent:

$$\Lambda(\psi) = -p_3^2 \cos^2(\psi) + 2(p_1 p_3 - p_2)\cos(\psi) + (1 - p_1^2 + p_2^2) \geq 0 \qquad (3.34)$$

which is nonnegative at feasible posture.

Erdman et al. and Söylemez claim that transmission angles should be no less than $40° - 45°$ and no greater than $135° - 140°$, depending on the design of the joint and lubrication [57], [75]:

$$45° \leq \mu \leq 135° \qquad (3.35)$$

Extreme transmission angles occur at the extreme positions of the mechanism (i.e. ground and the crank links are collinear). If the transmission angle reaches its extreme values at the outside of the limits given in equation (3.35), the crank link senses high bearing forces causing excessive wear. When the bearing forces exceed the transmitted torque, the mechanism will be locked and even break [72].

3.5 Kinematic Analysis of Planar Four-Bar Mechanisms

In this subsection, position, velocity and acceleration analyses of planar FB mechanisms are summarized.

3.5.1 Position Analysis

Position/displacement analysis of planar FB mechanisms can be done by using several methods. In this dissertation, a simplification of a robust input-output analysis method [76] is presented.

Consider a planar FB linkage shown as in Figure 3.2, following algorithm can be used to derive output angle, ϕ, in terms of feasible link lengths, $\{a_j\}_1^4$ and the input crank angle, ψ. Let us consider the Freudenstein input-output equation (3.6). This equation can be transformed into an algebraic quadratic polynomial equation by means of applying half-tangent identities which are:

$$\cos(\phi) \equiv \frac{1 - T^2}{1 + T^2}, \sin(\phi) \equiv \frac{2T}{1 + T^2}, T \equiv \tan\left(\frac{\phi}{2}\right) \qquad (3.36)$$

After substitution of equation (3.36) into the Freudenstein equation, following quadratic polynomial equation in terms of T can be obtained:

$$D(\psi)T^2 + 2E(\psi)T + F(\psi) = 0 \tag{3.37}$$

where

$$D(\psi) = p_1 - p_2 + (1 - p_3)\cos(\psi) \tag{3.38}$$

$$E(\psi) = -\sin(\psi) \tag{3.39}$$

$$F(\psi) = p_1 + p_2 - (1 + p_3)\cos(\psi) \tag{3.40}$$

and p_1, p_2, p_3 are the Freudenstein parameters.

As the crank rotates, the three coefficients, $D(\psi), E(\psi), F(\psi)$ will vary. Then the output angle can be computed if the two roots of T are available. In order to avoid pitfalls that Forsythe predicted [77], the first root, which has the larger absolute value, can be computed as:

$$T_1 = \frac{-E - \text{sgn}(E)\sqrt{E^2 - DF}}{D}, \phi_1 = 2\tan^{-1}(T_1) \tag{3.41}$$

where $\text{sgn}(\cdot)$ is the *signum function*. Now, calculation of T_2 can be divided into two cases:

If $E(\psi) = -\sin(\psi) \neq 0$, then the independent term is proportional to the product T_1T_2. Hence, T_2 is:

$$T_2 = \frac{F}{DT_1}, \phi_2 = 2\tan^{-1}(T_2) \tag{3.42}$$

If $E(\psi) = -\sin(\psi) = 0$, then the term linear in T vanishes. Hence, two roots of T become symmetrical:

$$T_{1,2} = \pm\sqrt{-\frac{F}{D}} \tag{3.43}$$

In any event, three possible cases arise according to the value of the root T:

If two roots, $\{T_j\}_1^2$, are real and distinct; two solutions of the output angle, $\{\phi_j\}_1^2$, correspond to the two conjugate posture of the linkage. Solutions in equations (3.42) and (3.43) lay into this case.

If two roots, $\{T_j\}_1^2$, are real but identical; two solutions of the output angle, $\{\phi_j\}_1^2$, are also identical and corresponds to the same posture of the linkage, which is the extreme position of the linkage also known as *deadpoint*.

If two roots, $\{T_j\}_1^2$, are complex conjugates; either the link lengths are not feasible (they do not define a quadrilateral) or the linkage is feasible but the crank does not make a full-turn.

3.5.2 Velocity and Acceleration Analyses

After computation of follower and coupler angles, ϕ, θ, velocity and acceleration analysis of planar FB linkages are quite straightforward. Angular velocities and accelerations of planar FB mechanisms can be determined by differentiating equation (3.2) and writing the equations in matrix form [56].

The first derivative of equation (3.2) is:

$$ia_2\dot{\psi}e^{i\psi} + ia_3\dot{\theta}e^{i\theta} = ia_4\dot{\phi}e^{i\phi} \tag{3.44}$$

Then angular velocities are:

$$\begin{Bmatrix}\dot{\theta}\\ \dot{\phi}\end{Bmatrix} = \begin{bmatrix}a_3\cos(\theta) & a_4\cos(\phi)\\ a_3\sin(\theta) & a_4\sin(\phi)\end{bmatrix}^{-1}\begin{Bmatrix}-a_2\dot{\psi}\cos(\psi)\\ -a_2\dot{\psi}\sin(\psi)\end{Bmatrix} \tag{3.45}$$

The second derivative of equation (3.2) is:

$$a_2\ddot{\psi}e^{i\psi} + ia_2\dot{\psi}^2e^{i\psi} + a_3\ddot{\theta}e^{i\theta} + ia_3\dot{\theta}^2e^{i\theta} = a_4\ddot{\phi}e^{i\phi} + ia_4\dot{\phi}^2e^{i\phi} \quad (3.46)$$

Then angular accelerations are:

$$\begin{Bmatrix}\ddot{\theta}\\ \ddot{\phi}\end{Bmatrix} = [A]^{-1}\begin{Bmatrix}-a_2\ddot{\psi}\cos(\psi) + a_2\dot{\psi}^2\sin(\psi) + a_3\dot{\theta}^2\sin(\theta) - a_4\dot{\phi}^2\sin(\phi)\\ -a_2\ddot{\psi}\sin(\psi) - a_2\dot{\psi}^2\cos(\psi) - a_3\dot{\theta}^2\cos(\theta) + a_4\dot{\phi}^2\cos(\phi)\end{Bmatrix} \quad (3.47)$$

where $[A]$ is the characteristic matrix and same with equation (3.45):

$$[A] = \begin{bmatrix}a_3\cos(\theta) & a_4\cos(\phi)\\ a_3\sin(\theta) & a_4\sin(\phi)\end{bmatrix} \quad (3.48)$$

3.6 Discussion and Conclusion

In this chapter, kinematic synthesis of planar FB linkages is explained. Kinematic synthesis can be categorized as number, type and dimensional synthesis. This chapter focuses on the dimensional synthesis of planar FB linkages. For three different purpose which are function generation, path generation and motion generation, two different approaches with related formulation are introduced. Defect in mechanism synthesis are mentioned briefly. Then two methods to select the correct mechanism are explained which are: transmission angle and Grashof criteria. This chapter ends with kinematic analysis of the FB linkages.

CHAPTER 4

KINEMATIC SYNTHESIS AND ANALYSIS OF THE PLANAR SCISSOR-STRUCTURAL MECHANISMS

In this chapter, a novel kinematic synthesis methodology is introduced. This methodology can be used to obtain planar scissor-structural mechanisms (SSMs) by means of several types of scissor-like-elements (SLEs). Therefore, typology of SLEs are introduced. The methodology to determine kinematic analysis of the synthesized mechanisms is also derived. This chapter finishes with the derived methodology for dynamic force analysis of the SSM both in-vacuo conditions and under aerodynamic loading.

4.1 Introduction

One of the most effective methods of meeting the large-scale change needs rapidly is to use the deployable structures. These deployable/ foldable/ movable/ convertible structures are often called as “structural mechanisms” [78], since they behave as a mechanism while conversion process and they resist loads when as bearing structure when they are fixed [79],[80].

Deployable structures gained its popularity with “movable theatre” of a Spain architect, Emilio Pérez Piñero [81], and widely surveyed and utilized in ordinary mechanical engineering [82]. After 1970s, deployable structures are used in complex space missions [83], small-scale structural applications [84], covering of swimming pools [85], bridge systems [86], and aerospace applications [87]. SSMs, which are a sub-class of deployable structures, are widely applied in above mentioned areas, because they show effective performance by providing significant volume expansion,

easy and quick assembling/ disassembling, requiring minimal damage to structural components during working [88].

The most popular deployable structure is the scissor-structural mechanism (SSM) which is based on scissor-like element (SLE). With the concept of SLE, several deployable truss-like structures can be developed in the form any geometrical shape such as equilateral triangles, squares, or normal hexagons [83].

4.2 Typology of Scissor-Like Elements

One type of planar mechanisms is the planar "scissor-structural mechanisms" (SSM) which is formed by a series of SLEs. A SLE consists of two or more bars/links which are assembled to each other at a point on them by a kinematic element often a revolute joint ("scissor hinge"), which allows large geometrical transformations.

The typology of the SLE determines the morphology and the movement characteristics of the structure. The shape and number of bars, type of the kinematic joint and the relative position of the attachment point of the bars are the key elements which create difference.

In general, there are four main categories of SLEs, which consist of only bar elements with revolute or prismatic joints: translational scissor-like elements, polar scissor-like elements, angulated scissor-like elements, and scissor-like elements which have additional degree-of-freedom a.k.a. modified scissor-like elements [89],[90].

4.2.1 Terms and Definitions

A SLE consists of two or more bars which are hinged together by a kinematic element often a revolute joint ("scissor-hinge") which allows large geometrical manipulations. Such elements are called differently by various researchers. Pinero used "pantograph", Akgün used "scissor-hinge unit" and Gantes used "scissor-like elements" in order to call these elements [91]. In this paper Gantes' terminology is used.

In the Figure 4.1, the most basic form of a SLE is shown. In its basic form, two straight bars or links are connected to each other with a revolute joint. This location can be called as "pivot". In the same figure, end nodes, where a SLE can be assembled to

another one, are shown as “hinge”. The portion of a straight bar from pivot location to the end nodes are called as “section”. SLEs are distinguished by imaginary lines which get through the hinge locations, which are called as “t-lines”.

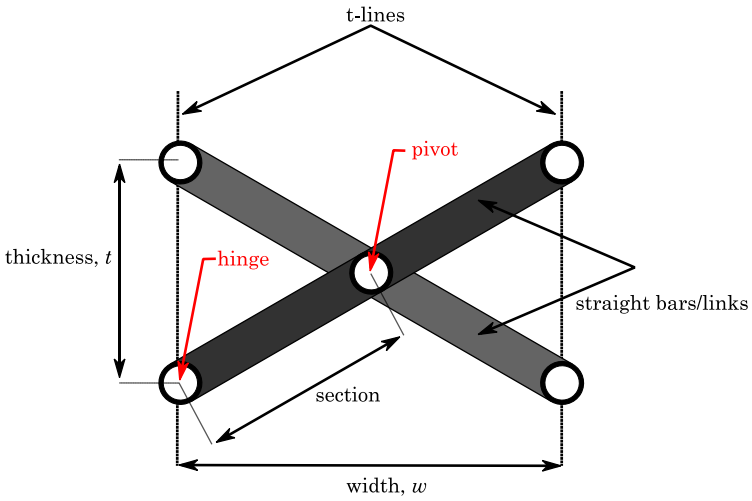

Figure 4.1: A Common Scissor-Like Element

Common property of SLEs is the inverse-proportion of the thickness and the width. It is clearly seen that, by changing the type of SLE, such inverse relation can take a complex form, which are used to stretch/shrink/bend any geometry in any direction. This relation can be brought out by defining a “foldability vector” which connects midpoints between the left-hand-side (LHS) and right-hand-side (RHS) end nodes [92].

4.2.2 Translational Scissor-Like Elements

SLEs are distinguished by imaginary lines which get through the joint locations where a SLE can be assembled to another one (i.e. end nodes) [93]. Calling those imaginary lines as “t-lines”, the group of translational SLEs covers the elements of which t-lines remain parallel throughout the deployment process.

In its basic form, a translational SLE consists of two identical straight bars, Figure 4.2a, assembled to each other from their centers; while deployment, results in a linear motion, or in three dimensional space, a planar motion. Therefore, they are called plane-translational units [93]. When the intermediate hinge location is changed, while

keeping the lengths of the both bars equal from the hinge location, the same motion can be obtained. Such element is the irregular form of the plane translational SLE, which is seen in Figure 4.2b.

As seen from Figure 4.2c, if straight bar lengths are not equal, i.e. proportional, then it is possible to generate curvilinear motion. Such elements are called curved-translational SLEs. In this case, it is also possible to obtain an irregular form by adding eccentricity to the hinge location, which is called irregular curved-translational SLE can be seen in Figure 4.2d.

Consider the most general case of translational SLEs (irregular curved-translational form), $l(k+1)$ and $l'(k+1)$ are the lengths of the straight bars where k determines the eccentricity of the hinge location, $e \equiv |l - l'|$ is the difference between link lengths up to the hinge location which determines the characteristics of the produced motion, φ is the angle between straight bars, t and kt are the vertical distance between the fore and aft end nodes respectively.

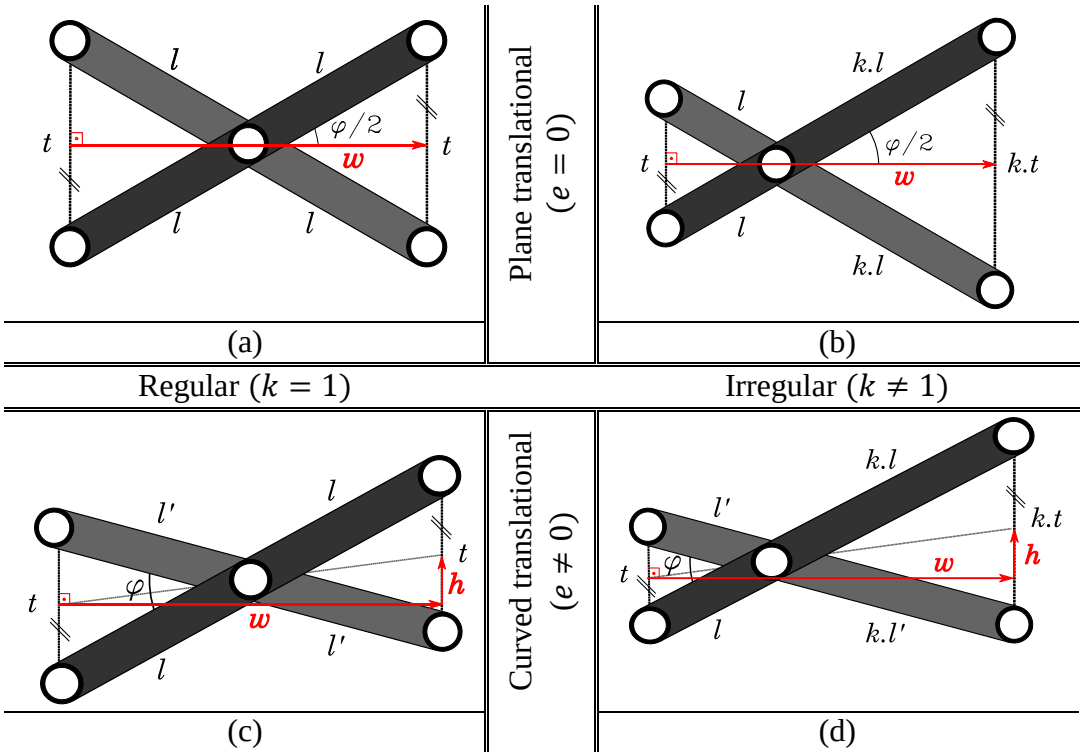

Figure 4.2: Translational Scissor-Like Elements: (a) Regular-plane t-SLE, (b) Irregular-plane t-SLE, (c) Regular-curved t-SLE, (d) Irregular-curved t-SLE

Langbecker derived foldability vectors for translational, polar and Hoberman's units [92]. By using that formulation, with the terminology introduced, foldability vectors can be found for the most complex ones of each type of SLE.

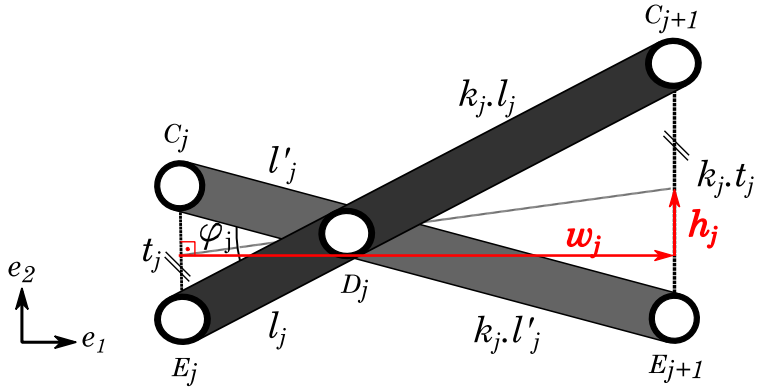

Figure 4.3: Irregular-curved t-SLE with Labels

As seen from the Figure 4.3, triangles $C_jD_jE_j$ and $C_{j+1}D_jE_{j+1}$, which forms j^{th} SLE of the SSM, are similar for all $j = 1 \dots N$. Therefore:

$$k_j = \frac{D_jE_{j+1}}{C_jD_j} = \frac{D_jC_{j+1}}{E_jD_j} = \frac{t_{j+1}}{t_j} \tag{4.1}$$

For known foldability parameters (w_j, h_j), using Pythagoras theorem, the lengths C_jD_j and D_jE_j can be found as:

$$l_j = \frac{\sqrt{w_j^2 + \frac{(2h_j + t_j(k_j+1))^2}{4}}}{k_j + 1} \tag{4.2}$$

$$l'_j = \frac{\sqrt{w_j^2 + \frac{(2h_j - t_j(k_j+1))^2}{4}}}{k_j + 1} \tag{4.3}$$

And the angle between the straight bars, φ_j, becomes:

$$\varphi_j = \cos^{-1}\left(\frac{l_j^2 + l_j'^2 - t_j^2}{2l_jl'_j}\right) \tag{4.4}$$

Alternatively, for known straight bar lengths (l_j, l'_j, k_j), foldability vector parameters and foldability vector can be written as:

$$w_j = l_j(k_j + 1)\sqrt{1 - \left(\frac{t_j}{2l_j}\right)^2 \left(\frac{l_j^2 - l'^2_j}{t_j^2} + 1\right)^2} \tag{4.5}$$

$$h_j = \frac{(l_j^2 - l'^2_j)(k_j + 1)}{2(t_j)} \tag{4.6}$$

Hence the foldability vector $\vec{M}$ becomes in terms of global coordinates:

$$\vec{M}_j(t_j) = w_j\vec{e}_1 + h_j\vec{e}_2 \tag{4.7}$$

Where the limits for t_j are $l_j - l'_j \leq t_j \leq l_j + l'_j$. for all $j = 1 \dots N$.

4.2.3 Polar Scissor-Like Elements

If the imaginary lines which get through the joint locations where a SLE can be assembled to another one (t-lines), do not remain parallel throughout the deployment process, then this type of SLEs are called polar SLEs a.k.a. curvilinear SLEs.

Similarly, in its basic form, a polar SLE consists of two identical straight bars; however, they are assembled to each other with an eccentricity, by ensuring that the section lengths of two bars are the same. As seen from Figure 4.4a, such a SLE can be called as regular-proportional polar SLE. The term "proportional" is used to emphasize the similarity of the triangles emerged from the SLE geometry; moreover, in the case of regular-proportional polar SLE, those triangles are the same. Regular-proportional polar SLEs have the same geometry with the irregular form of the plane translational SLEs. The only difference between them is the way of assembly. In other words, when the irregular form of the plane-translational SLE is assembled to another SLE with its end nodes which have different section lengths, then it behaves as a polar SLE, results in a curvilinear motion in two dimensional space instead of a linear motion.

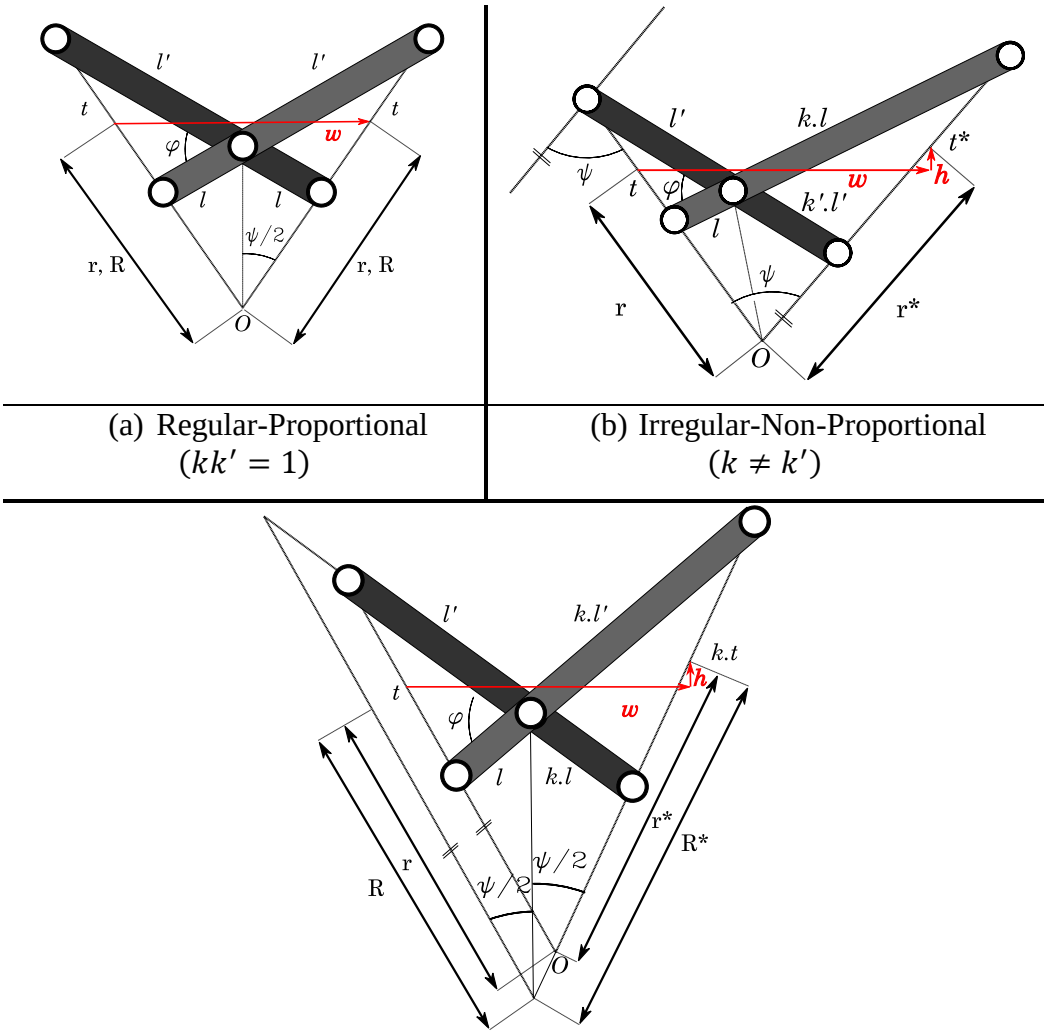

Figure 4.4: Polar Scissor-Like Elements: (a) Regular-Proportional p-SLE, (b) Irregular-non-Proportional p-SLE, (c) Irregular-Proportional p-SLE

Irregular-proportional polar SLEs are widely used to generate cylindrical and spherical grids. For that form of the polar SLE, its foldability vector can be derived as follows:

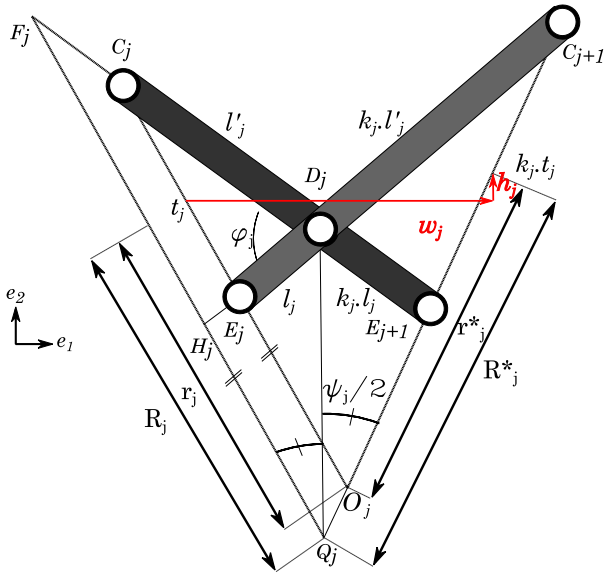

Figure 4.5: Irregular-proportional p-SLE with Labels

As seen from the Figure 4.5, triangles $C_jD_jE_j$ and $C_{j+1}D_jE_{j+1}$ are similar for all $j = 1 \dots N$. Therefore, the similarity factor is:

$$k_j = \frac{D_jC_{j+1}}{C_jD_j} = \frac{D_jE_{j+1}}{E_jD_j} = \frac{t_{j+1}}{t_j} \tag{4.8}$$

Considering the similarity between triangles $H_jQ_jE_{j+1}$ & $F_jQ_jC_{j+1}$ and triangles $H_jD_jE_{j+1}$ & $F_jD_jC_{j+1}$, ratio of section lengths can be found as:

$$\frac{l_j}{l'_j} = \frac{2r_j - t_j}{2r_j + t_j} = \frac{2r_{j+1} - t_{j+1}}{2r_{j+1} + t_{j+1}} \tag{4.9}$$

Using the law of cosines for triangle $F_jQ_jE_{j+1}$ with the equation (4.9) and manipulating using trigonometric identities, section lengths of the links can be written as:

$$l_j = r_j\left(1 - \frac{t_j}{2r_j}\right)\sqrt{\sin^2\left(\frac{\psi_j}{2}\right) + \left(\frac{t_j}{2r_j}\right)\cos^2\left(\frac{\psi_j}{2}\right)} \tag{4.10}$$

$$l'_j = r_j\left(1+\frac{t_j}{2r_j}\right)\sqrt{\sin^2\left(\frac{\psi_j}{2}\right)+\left(\frac{t_j}{2r_j}\right)\cos^2\left(\frac{\psi_j}{2}\right)} \tag{4.11}$$

If parameters k_j, l_j, l'_j are known for all $j = 1 \dots N$, it means that all link lengths are determined. Considering the geometry of the triangle $O_j Q_j I_j$, below relations can be derived as

$$R_j = \frac{r_j}{2}(1+k_j)+\frac{t_j^2}{8r_j}(1-k_j) \tag{4.12}$$

$$R_{j+1} = \frac{r_j}{2}(1+k_j)-\frac{t_j^2}{8r_j}(1-k_j) \tag{4.13}$$

Above equations can be rewritten in terms of ratio of section lengths $\left(l_j/l'_j\right)$ and distance of end nodes (t_j) as follows

$$R_j = \frac{t_j}{2}\frac{1+2k_j\left(\frac{l_j}{l'_j}\right)+\left(\frac{l_j}{l'_j}\right)^2}{1-\left(\frac{l_j}{l'_j}\right)^2} \tag{4.14}$$

$$R_{j+1} = \frac{t_j}{2}\frac{k_j+2\left(\frac{l_j}{l'_j}\right)+k_j\left(\frac{l_j}{l'_j}\right)^2}{1-\left(\frac{l_j}{l'_j}\right)^2} \tag{4.15}$$

Again using the trigonometric relations, below relations can be written

$$\sin\left(\frac{\psi_j}{2}\right) = \frac{1-\left(\frac{l_j}{l'_j}\right)}{2}\sqrt{\frac{\left(\frac{l'_j}{l_j}\right)^2\left(1+\frac{l_j}{l'_j}\right)^2-1}{\left(\frac{l_j}{l'_j}\right)}} \tag{4.16}$$

$$\cos\left(\frac{\psi_j}{2}\right) = \frac{1+\left(\frac{l_j}{l'_j}\right)}{2}\sqrt{\frac{1-\left(\frac{l'_j}{l_j}\right)^2\left(1-\frac{l_j}{l'_j}\right)^2}{\left(\frac{l_j}{l'_j}\right)}} \tag{4.17}$$

Hence the foldability vector $\vec{M}$ can be found about the coordinate system in which the ray D_jQ_j is assumed to be perpendicular about the axis $\vec{e}_1$. In other words, the cross-product of the vector (D_jQ_j) any dummy vector along the vertical axis $(\delta\vec{e}_2)$ is zero. (i.e. $\overrightarrow{D_jQ_j} \times \delta\vec{e}_2 = \vec{0}$.) This means, while designing a series of irregular-proportional polar SLEs, one should take into consideration that every foldability vector $\vec{M}_j$ of every j^{th} SLE is derived for its own coordinate system. In order to write them in global coordinate system related transformation should be done. The foldability vector $\vec{M}_j$ of j^{th} SLE in its own coordinate system is

$$\vec{M}_j(t_j) = (R_{j+1} + R_j)\cos\left(\frac{\psi_j}{2}\right)\vec{e}_1 + (R_{j+1} - R_j)\sin\left(\frac{\psi_j}{2}\right)\vec{e}_2 \qquad (4.18)$$

where the limits for t_j are $l_j - l'_j \leq t_j \leq l_j + l'_j$. for all $j = 1 \ldots N$.

4.2.4 Other Type of Scissor-Like Elements

It is also possible to derive different types of SLEs other than translational and polar SLEs. In Figure 4.6, angulated and modified SLEs are shown:

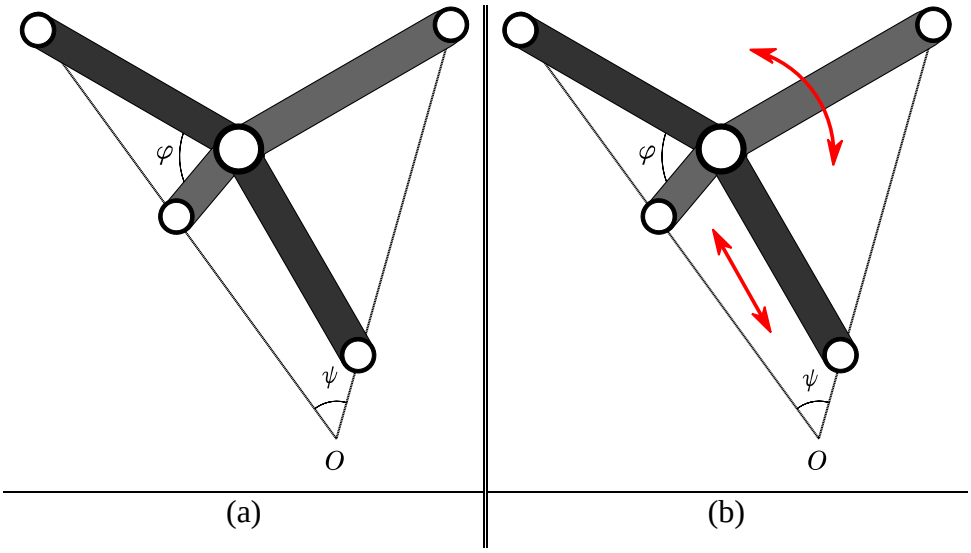

Figure 4.6: Other Type of Scissor-Like Elements: (a) Angulated Scissor-Like Element (a-SLE), (b) Modified Scissor-Like Element (m-SLE)

The "angulated SLEs", a.k.a. "the Hoberman's angulated element" [94], are very similar to the p-SLEs; whereas, in the type of a-SLEs, the angle between the links (φ)

of a SLE is not a unique value. In other words, if the links of a polar SLE are converted from bars to ternary links, one can obtain angulated-SLEs.

When one of links or both of them that form a SLE are substituted with a RR, RP, PR or PP pairs, the SLE can gain an additional freedom. By doing so, any type of standard SLE can be modified to get more flexible designs. Such elements are called "angulated SLEs" (m-SLE) [95].

In this study, both angulated and modified elements are not used due to lack of need.

4.3 Mobility of Scissor-Structural Mechanisms

Mobility can be defined as the number of input parameters (prime movers or actuators) that must be independently controlled to bring the mechanism into a desired position. It is also called as the degree-of-freedom (DOF) of a mechanism [54]. Although there are some exceptions, it is possible to calculate the mobility of the mechanism directly counting the number of links and joints considering the types of mechanism, links and joints.

In his paper, Gogu presented that, there are dozens of approaches which have been proposed in the last decade for the calculation of mobility of the mechanism [96]. A "magic formula" to calculate the mobility of all kind of mechanisms cannot be found yet. However, some of these methods can be simplified to the same well-known formula which is called Chebychev–Grübler–Kutzbach's criterion [96]. This Chebychev–Grübler–Kutzbach's formula is very simple and sufficient to analyze the mobility of the simple planar linkages. The Chebychev–Grübler–Kutzbach's criterion generally presented as follows [97]:

$$M = \lambda\left(n_l - n_j - 1\right) + \sum_{i=1}^{n_j} f_i \tag{4.19}$$

In the above equation, λ represents the space in which the mechanism works. $\lambda = 3$ for planar and spherical mechanisms, while $\lambda = 6$ for spatial mechanisms. M is the DOF of the mechanism, n_l is the total number of links, n_j is the total number of joints and the f_i is the independent DOF of the i^{th} joint.

For the proposed planar SSM which consists of N translational or polar SLEs of any kind, $\lambda = 3$. If one consider only plain (only constructed with SLEs) SSMs as seen from Figure 4.7; the total number of the links (where the ground should be accepted as a link as explained) is: $n_l = 2N + 1$, the total number of joints is: $n_j = 3N$, if two of first joints are fixed. Since all joints are the type of revolute, $f = 1$ for all joints. If the DOF of the proposed SSM is calculated one can get: $M = 3(2N + 1 - 3N - 1) + 3N = 0$. When one fixed joint is set free, then mobility becomes $M = 2$.

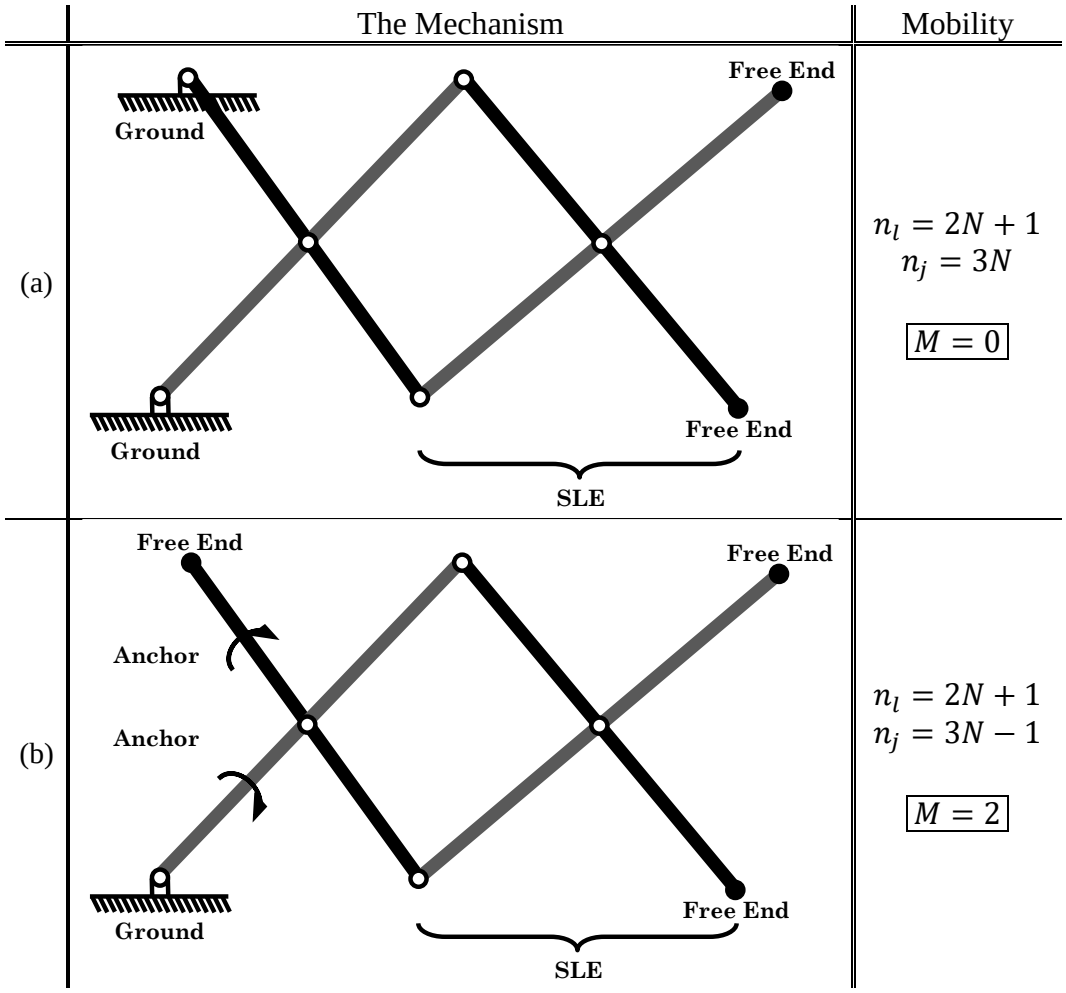

Figure 4.7: Mobility of Plain SSMs (a) Fixed-Fixed, (b) Fixed-Free

According to the results $(M = 0, 2)$, the proposed SSM cannot move (behaves as a structure) or needs two actuators to deploy; therefore, in order to obtain a single-DOF mechanism, one needs an additional input linkage system. To overcome such problem,

in this conceptual design/ type synthesis phase, an additional planar FB linkage is assumed to be attached to manipulate the whole planar SSM.

In Figure 4.8, simple drawings of SSMs with FB linkages, function generator and motion/path generator, are shown respectively. As seen from the same figure, both mechanisms yield the same mobility result which is: $M = 1$.

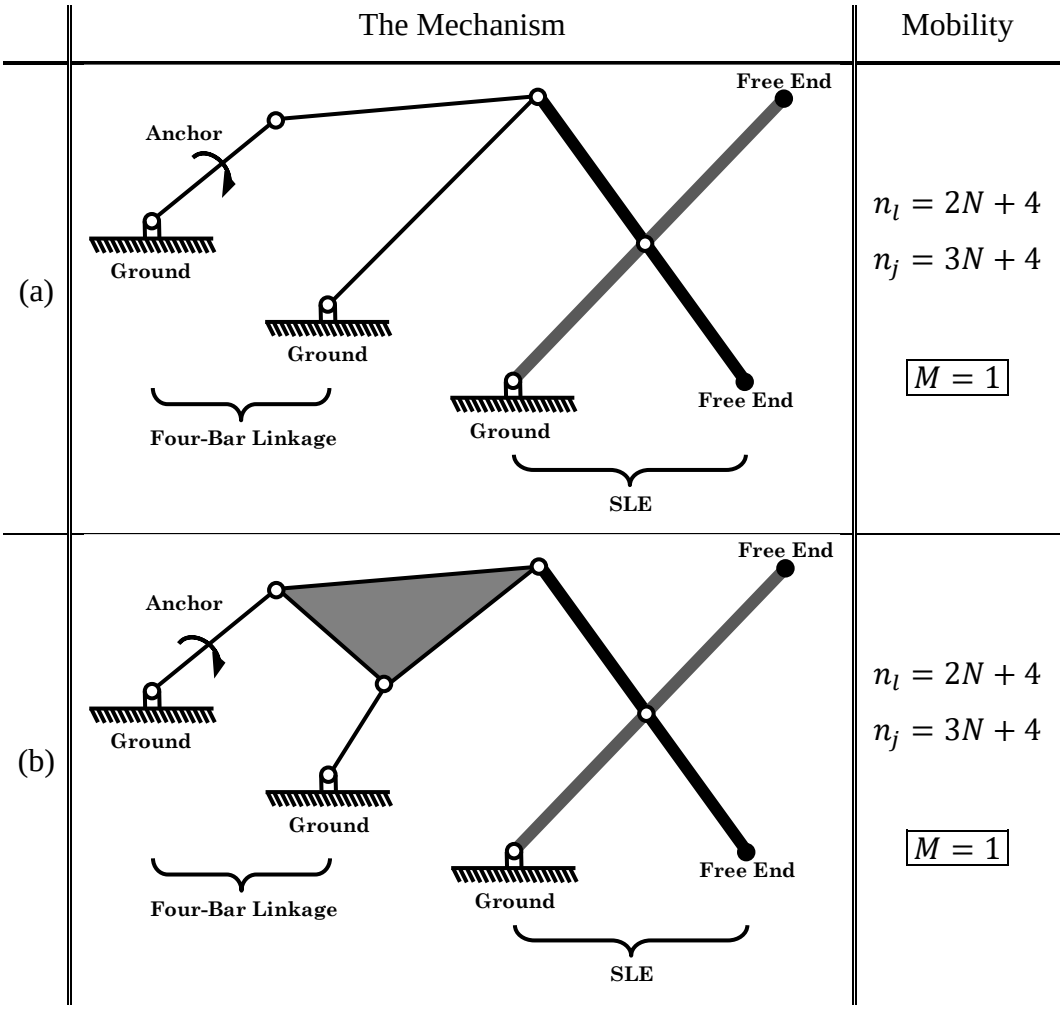

Figure 4.8: Mobility of SSMs with a Four-Bar Linkage (a) Function Generator, (b) Function Generator

It is also possible to increase the degree-of-freedom of the mechanism by converting ordinary SLEs into modified ones. By doing so, one can get further complex but accurate SSM. As seen from Figure 4.9, if modified SLEs do not include a prismatic joint (slider), then it is also possible to add a pre-synthesized FB linkage to the system.

As the number of additional FB linkage increases, the mobility of the SSM will increase with the number of added FB linkage.

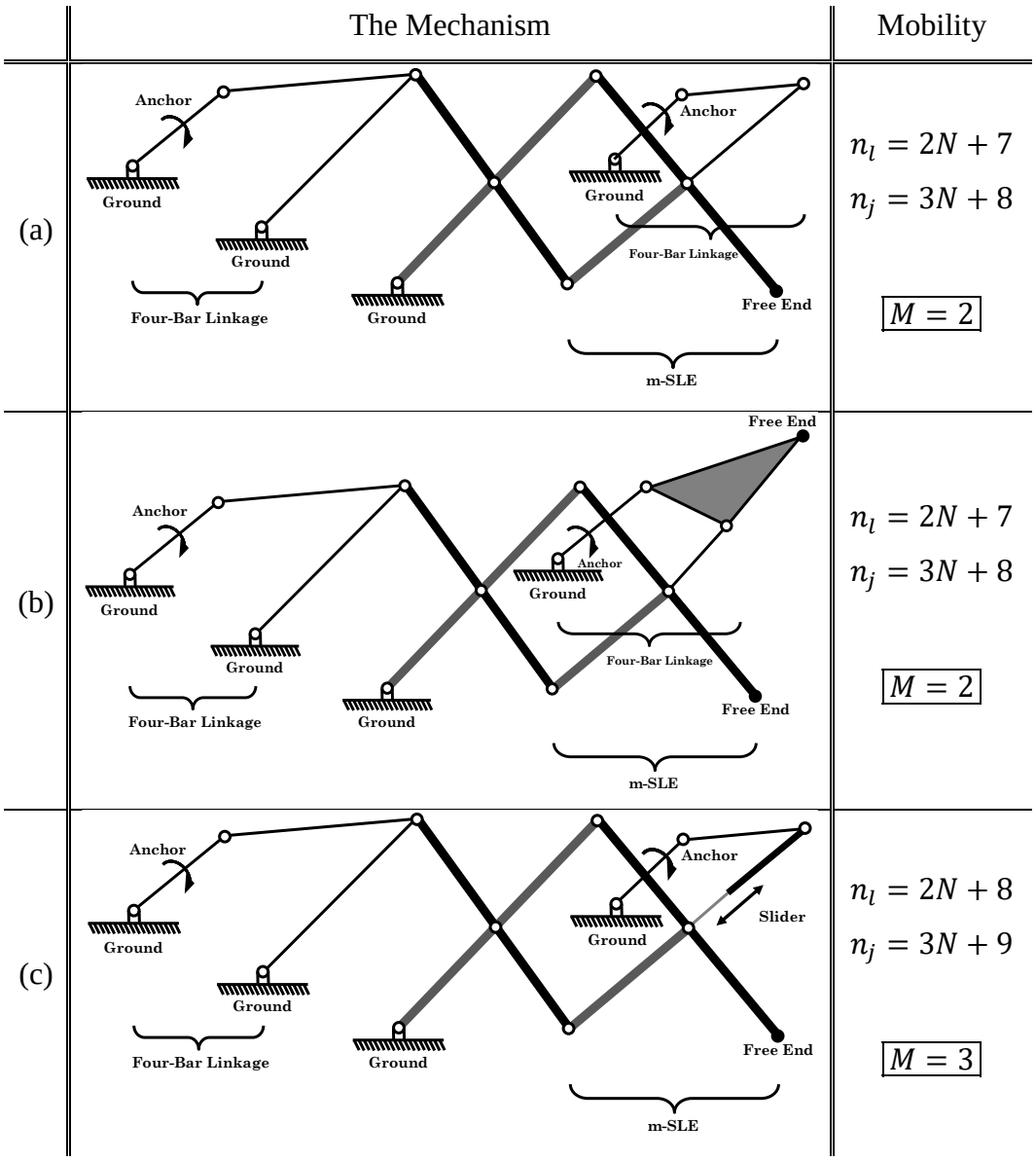

Figure 4.9: Mobility of SSMs with m-SLEs (a) Function Generator m-SLE, (b) Motion Generator m-SLE, (c) Five-Bar m-SLE

4.4 Kinematic Analysis of Scissor-Structural Mechanisms

In order to find out the kinematic capability of the designed scissor-like structure, determine the inertial forces, and compute the required torque, kinematic analysis of the mechanism should be done properly. As mentioned above, if a FB linkage is

attached to manipulate the whole SSM, the system becomes a 1-DOF mechanism. In other words, one needs only one actuator to manipulate the whole system. If the output angle of the FB linkage in terms of time is known; then, the position analysis of whole system can be done in terms of that output angle.

4.4.1 Position Analysis

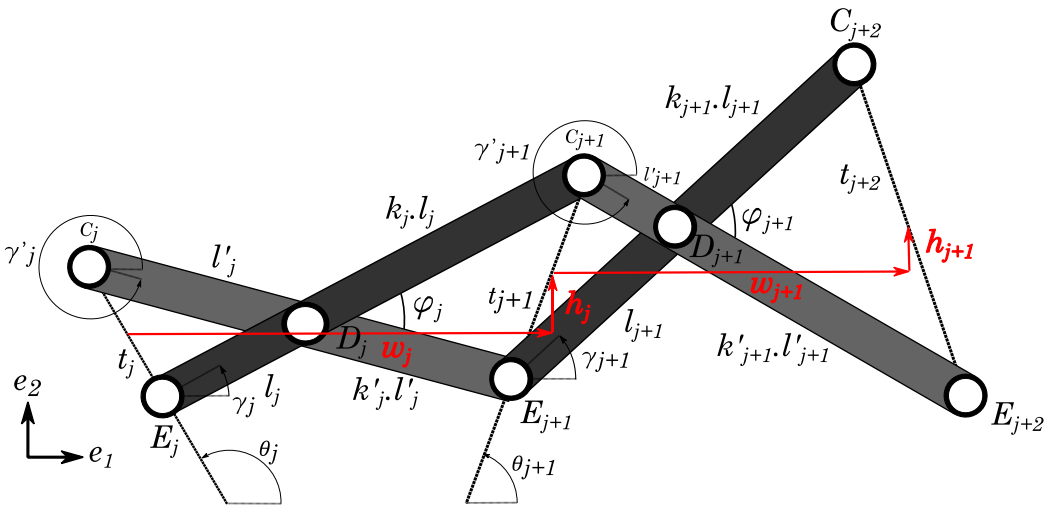

Figure 4.10: A Planar Scissor-Structural Mechanism

In Figure 4.10, C_jE_{j+1} and E_jC_{j+1} are two straight bars which form the j^{th} SLE of the SSM. l_j, k_jl_j and l'_j, $k'_jl'_j$ represent section lengths, γ_j and γ'_j represent orientations about global coordinates of those straight bars respectively. When another SLE is attached to the j^{th} SLE, let $(j+1)^{th}$ SLE, there occurs a closed loop $D_jC_{j+1}\ D_{j+1}\ E_{j+1}$, which is a "quadrilateral". The loop-closure equation can be written as follows:

$$\overrightarrow{D_jC_{j+1}} + \overrightarrow{C_{j+1}D_{j+1}} = \overrightarrow{D_jE_{j+1}} + \overrightarrow{E_{j+1}D_{j+1}} \tag{4.20}$$

The closed-loop equation of that quadrilateral given in equation (4.20) can be re-written in complex notation as:

$$k_jl_je^{i\gamma_j} + l'_{j+1}e^{i\gamma'_{j+1}} = k'_jl'_je^{i\gamma'_j} + l_{j+1}e^{i\gamma_{j+1}} \tag{4.21}$$

Equation (4.21) can be solved if the orientation angles of j^{th} SLE (γ_j and γ_j') are known. Assume that the angle γ_j varies, then multiplying both sides of equation (5) with $e^{i\gamma_j'}$ gives an equation in terms of $\varphi_j \equiv \gamma_j - \gamma_j'$, $\mu_{j+1} \equiv \gamma_{j+1} - \gamma_j'$ and $\mu_{j+1}' \equiv \gamma_{j+1}' - \gamma_j'$:

$$k_j l_j e^{i\varphi_j} + l_{j+1}' e^{i\mu_{j+1}'} = k'_j l'_j + l_{j+1} e^{i\mu_{j+1}} \tag{4.22}$$

In the equation (4.22), the angle μ_{j+1}' can also be eliminated by multiplying both sides of equation (4.22) with $e^{i\mu_{j+1}'}$. Hence, the resulting equation takes the form of well-known Freudenstein equation when the Euler's identity of $e^{i\theta} = \cos(\theta) + i\sin(\theta)$ is applied:

$$F(\varphi_j, \mu_{j+1}) = p_1 + p_2\cos(\mu_{j+1}) - p_3\cos(\varphi_j) - \cos(\mu_{j+1} - \varphi_j) = 0 \tag{4.23}$$

where Freudenstein parameters (p_1, p_2, p_3) are:

$$p_1 \equiv \frac{k_j'^2 l_j'^2 + k_j^2 l_j^2 - l_{j+1}'^2 + l_{j+1}^2}{2k_j l_j l_{j+1}},\ p_2 \equiv \frac{k'_j l'_j}{k_j l_j},\ p_3 \equiv \frac{k'_j l'_j}{l_{j+1}} \tag{4.24}$$

Freudenstein equation (4.23) gives an implicit relation between the position variables φ_j and μ_{j+1}. This equation can be solved by applying half-tangent representation of the sine and cosine function of unknown μ_{j+1} and solving the arising quadratic equation in terms of $T \equiv \tan\left(\frac{\mu_{j+1}}{2}\right)$. The solution procedure and arising cases are identical with the planar FB linkages. Related formulation is given in the equations (3.36)-(3.43).

From the designed FB linkage, the first orientation angles γ_1 and γ_1', afterwards the other orientation angles, $\{\gamma_j\}_2^N$ and $\{\gamma_j'\}_2^N$ can be determined. Hence, position vectors of all joints can be written in complex form as

$$\vec{r}_{C_{j+1}} = \vec{r}_{E_j} + (l_j)(k_j + 1)e^{i\gamma_j(t)} \tag{4.25}$$

$$\vec{r}_{D_{j+1}} = \vec{r}_{C_j} + l'_j e^{i\gamma_j'(t)} \tag{4.26}$$

$$\vec{r}_{E_{j+1}} = \vec{r}_{C_j} + \left(l'_j\right)\left(k'_j + 1\right)e^{i\gamma'_j(t)} \tag{4.27}$$

4.4.2 Velocity and Acceleration Analyses

It is possible to calculate the velocity and acceleration of the SSMs. If the rotational velocity and acceleration of one of the input link ($(\dot{\gamma}_1, \ddot{\gamma}_1)$ or $(\dot{\gamma'}_1, \ddot{\gamma'}_1)$ are prescribed, then velocities and accelerations of the whole system can be calculated.

Assuming the prescribed angular velocity and acceleration belong to the underlying links, (i.e. $\dot{\gamma}_1, \ddot{\gamma}_1$), then the other initial link behaves as a fixed link ($\dot{\gamma'}_1 = \ddot{\gamma'}_1 = 0$) or vice-versa. Then, *the first derivative* of the equation (4.22) with respect to time gives:

$$ik_j l_j \dot{\varphi}_j e^{i\varphi_j} + il'_{j+1}\dot{\mu}'_{j+1}e^{i\mu'_{j+1}} = il_{j+1}\dot{\mu}_{j+1}e^{i\mu_{j+1}} \tag{4.28}$$

Then, manipulating and writing the equation (4.28) in matrix form gives:

$$[A]\{\dot{\mu}\} = \dot{\varphi}_j\{B_v\} \tag{4.29}$$

where $[A]$ is known as "characteristic matrix", $\{\dot{\mu}\}$ is the unknown angular velocity vector and $\{B_v\}$ is the known vector:

$$[A] \equiv \begin{bmatrix} l_{j+1}\cos\mu_{j+1} & -l'_{j+1}\cos\mu'_{j+1} \\ l_{j+1}\sin\mu_{j+1} & -l'_{j+1}\sin\mu'_{j+1} \end{bmatrix} \tag{4.30}$$

$$\{\dot{\mu}\} \equiv \begin{Bmatrix} \dot{\mu}_{j+1} \\ \dot{\mu}'_{j+1} \end{Bmatrix} \tag{4.31}$$

$$\{B_v\} \equiv \begin{Bmatrix} k_j l_j \cos\varphi_j \\ k_j l_j \sin\varphi_j \end{Bmatrix} \tag{4.32}$$

Then angular velocities can be determined as:

$$\{\dot{\mu}\} = [A]^{-1}\dot{\varphi}_j\{B_v\} \tag{4.33}$$

Since the angular velocity, $\dot{\gamma}_1$ is prescribed and $\dot{\gamma}'_1 = 0$; the other angular velocities, $\{\dot{\gamma}_j\}_2^N$ and $\{\dot{\gamma}'_j\}_2^N$ can be determined by following the given algorithm. Hence, velocities of all joints can be written in complex form as:

$$\vec{v}_{C_{j+1}} = \vec{v}_{E_j} + i\left(l_j\right)\left(k_j + 1\right)\dot{\gamma}_j(t)e^{i\gamma_j(t)} \tag{4.34}$$

$$\vec{v}_{D_{j+1}} = \vec{v}_{C_j} + il'_j\dot{\gamma}'_j(t)e^{i\gamma'_j(t)} \tag{4.35}$$

$$\vec{v}_{E_{j+1}} = \vec{v}_{C_j} + i\left(l'_j\right)\left(k'_j + 1\right)\dot{\gamma}'_j(t)e^{i\gamma'_j(t)} \tag{4.36}$$

The second derivative of the equation (4.22) with respect to time gives:

$$k_j l_j \ddot{\varphi}_j e^{i\varphi_j} + i k_j l_j \left(\dot{\varphi}_j\right)^2 e^{i\varphi_j} + l'_{j+1}\ddot{\mu}'_{j+1} e^{i\mu'_{j+1}} + i l'_{j+1}\left(\dot{\mu}'_{j+1}\right)^2 e^{i\mu'_{j+1}} = l_{j+1}\ddot{\mu}_{j+1} e^{i\mu_{j+1}} + i l_{j+1}\left(\dot{\mu}_{j+1}\right)^2 e^{i\mu_{j+1}} \quad (4.37)$$

Then, manipulating and writing the equation (4.37) in matrix form gives:

$$[A]\{\ddot{\mu}\} = \{B_a\} \quad (4.38)$$

where the characteristic matrix $[A]$ is the same with equation (4.30). $\{\ddot{\mu}\}$ is unknown angular acceleration vector and $\{B_a\}$ is the known vector, which are:

$$\{\ddot{\mu}\} \equiv \begin{Bmatrix} \ddot{\mu}_{j+1} \\ \ddot{\mu}'_{j+1} \end{Bmatrix} \quad (4.39)$$

$$\{B_a\} \equiv \begin{Bmatrix} k_j l_j \ddot{\varphi}_j \cos\varphi_j - k_j l_j \dot{\varphi}_j^2 \sin\varphi_j + l_{j+1}\dot{\mu}_{j+1}^2 \sin\mu_{j+1} - l'_{j+1}\dot{\mu}'^2_{j+1} \sin\mu'_{j+1} \\ k_j l_j \ddot{\varphi}_j \sin\varphi_j + k_j l_j \dot{\varphi}_j^2 \cos\varphi_j - l_{j+1}\dot{\mu}_{j+1}^2 \cos\mu_{j+1} + l'_{j+1}\dot{\mu}'^2_{j+1} \cos\mu'_{j+1} \end{Bmatrix} \quad (4.40)$$

Then angular accelerations can be determined as:

$$\{\ddot{\mu}\} = [A]^{-1}\{B_a\} \quad (4.41)$$

Since the angular acceleration, $\ddot{\gamma}_1$ is prescribed and $\ddot{\gamma}'_1 = 0$; other angular accelerations, $\{\ddot{\gamma}_j\}_2^N$ and $\{\ddot{\gamma}'_j\}_2^N$ can be determined by following the given algorithm. Hence, accelerations of all joints can be written in complex form as:

$$\vec{a}_{C_{j+1}} = \vec{a}_{E_j} - (l_j)(k_j + 1)\left(\dot{\gamma}_j(t)\right)^2 e^{i\gamma_j(t)} + i(l_j)(k_j + 1)\ddot{\gamma}_j(t) e^{i\gamma_j(t)} \quad (4.42)$$

$$\vec{a}_{D_{j+1}} = \vec{a}_{C_j} - l'_j\left(\dot{\gamma}'_j(t)\right)^2 e^{i\gamma'_j(t)} + i l'_j \ddot{\gamma}'_j(t) e^{i\gamma'_j(t)} \quad (4.43)$$

$$\vec{a}_{E_{j+1}} = \vec{a}_{C_j} - (l'_j)(k'_j + 1)\left(\dot{\gamma}'_j(t)\right)^2 e^{i\gamma'_j(t)} + i(l'_j)(k'_j + 1)\ddot{\gamma}'_j(t) e^{i\gamma'_j(t)} \quad (4.44)$$

4.5 Dynamic Force Analysis of Scissor-Structural Mechanisms

When the inertia forces are considered in the analysis of the mechanism, the analysis known as "dynamic force analysis". The dynamic force analysis problem can be solved using the matrix method by reducing it to one requiring static analysis. For this purpose, Newton's 2nd law, which assumes the inertial frame is the frame of reference, can be applied which states that the kinematic behavior of an objects for which all existing forces are not balanced. In other words, the inertia forces and couples, and the external forces and torques on the body together are balanced.

4.5.1 Dynamic Force Analysis of Scissor-Structural Mechanisms in In-Vacuo Condition

For scissor-structural mechanisms, deriving equations only one SLE is adequate to calculate the whole system. Figure 4.11 shows the eccentric locations of the mass centers of a common SLE.

In Figure 4.11, G_j' and G_j represent the mass centers of links that construct a SLE. l_{g_j}', l_{g_j} and δ_j', δ_j represent the position vectors of the mass centers, and the interjacent angle between the corresponding link and mass center vector of that link respectively.

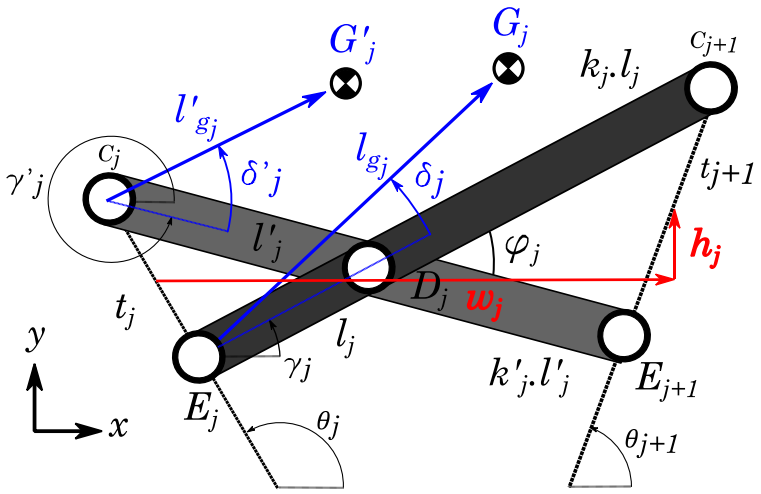

Figure 4.11: Representation of Mass Centers of a SLE

Figure 4.12a shows the internal and external forces and moments on a common scissor-like elements, while Figure 4.12b shows inertia forces and moment.

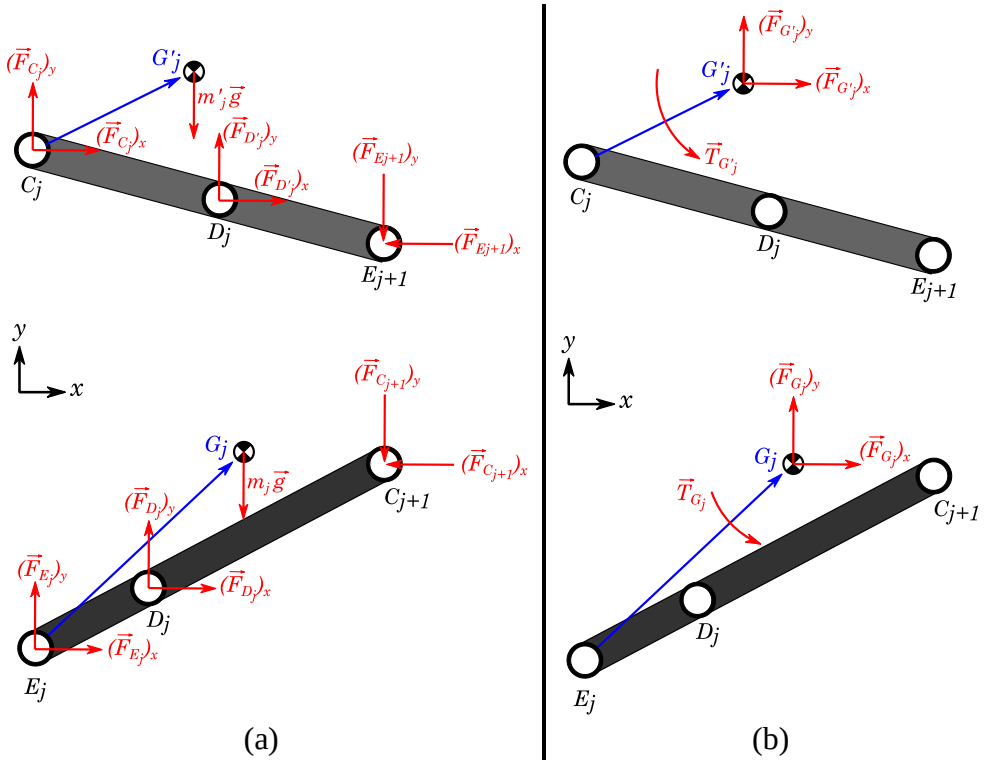

Figure 4.12: Free-body-diagram of a SLE: (a) External Forces, (b) Effective Forces

Note that, as a standard terminology, internal forces of constraint are indicated as $\vec{F}_{ij}$ to denote the force exerted by the i^{th} link on the j^{th} link. However, for simplicity of formulation and legibleness of the thesis, all internal forces are indicated by a single joint label; which represent the force exerted by current link to the former joint. For example, $\vec{F}_{C_j}$ represents the force exerted by ipsilateral j^{th} link to the $(j-1)^{th}$ link.

As seen from Figure 4.12b, the inertia forces $\left\{\vec{F}_{G_j}\right\}_1^N$, $\left\{\vec{F}_{G'_j}\right\}_1^N$ are given by:

$$\vec{F}_{G_j} = m_j \vec{a}_{G_j}(t) \tag{4.45}$$

$$\vec{F}_{G'_j} = m'_j \vec{a}_{G'_j}(t) \tag{4.46}$$

where accelerations of mass centers, $\vec{a}_{G_j}(t)$ and $\vec{a}_{G'_j}(t)$ can be calculated through below given formulas which are:

$$\vec{a}_{G_{j+1}} = \vec{a}_{E_j} - l_{g_j}\left(\dot{\gamma}_j(t)\right)^2 e^{i(\gamma_j(t)+\delta_j)} + i l_{g_j}\ddot{\gamma}_j(t)e^{i(\gamma_j(t)+\delta_j)} \tag{4.47}$$

$$\vec{a}_{G'_{j+1}} = \vec{a}_{C_j} - l'_{g_j}\left(\dot{\gamma}'_j(t)\right)^2 e^{i\left(\gamma'_j(t)+\delta'_j\right)} + i l'_{g_j}\ddot{\gamma}'_j(t)e^{i\left(\gamma'_j(t)+\delta'_j\right)} \tag{4.48}$$

The inertia moments $\left\{\vec{T}_{G_j}\right\}_1^N$, $\left\{\vec{T}_{G'_j}\right\}_1^N$ are:

$$\vec{T}_{G_j} = I_j \ddot{\gamma}_j(t) \tag{4.49}$$

$$\vec{T}_{G'_j} = I'_j \ddot{\gamma}'_j(t) \tag{4.50}$$

where I_j and I'_j represent corresponding *moment of inertias* of links $E_j D_j C_{j+1}$ and $C_j D_j E_{j+1}$ respectively.

Note that, Newton's 2nd law states that:

$$\left(\sum \vec{F}\right)_{external} = \left(\sum \vec{F}\right)_{effective} \tag{4.51}$$

$$\left(\sum \vec{M}_G\right)_{external} = \left(\sum \vec{M}_G\right)_{effective} \tag{4.52}$$

Applying Newton's 2nd law for a single common type of SLE gives six relations, in which four of them are force equilibrium and two of them are moment equilibrium. Four force equilibrium equations can be written as:

$$\left(F_{C_j}\right)_x + \left(F_{D'_j}\right)_x - \left(F_{E_{j+1}}\right)_x = \left(F_{G'_j}\right)_x \tag{4.53}$$

$$\left(F_{E_j}\right)_x + \left(F_{D_j}\right)_x - \left(F_{C_{j+1}}\right)_x = \left(F_{G_j}\right)_x \tag{4.54}$$

$$\left(F_{C_j}\right)_y + \left(F_{D'_j}\right)_y - \left(F_{E_{j+1}}\right)_y - m'_j g = \left(F_{G'_j}\right)_y \tag{4.55}$$

$$\left(F_{E_j}\right)_y + \left(F_{D_j}\right)_y - \left(F_{C_{j+1}}\right)_y - m_j g = \left(F_{G_j}\right)_y \tag{4.56}$$

In order to write the moment relations, vectors from the mass centers to the joint locations should be defined. These vectors and their orientations can be defined as:

$$\vec{g}_{D_j} \equiv l_{g_j} e^{i(\gamma_j + \delta_j)} - l_j e^{i\gamma_j} \text{ and } \eta_{D_j} \equiv \arg \vec{g}_{D_j} \tag{4.57}$$

$$\vec{g}_{C_{j+1}} \equiv l_{g_j} e^{i(\gamma_j + \delta_j)} - l_j (k_j + 1) e^{i\gamma_j} \text{ and } \eta_{C_{j+1}} \equiv \arg \vec{g}_{C_{j+1}} \tag{4.58}$$

$$\vec{g}_{D'_j} \equiv l'_{g_j} e^{i\left(\gamma'_j + \delta'_j\right)} - l'_j e^{i\gamma'_j} \text{ and } \eta_{D'_j} \equiv \arg \vec{g}_{D'_j} \tag{4.59}$$

$$\vec{g}_{E_{j+1}} \equiv l'_{g_j} e^{i\left(\gamma'_j + \delta'_j\right)} - l'_j (k'_j + 1) e^{i\gamma'_j} \text{and } \eta_{E_{j+1}} \equiv \arg \vec{g}_{E_{j+1}} \tag{4.60}$$

By using the property $\vec{r} \times \vec{F} = rF \sin(\theta_F - \theta_r)$ and position vectors from hinge locations to the mass centers which are defined above, two moment equilibrium equations can be written as:

$$
\begin{aligned}
& l'_{g_j}\left(F_{C_j}\right)_x \sin(\pi-\gamma'_j-\delta'_j)+g_{D'_j}\left(F_{D'_j}\right)_x \sin\left(-\pi-\eta_{D'j}\right) \\
& \quad -g_{E_{j+1}}\left(F_{E_{j+1}}\right)_x \sin\left(-\pi-\eta_{E\,j+1}\right) \\
& \quad +l'_{g_j}\left(F_{C_j}\right)_y \sin\left(\frac{3\pi}{2}-\gamma'_j-\delta'_j\right) \\
& \quad +g_{D'_j}\left(F_{D'_j}\right)_y \sin\left(-\frac{\pi}{2}-\eta_{D'j}\right) \\
& \quad -g_{E_{j+1}}\left(F_{E_{j+1}}\right)_y \sin\left(-\frac{\pi}{2}-\eta_{E\,j+1}\right)=T_{G'j}
\end{aligned} \tag{4.61}
$$

$$
\begin{aligned}
& l_{g_j}\left(F_{E_j}\right)_x \sin(\pi-\gamma_j-\delta_j)+g_{D_j}\left(F_{D_j}\right)_x \sin\left(-\pi-\eta_{Dj}\right) \\
& \quad -g_{C_{j+1}}\left(F_{C_{j+1}}\right)_x \sin\left(-\pi-\eta_{C\,j+1}\right) \\
& \quad +l_{g_j}\left(F_{E_j}\right)_y \sin\left(\frac{3\pi}{2}-\gamma_j-\delta_j\right) \\
& \quad +g_{D_j}\left(F_{D_j}\right)_y \sin\left(-\frac{\pi}{2}-\eta_{Dj}\right) \\
& \quad -g_{C_{j+1}}\left(F_{C_{j+1}}\right)_y \sin\left(-\frac{\pi}{2}-\eta_{C\,j+1}\right)=T_{Gj}
\end{aligned} \tag{4.62}
$$

Note that, from Newton's 3rd law:

$$\vec{F}_{D'_j}=-\vec{F}_{D_j} \tag{4.63}$$

Since the SSM has free ends (i.e. $\vec{F}_{C_{N+1}}=\vec{F}_{E_{N+1}}=\vec{0}$), internal forces on the revolute joints can be calculated solving the below linear system starting from the N^{th} SLE to the 1^{st} SLE. Below system should be constructed for every SLE separately.

$$\{f\}=\left[A_f\right]^{-1}\{B_f\} \tag{4.64}$$

where the force vector, $\{f\}$, is:

$$\{f\}=\left\{\left(F_{C_j}\right)_x \quad \left(F_{D_j}\right)_x \quad \left(F_{E_j}\right)_x \quad \left(F_{C_j}\right)_y \quad \left(F_{D_j}\right)_y \quad \left(F_{E_j}\right)_y\right\}^T \tag{4.65}$$

Using trigonometric identities of $\sin(\pi-x)=\sin(x)$, $\sin(-x)=-\sin(x)$ and $\sin\left(\frac{\pi}{2}-x\right)=\sin\left(\frac{\pi}{2}+x\right)=\cos(x)$, the matrix $\left[A_f\right]$ can be constituted as:

$$
[A_f]=\begin{bmatrix}
1 & -1 & 0 & 0 & 0 & 0 \\
0 & 1 & 1 & 0 & 0 & 0 \\
0 & 0 & 0 & 1 & -1 & 0 \\
0 & 0 & 0 & 0 & 1 & 1 \\
l'_{g_j}\mathrm{s}(\gamma'_j+\delta'_j) & -g_{D'_j}\mathrm{s}\left(\eta_{D'j}\right) & 0 & -l'_{g_j}\mathrm{c}(\gamma'_j+\delta'_j) & g_{D'_j}\mathrm{c}\left(\eta_{D'j}\right) & 0 \\
0 & g_{D_j}\mathrm{s}\left(\eta_{Dj}\right) & l_{g_j}\mathrm{s}(\gamma_j+\delta_j) & 0 & -g_{D_j}\mathrm{c}\left(\eta_{Dj}\right) & -l_{g_j}\mathrm{c}(\gamma_j+\delta_j)
\end{bmatrix}
\tag{4.66}
$$

where $\mathrm{s}(x) \equiv \sin(x)$ and $\mathrm{c}(x) \equiv \cos(x)$.

The known vector $\{B_f\}$ can be constituted as:

$$\{B_f\} = \begin{Bmatrix} \left(F_{G_j'}\right)_x + \left(F_{E_{j+1}}\right)_x \\ \left(F_{G_j}\right)_x + \left(F_{C_{j+1}}\right)_x \\ \left(F_{G_j'}\right)_y + \left(F_{E_{j+1}}\right)_y + m_j' g \\ \left(F_{G_j}\right)_y + \left(F_{C_{j+1}}\right)_y + m_j g \\ T_{G'j} + g_{E_{j+1}}\left(F_{E_{j+1}}\right)_x \mathrm{s}\left(\eta_{E\,j+1}\right) - g_{E_{j+1}}\left(F_{E_{j+1}}\right)_y \mathrm{c}\left(\eta_{E\,j+1}\right) \\ T_{G\,j} + g_{C_{j+1}}\left(F_{C_{j+1}}\right)_x \mathrm{s}\left(\eta_{C\,j+1}\right) - g_{C_{j+1}}\left(F_{C_{j+1}}\right)_y \mathrm{c}\left(\eta_{C\,j+1}\right) \end{Bmatrix} \quad (4.67)$$

4.5.2 Dynamic Force Analysis of Scissor-Structural Mechanisms Under Aerodynamic Loading

If the pressure distribution over the surface formed by the SSM is considered and converted into the nodal forces on the upper and lower hinges of a SLE, the free-body-diagram of a generic SLE becomes:

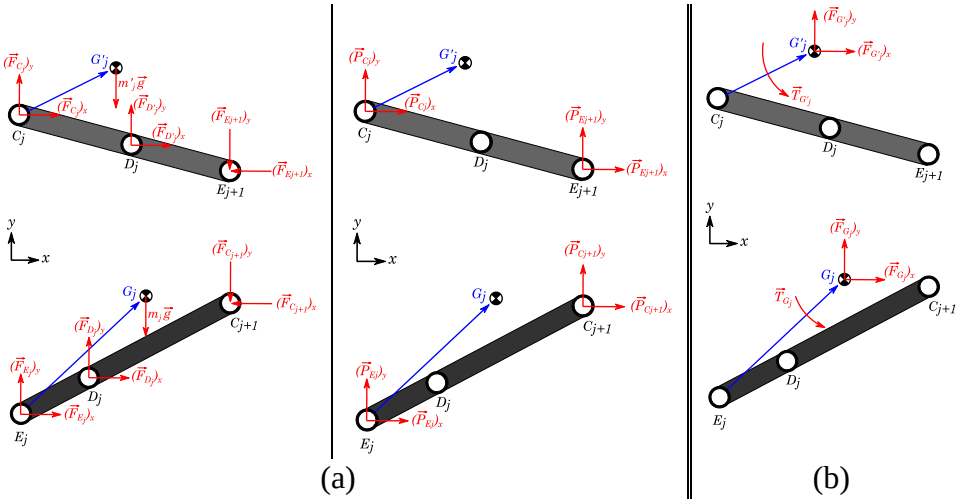

Figure 4.13: Free-body-diagram of a SLE: (a) External Forces (including Pressure), (b) Effective Forces

Figure 4.13a shows the internal and external forces and moments on a common scissor-like elements where pressure over the surface of the SSM converted into nodal forces, while Figure 4.13b shows inertia forces and moment.

With those considerations, the known vector $\{B_f\}$ can be updated as:

$$\{B_f\} = \begin{Bmatrix} \left(F_{G_j'}\right)_x + \left(F_{E_{j+1}}\right)_x - \left(P_{C_j}\right)_x - \left(P_{E_{j+1}}\right)_x \\ \left(F_{G_j}\right)_x + \left(F_{C_{j+1}}\right)_x - \left(P_{E_j}\right)_x - \left(P_{C_{j+1}}\right)_x \\ \left(F_{G_j'}\right)_y + \left(F_{E_{j+1}}\right)_y - \left(P_{C_j}\right)_y - \left(P_{E_{j+1}}\right)_y + m_j' g \\ \left(F_{G_j}\right)_y + \left(F_{C_{j+1}}\right)_y - \left(P_{E_j}\right)_y - \left(P_{C_{j+1}}\right)_y + m_j g \\ T_{G'j} - l'_{g_j}\left(P_{C_j}\right)_x \mathrm{s}(\gamma_j' + \delta_j') + l'_{g_j}\left(P_{C_j}\right)_y \mathrm{c}(\gamma_j' + \delta_j') + g_{E_{j+1}}\left(\left(F_{E_{j+1}}\right)_x - \left(P_{E_{j+1}}\right)_x\right)\mathrm{s}\left(\eta_{E\,j+1}\right) - g_{E_{j+1}}\left(\left(F_{E_{j+1}}\right)_y - \left(P_{E_{j+1}}\right)_y\right)\mathrm{c}\left(\eta_{E\,j+1}\right) \\ T_{G_j} - l_{g_j}\left(P_{E_j}\right)_x \mathrm{s}(\gamma_j + \delta_j) + l_{g_j}\left(P_{E_j}\right)_y \mathrm{c}(\gamma_j + \delta_j) + g_{C_{j+1}}\left(\left(F_{C_{j+1}}\right)_x - \left(P_{C_{j+1}}\right)_x\right)\mathrm{s}\left(\eta_{C\,j+1}\right) - g_{C_{j+1}}\left(\left(F_{C_{j+1}}\right)_y - \left(P_{C_{j+1}}\right)_y\right)\mathrm{c}\left(\eta_{C\,j+1}\right) \end{Bmatrix} \quad (4.68)$$

torque After all the internal forces and moments have been calculated, the required driving torque value of the attached FB linkage can be determined. In equation (4.68) $F's$ denotes the internal forces and $P's$ stands for the pressure, aerodynamic loading; hence the same equation can also be used for the calculation of in-vacuo conditions by simply assigning $P's$ equal to zero .

4.6 Design of Scissor-Structural Mechanisms

Any planar SSM constructed by using proposed translational and polar SLEs, can generate three different 2D curves. As seen from the Figure 4.14, those three curves are assumed to pass through joint locations $\{C_j\}_1^N$, $\{D_j\}_1^N$, $\{E_j\}_1^N$ respectively. This property of planar SSMs can be used to morph structures which are described by curves.

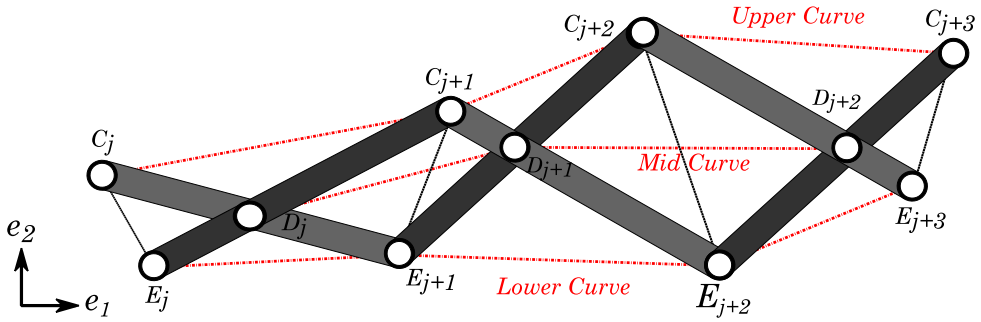

Figure 4.14: Curves Generated by a Planar SSM

In order to design a SSM, which is used to transform a structure characterized by two different curves into another form, the total number of SLEs, their types and the other initial parameters should be selected/optimized correctly to satisfy the both geometries.

4.6.1 Segmentation

It is convenient to start the design with the selection of the total number of used SLEs (N). This is the first step of the whole design. By segmentation, baseline curves which characterize the original structure and target curves which is the morphed form of the structure can be analyzed to find the correct number of used SLE. In the literature, there are many approaches related segmentation, which divide the design and target curves into several portion and analyze these portions in terms of their shape to find the best matches [98].

Then given curves can be divided into N segments to determine related width and thickness of each SLEs; however, the critical parameter which determines the final values of width or thickness is the orientation of t-lines, $\{\theta_j\}_1^N$. In other words, since each SLE is separated from each other with t-lines, the orientation of t-lines should be chosen reasonably. If two of three parameter set ($\{w_j\}_1^N, \{t_j\}_1^N, \{\theta_j\}_1^N$) are determined, the other parameter set can automatically arise. All in all, after selection of the type of designed mechanism which is called "type synthesis"; segmentation step is the second step of kinematic synthesis procedure ("number synthesis") in which the number of used links and joints are determined.

4.6.2 Determination of Link Parameters

After segmentation procedure, foldability vector parameters $\{t_j\}_1^N$, $\{w_j\}_1^N$, $\{h_j\}_1^N$, $\{\psi_j\}_1^N$, can be identified. By using foldability vector parameters, the parameters which describe the lengths of straight bars $\{k_j\}_1^N$, $\{l_j\}_1^N$, $\{k'_j\}_1^N$ $\{l'_j\}_1^N$, and their orientations $\{\gamma_j\}_1^N$, $\{\gamma'_j\}_1^N$ can be calculated by following formulas given in the Section 4.2.

As an alternative approach, the lengths of straight bars and their orientations can be directly selected by skipping the segmentation step. Yet, using segmentation is very important to see the behave of the curves. Due to its complexity, direct selection of link parameters is not recommended.

4.6.3 Joining the Chain

When segmentation and determination of link parameters are completed, position analysis of the SSM gives answer to the question of "Whether the designed SSM satisfies the target shape or not?". If the designed SSM cannot satisfy the target shape, then design parameters (especially orientation of t-lines) can be updated.

With the power of computer, above design procedure can be expedited by perturbing the design parameters. The obtained SSMs can be compared by their errors, and the final SSM which best matches with both baseline and target curves can be selected. Such type of errors, which originate to the design, is named as "structural error" and can be defined as:

$$err_j = \frac{d_j}{s} \tag{4.69}$$

where d_j is the shortest distance from the newest joint locations of j^{th} SLE to the target curves, and s is the characteristic dimension selected to reveal the percentage error.

Since all errors are lengths, so positive, $(\{err_j\}_1^N \geq 0)$, the mean error can be calculated as:

$$err_m = \frac{1}{N}\sum_{1}^{N} err_j \tag{4.70}$$

which is the only parameter to compare different SSMs with each other.

If the above procedure is finished, then the mechanism can be analyzed in order to reveal its kinematic and dynamic characteristics by following described formulation in the chapter.

In this thesis, this formulated is coded in the METU licensed MATLAB software [99]. MATLAB is chosen since all equations presented have analytic solution; therefore, the codded computer-routine requires less computational time. Summary of the computer-routine can be found as a flowchart in Appendix A.

4.7 Discussion and Conclusion

This chapter focuses on the design of SSMs. SSMs are used for if there is a requirement of deployment. The basic element which form the structure is SLEs. In this chapter, only two type of SLEs are investigated geometrically, which are translational and polar SLEs. New derivations, which are kinematic analysis and dynamic force analysis of scissor-structural mechanisms, have been introduced into the literature. A novel synthesis algorithm is introduced, which can help designer to synthesize a SSM which morph a 2D curve into another shape. Chapter ends with details of that algorithm.

CHAPTER 5

DESIGN OF A SCISSOR-STRUCTURAL MECHANISM FOR AIRFOIL PROFILE ADJUSTMENT

In this chapter, examples of designed SSMs have been presented. Then, those SSMs' effects on wing skin have been investigated. After elongation analysis, aerodynamic analyses of the skin formed by SSMs have been performed. When aerodynamic analyses are completed, the parameters required to design FB linkages which drive the SSM have been presented and some examples of those FB linkages are shown. Chapter 5 ends with kinematic analyses and dynamic force analyses of the proposed SSMs.

5.1 Introduction

With the developed computer-routine, several SSMs can be obtained and compared to find out the best SSM which has the minimum design error. In order to design a planar SSM for the morphing of trailing edge of an aircraft wing, mentioned base and target curves are the upper and lower coordinates of the wing section. For convenience, those wing sections are taken as of 4-digit NACA airfoils, which are highly studied and easy to compute, and related computer-routine is coded which generate the coordinates of NACA 4-digit airfoils [100].

The chord length of the airfoil can be taken as 0.6 [m], and characteristic dimension for convenience with [101], [102]. Assuming the rear spar of the wing at the 60% of the chord length, starting from the rear spar to the trailing edge of the airfoil, various SSMs have been designed with various parameters.

The NACA 4412 is taken as baseline airfoil, and it is aimed to morph this airfoil into NACA 8412. For the five different total number of SLEs ($N = 4,6,8,10,12$),

perturbing the design parameters, several SSMs have been designed. Those SSMs are also investigated whether they satisfy the other airfoils (i.e. NACA 2412, NACA 6412) which have the same thickness and the maximum camber location.

Table 5.1 summarizes the primary design parameters, where $\bar{\theta}$ is the mean t-line orientation angle of the whole SSM, $\Delta\theta$ is the difference of t-line orientation angle between two consecutive SLEs, k_0 is the coefficient which determines the output link length of the FB linkage assumed to be assembled (assuming a_4 represents the length of the output link of the FB linkage assumed to be attached, $a_4 \equiv k_0 l_1$, where the l_1 is the section length of the initial SLE which is anchored), k_γ is the coefficient which determines the output link installation angle of the FB linkage assumed to be assembled (assuming ϕ represents the angle of the output link of the FB linkage assumed to be attached, $\phi(t=0) \equiv k_\gamma \gamma_1(t=0)$, where the γ_1 is the angle of the initial SLE which is anchored).

Table 5.1: Design Parameters for Various SSMs with Different Number of SLEs

	$\bar{\theta}$	$\Delta\theta$	k_0	k_{γ_1}
$N = 4$	110°	6°	0.7	2.0
$N = 6$	105°	5°	0.6	1.8
$N = 8$	100°	4°	0.5	1.6
$N = 10$	95°	3°	0.4	1.4
$N = 12$	90°	2°	0.3	1.2

Note that the parameters presented in Table 5.1 are not the optimum values; however, it is obvious from the characteristic of the SSMs that as the total number of SLEs is increasing, the structure becomes more prone to be convertible with little divergence form the core values, where the core values are $\bar{\theta} = 90°$, $\Delta\theta = 0$, $k_0 = 0$, $k_{\gamma_1} = 1$.

5.2 Design of a Scissor-Structural Mechanism for Various Total Number of Scissor-Like Elements

In the developed computer-routine, the user can define design parameters N, $\{w_j\}_1^N$, $\{\theta_j\}_1^N$, $\{\psi_j\}_1^N$. Since the airfoil geometry encloses the SSM from upper and lower surfaces, the other design parameters $\{h_j\}_1^N$ and $\{t_j\}_1^N$ can automatically be adjusted.

By using the design parameters represented in Table 5.1, five different SSMs can be designed assuming widths of all SLEs are equal to each other (i.e. $w_j = w_{j+1}$ for $j = 1 \dots N-1$). Table 5.2 gives a summary of mean design errors calculated:

Table 5.2: Mean Percentage Design Errors for Various SSMs with Different Number of SLEs

	NACA 2412	**NACA 6412**	**NACA 8412**
$\boldsymbol{N = 4}$	0.00235	0.00179	0.00206
$\boldsymbol{N = 6}$	0.00311	0.00148	0.00200
$\boldsymbol{N = 8}$	0.00310	0.00149	0.00205
$\boldsymbol{N = 10}$	0.00225	0.00104	0.00139
$\boldsymbol{N = 12}$	0.00132	0.00077	0.00145

In Figure 5.1, SSM with $N = 8$ SLEs at its initial position is shown. In this case, mean t-line orientation angle is chosen a hundred degrees, $\bar{\theta} = 100°$; all SLEs are the type of p-SLE with constant $\{\psi_j\}_1^N = 4°$; the segmentation is done linearly (widths of each SLE is equal to each other). Then, when the anchor-link is rotated $\Delta\phi = 23°$ clockwise, the designed SSM will satisfy the NACA 8412 geometry with 0.145% mean design error. In Figure 5.2, deployment process of the mechanism is shown:

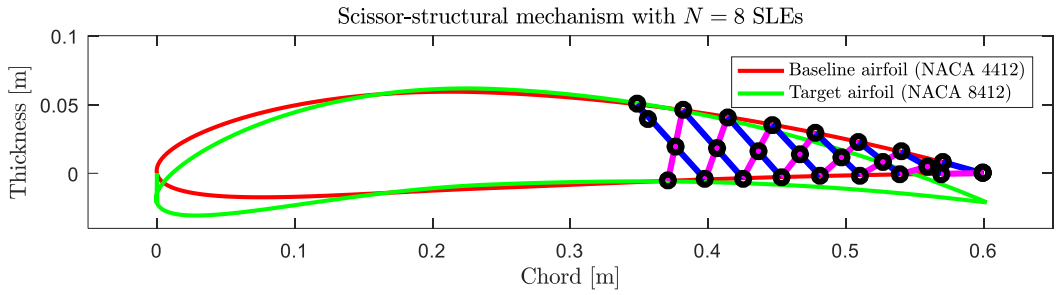

Figure 5.1: Scissor-Structural Mechanism with $N = 8$ SLEs at its Initial Position

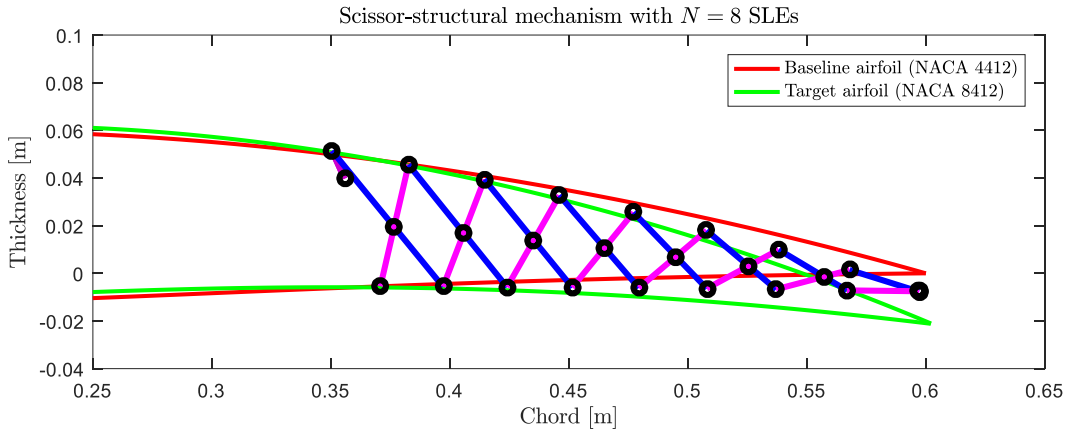

(a)

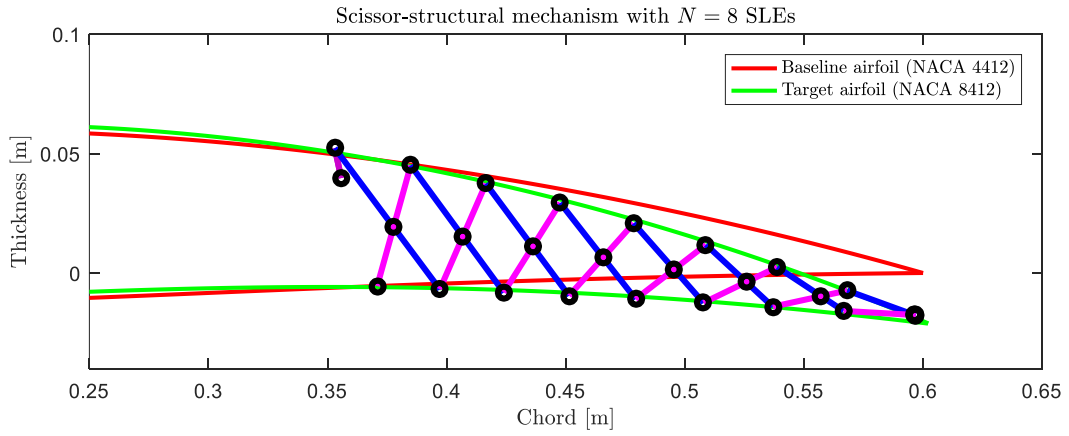

(b)

Figure 5.2: Scissor-Structural Mechanism with $N = 8$ SLEs (a) While Deploying, (b) at Its Deployed Position

As seen from the Figure 5.3a, if the anchor-link is rotated counter-clockwise, the mechanism adds decamber property to the aircraft wing also. The same SSM with $N = 8$ SLEs, can satisfy NACA 2412 and NACA 6412 profiles with 0.310% and 0.149% mean design errors respectively.

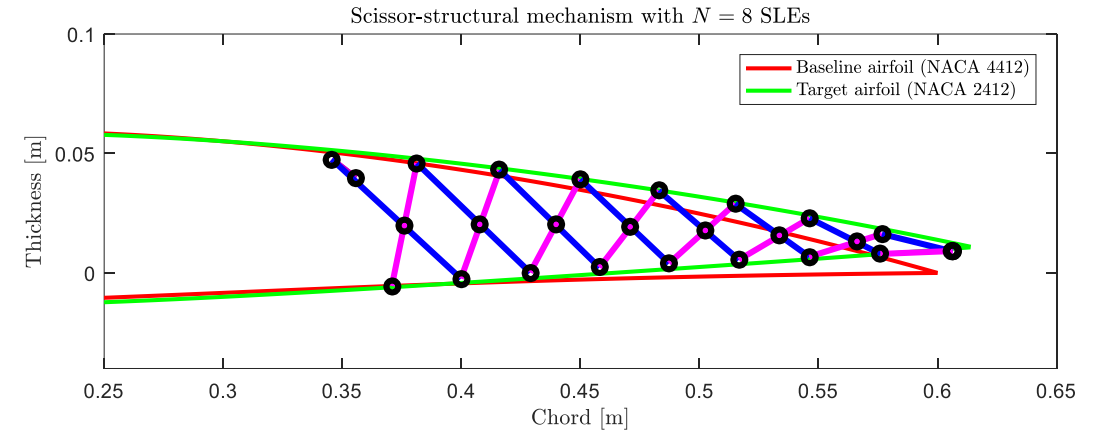

(a)

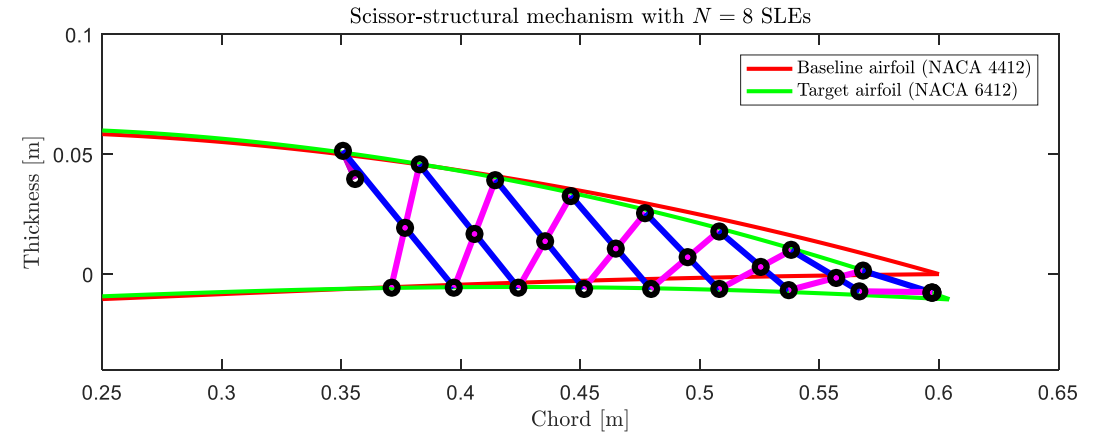

(b)

Figure 5.3: Scissor-Structural Mechanism with $N = 8$ SLEs at the Deployed Position when the Target Airfoil is (a) NACA 2412, (b) NACA 6412

As seen from the Figure 5.4 and Figure 5.5, four different SSMs with $N = 4,6,10,12$ SLEs have also been designed. For those cases, values of the design parameters are in descending trend. Then, when the anchor-link is rotated $\phi = 10.5°$, $\phi = 18°$, $\phi = 24°$ and $\phi = 26°$ clockwise, the designed SSMs will satisfy the NACA 8412

geometry with 0.206% , 0.200% , 0.139% and 0.145% mean design errors respectively.

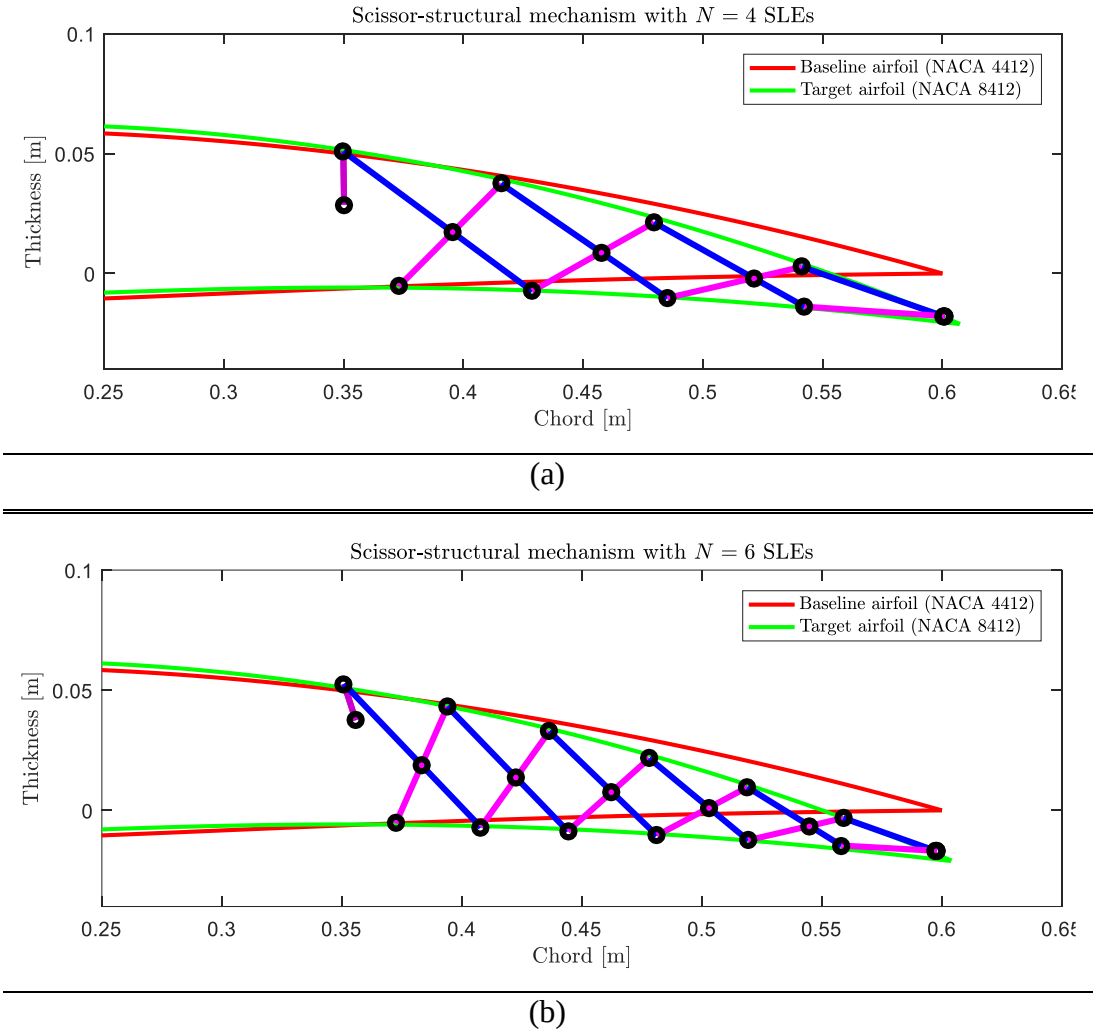

Figure 5.4: Scissor-Structural Mechanisms with (a) $N = 4$ SLEs, (b) $N = 6$ SLEs at Their Deployed Positions.

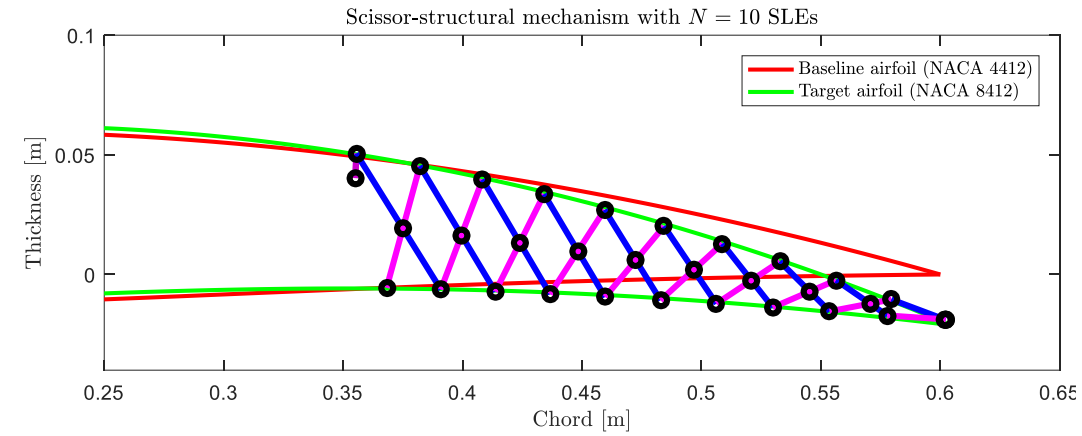

(a)

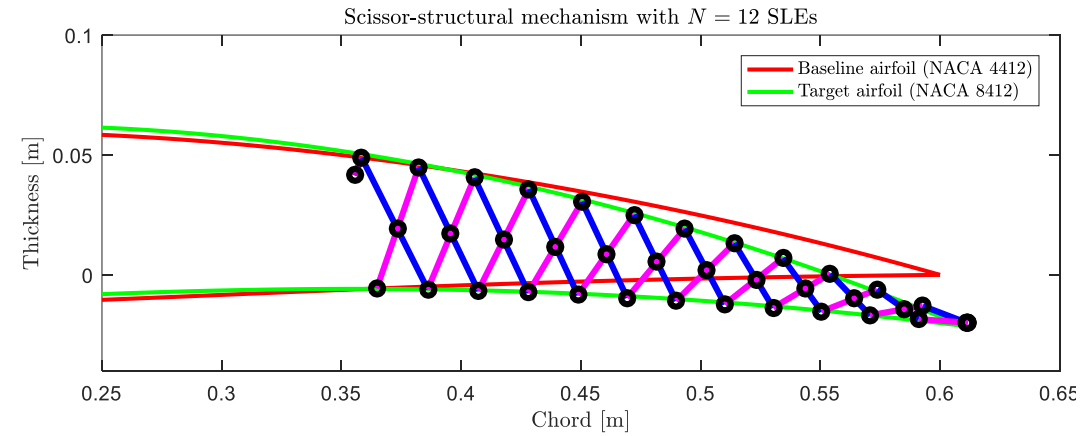

(b)

Figure 5.5: Scissor-Structural Mechanisms with (a) $N = 10$ SLEs, (b) $N = 12$ SLEs at Their Deployed Positions.

5.3 Effect of Scissor-Structural Mechanisms on Wing Skin

As seen for the designed SSMs, As the SSM deploys, the wing skin deforms. That why the SSMs are designed with the assumption of a fully-compliant aircraft wing skin which performs the imposed motion.

In spite of the assumption made above, required performances of the upper and lower wing skins have been investigated also. In order to see the percentage elongation of the wing skin segments divided by SLEs, the segment lengths are compared with their difference between initial and final positions.

As seen from the Figure 5.6, the SSM with $N = 8$ SLEs, produce negative elongation with the magnitude of at most 2.5% when it satisfied the NACA 8412 and produce positive elongation with the magnitude of at most 8% when it satisfied the NACA 8412.

As seen from the Figure 5.7 and Figure 5.8, four different SSMs with $N = 4,6,10,12$ SLEs have also been investigated in terms of their effects on the wing skin as those SSMs satisfying the NACA 8412. As seen from the same figures, the results are not in a certain trend, since the SSMs are not designed to minimize the elongations. However, one can conclude that, usage of SSMs are better than conventional systems, because the deformation at hinge point of conventional control surfaces is distributed throughout the trailing edge.

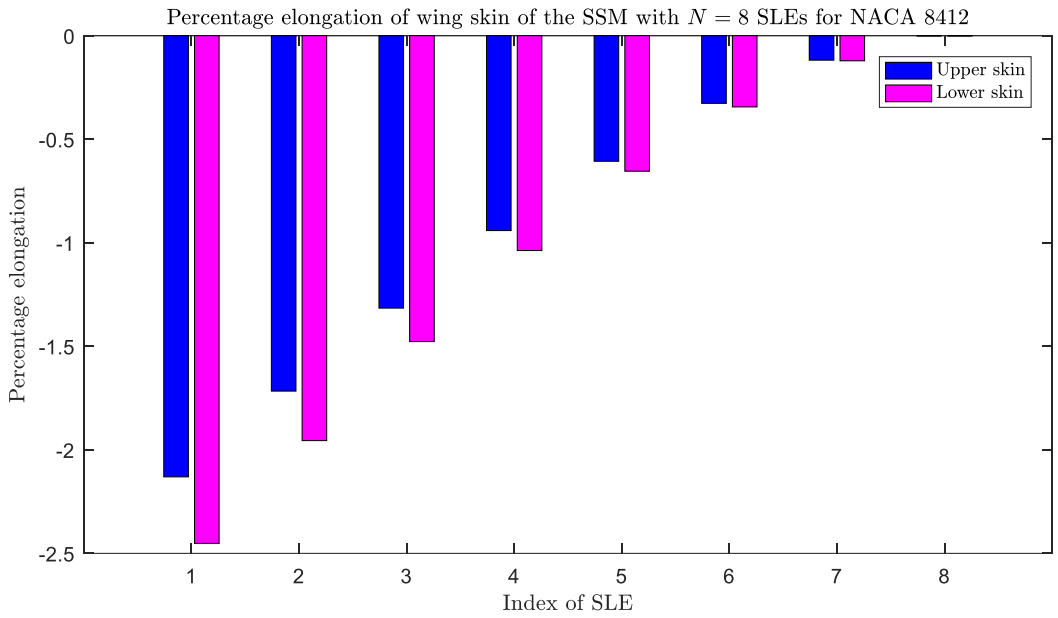

(a)

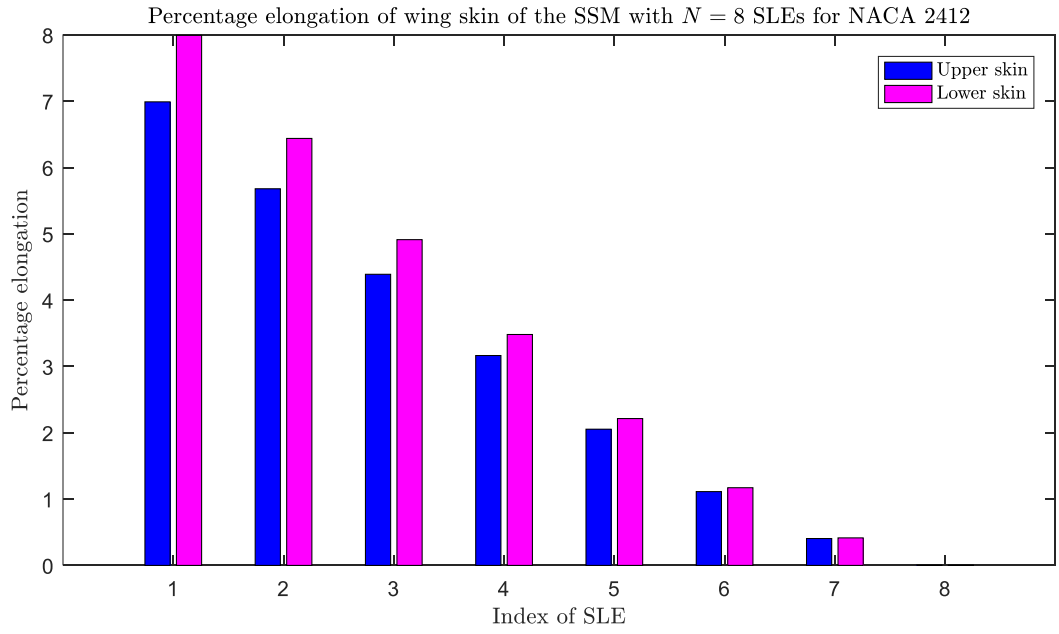

(b)

Figure 5.6: Percentage Elongation of Wing Skin Segments of the SSM with $N = 8$ SLEs, (a) for NACA 8412 (b) NACA 2412

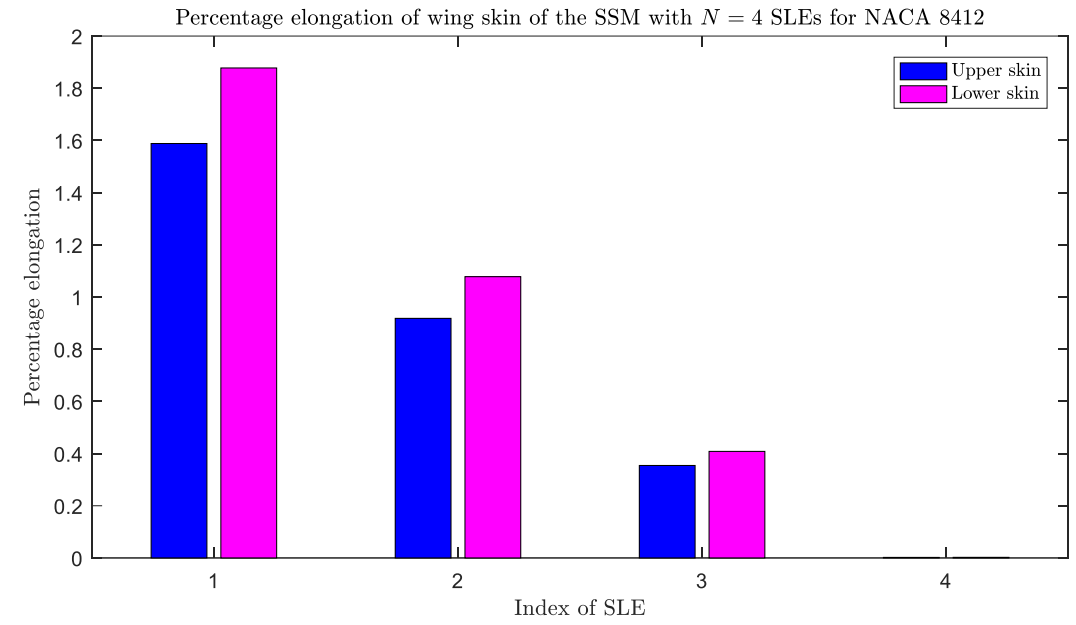

(a)

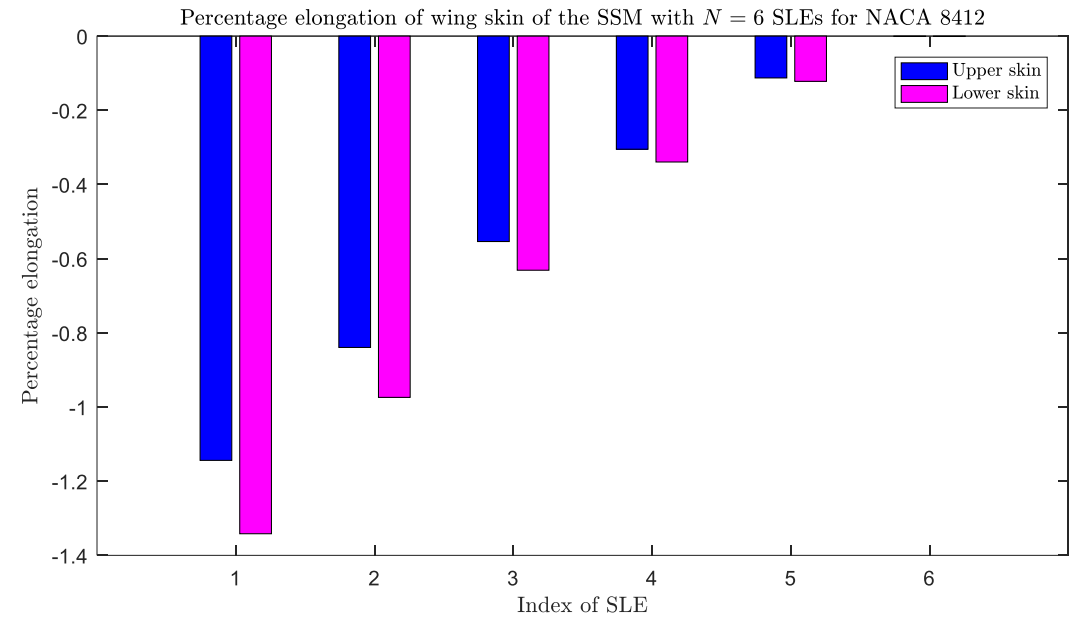

(b)

Figure 5.7: Percentage Elongation of Wing Skin Segments of the SSMs with (a) $N = 4$ SLEs, (b) $N = 6$ SLEs for NACA 8412

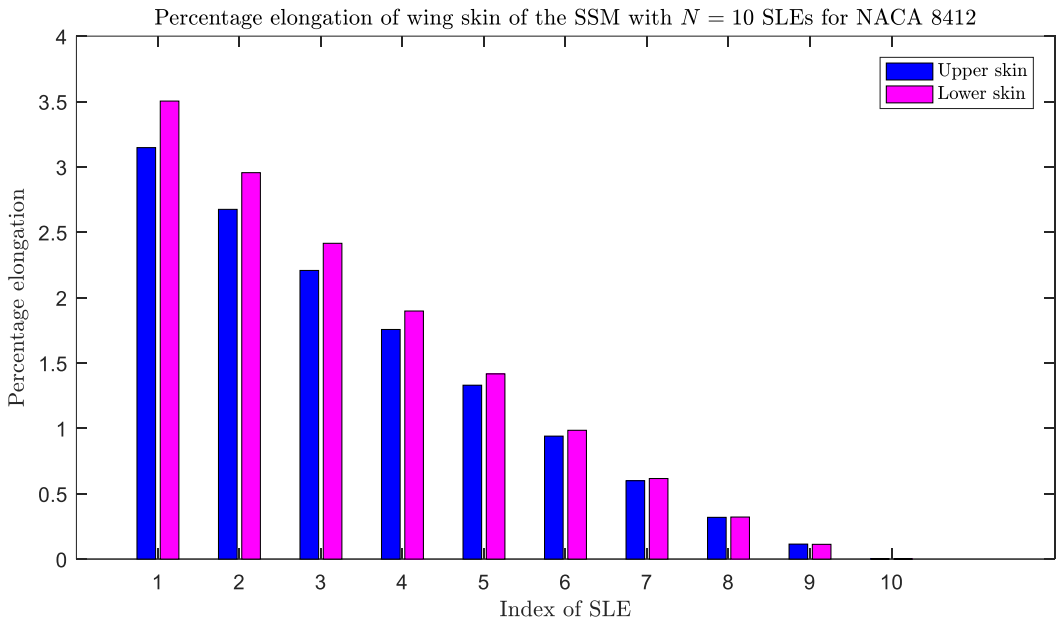

(a)

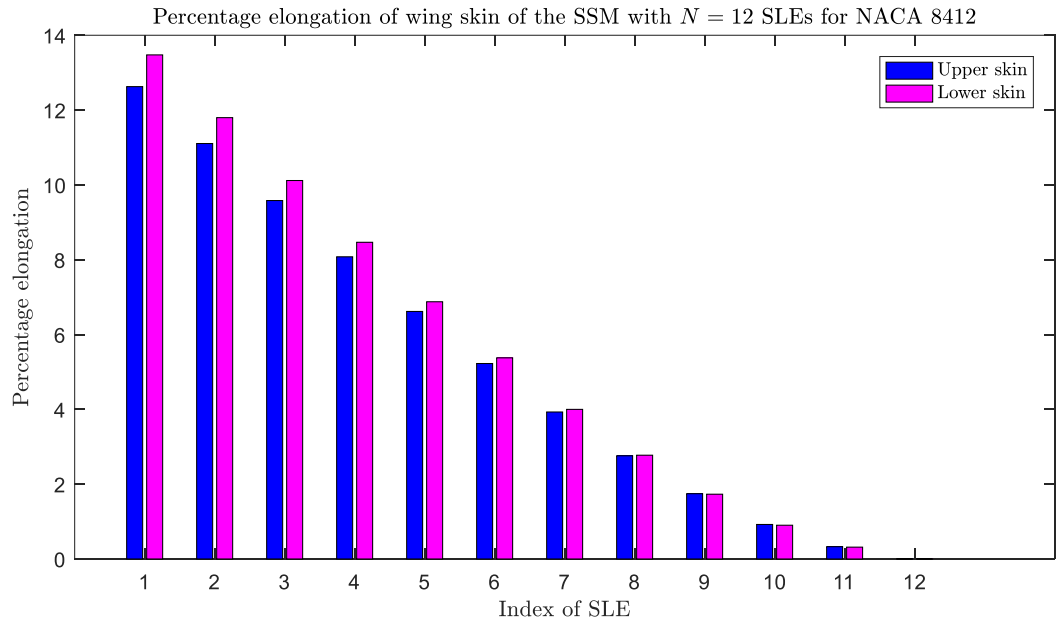

(b)

Figure 5.8: Percentage Elongation of Wing Skin Segments of the SSMs with (a) $N = 10$ SLEs, (b) $N = 12$ SLEs for NACA 8412

5.4 Aerodynamic Analyses of the Surface Formed by Scissor-Structural Mechanisms

5.4.1 XFOIL: Panel Method

Panel method provides solutions for linear, inviscid, irrotational flows around solid surfaces subjected to subsonic speeds. The solution algorithm employs panels to construct the solid interfaces with vortices and sources inducing a velocity field around the body. Then, the system of equations is solved by corresponding boundary conditions defined over the airfoil matching the number of panels. The corresponding pressure distribution is calculated using the tangential velocity components distributed over the surface, which also leads by integration over the airfoil contour to the computation of lift and drag forces. Nevertheless, owing to the fact that formulation of panel method considers inviscid flow conditions; skin friction component caused by interactions between a solid body and a viscous fluid is not taken into account. Thus, the total drag force calculated with panel method, normally consisting of skin friction and pressure drag components, lacks the skin friction drag component which leads to significant undershoots in terms of drag force and significant overshoots in terms of lift force computations. Furthermore, not only miscalculation of drag force but also absence of boundary layer interactions contributes to the possible inaccuracies of panel method especially for high angle-of-attack (AoA) values. These effects and their various performance characteristics are well-defined in literature including comparisons with experimental results [103],[104].

In order provide a solution to the problem of lacking viscous contribution, XFOIL is developed with a viscous coupling formulation where the entire viscous solution (boundary layers and wake) is strongly interacted with the incompressible potential flow via the surface transpiration model. This permits proper calculation of limited separation regions. The drag is determined from the wake momentum thickness far downstream. A special treatment is used for a blunt trailing edge, which fairly and accurately accounts for base drag [105].

5.4.2 Validation of the Solver

Owing to the fact that NACA 4412 airfoil is used as the baseline airfoil for the morphing modifications, XFOIL, which is based on panel method, is validated over experimental results presented at NACA Report No. 586 [106] and NACA Report No. 646 [107]. Viscous solutions of six different Reynolds numbers attained from XFOIL are compared with the experimental results in terms of pressure coefficient distributions over the chord length and variation of lift coefficient with different AoA values. In order to keep the validation process compatible with the solutions, $n_{panel} = 200$ panels are assigned over the airfoil coordinates focused on leading and trailing edges, and the results are compared considering the uncertainty limits included in the experimental data.

Throughout the solutions performed using XFOIL iteration number is limited to $n_{iter} = 100$ which is accompanied with a root-mean-square (RMS) tolerance of $tol = 10^{-4}$ for convergence. Since the panel method provides an inviscid solution for the flow around an airfoil, XFOIL possess an additional viscous coupling to be able to generate viscous solutions and boundary layer interactions over the airfoil surfaces. However, it is well documented in the literature that, for high AoA values, it has a tendency to overshoot the lift coefficient values with reduced effect of boundary layer interactions and separation due to adverse pressure gradient [108]. Hence, both for the validation and the solution processes, AoA values higher than $\alpha = 15°$ and lower than $\alpha = -5°$ were avoided. Consequently, according to the limitations and parameters selected, solutions obtained with Reynolds number of $Re = 330000$ revealed best agreement with the experimental data.

As seen from Figure 5.9b, XFOIL predict the pressure distribution quite well except the deviation around 70% of the chord. Therefore, the lift coefficient vs AoA differs a bit due to that deviation as seen from Figure 5.9a. In other words, XFOIL predicts more lift that the original airfoil.

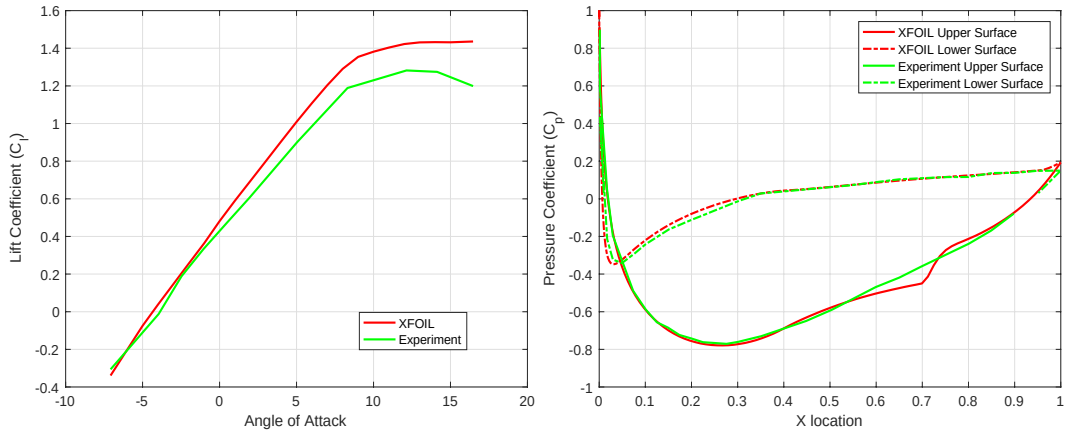

(a) (b)

Figure 5.9: Comparison of (a) Lift Coefficient (C_l) vs. Angle-of-attack (α), (b) Pressure Coefficient Distribution (C_p) Obtained by XFOIL and Experimental Data for NACA 4412 Airfoil

5.4.3 Results

Aerodynamic analyses have been conducted for all designed SSMs with the package XFLR5, which is an analysis tool for airfoils, wings and planes operating at low Reynolds Numbers. XFLR5 includes XFOIL's direct and inverse analysis capabilities with wing design and analysis capabilities based on the lifting line theory, on the vortex lattice method, and on a 3D panel method [109].

In Figure 5.10, the results obtained from the XFLR5 for SSM with $N = 8$ SLEs when the SSM at the position of NACA 8412 are shown. The same figure also includes the comparison of the panel numbers. As seen from the figure, for all panel numbers, which are $n_{panel} = 80, 120, 160, 200$, the results are nearly same if one ignore little variations. Since using large number of panels does not require large computational time, for the solutions $n_{panel} = 200$ is selected.

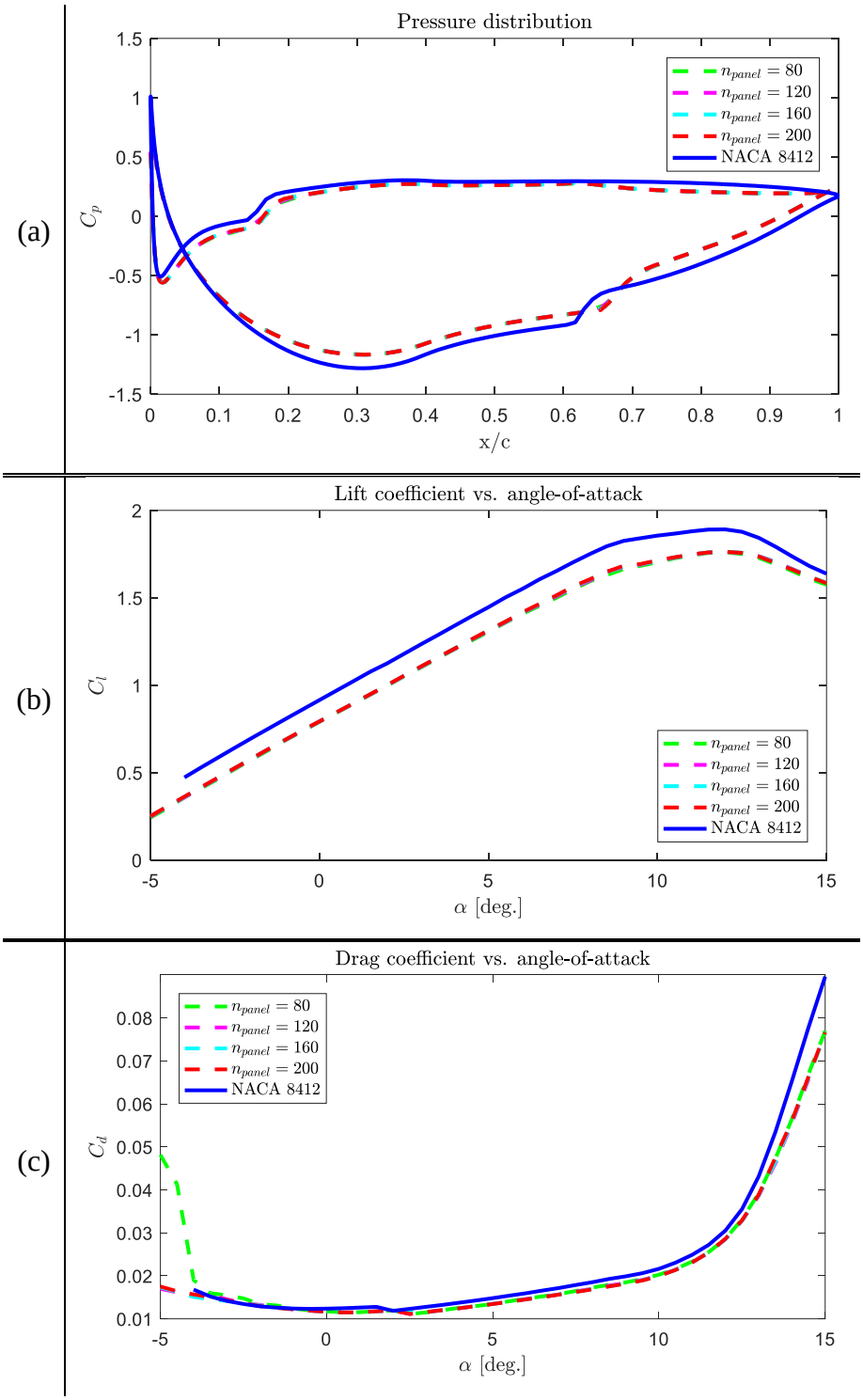

Figure 5.10: Comparison of Aerodynamic Behavior of the Surface Formed by Proposed SSM with $N = 8$ SLEs for NACA 8412 with NACA 8412 Profile: (a) Pressure Distribution, (b) Lift Coefficient vs. AoA, (c) Drag Coefficient vs. AoA

Figure 5.11 shows the aerodynamic behavior of the surfaces formed by the same mechanism at the other poses (NACA 2412 and NACA 6412). As seen from Figure 5.10 and Figure 5.11, the results nearly overlap with the original NACA airfoils; however, at the point, where the anchor-link of the mechanism is located and assembled to the whole SSM, pressure coefficients deviates from the NACA airfoils. Due to this effect, the surfaces formed by proposed SSM generate less lift than NACA airfoils. Since the SSM designed for NACA 8412 with little design error, satisfies the other airfoils (NACA 2412 and NACA 6412) with larger design errors and manipulates the chord length very little, all deviations are expected and normal.

Figure 5.12 shows the aerodynamic behavior of the surfaces formed by the SSMs with $N = 4$ and $N = 6$ SLEs and Figure 5.13 shows the aerodynamic behavior of the surfaces formed by the SSMs with $N = 10$ and $N = 12$ SLEs respectively. As seen from the figures, the same scenario with the SSM with $N = 6$ SLEs remains valid.

From the performance of the surfaces formed by SSMs, one can conclude that the location where the anchor-link is assembled to the SSM is very critical to design and designed SSMs for each case satisfy the target airfoil profiles successfully with little lift penalty. Since the proposed SSMs have the capability to obtain high camber rates, they can also generate higher lifts than NACA airfoils.

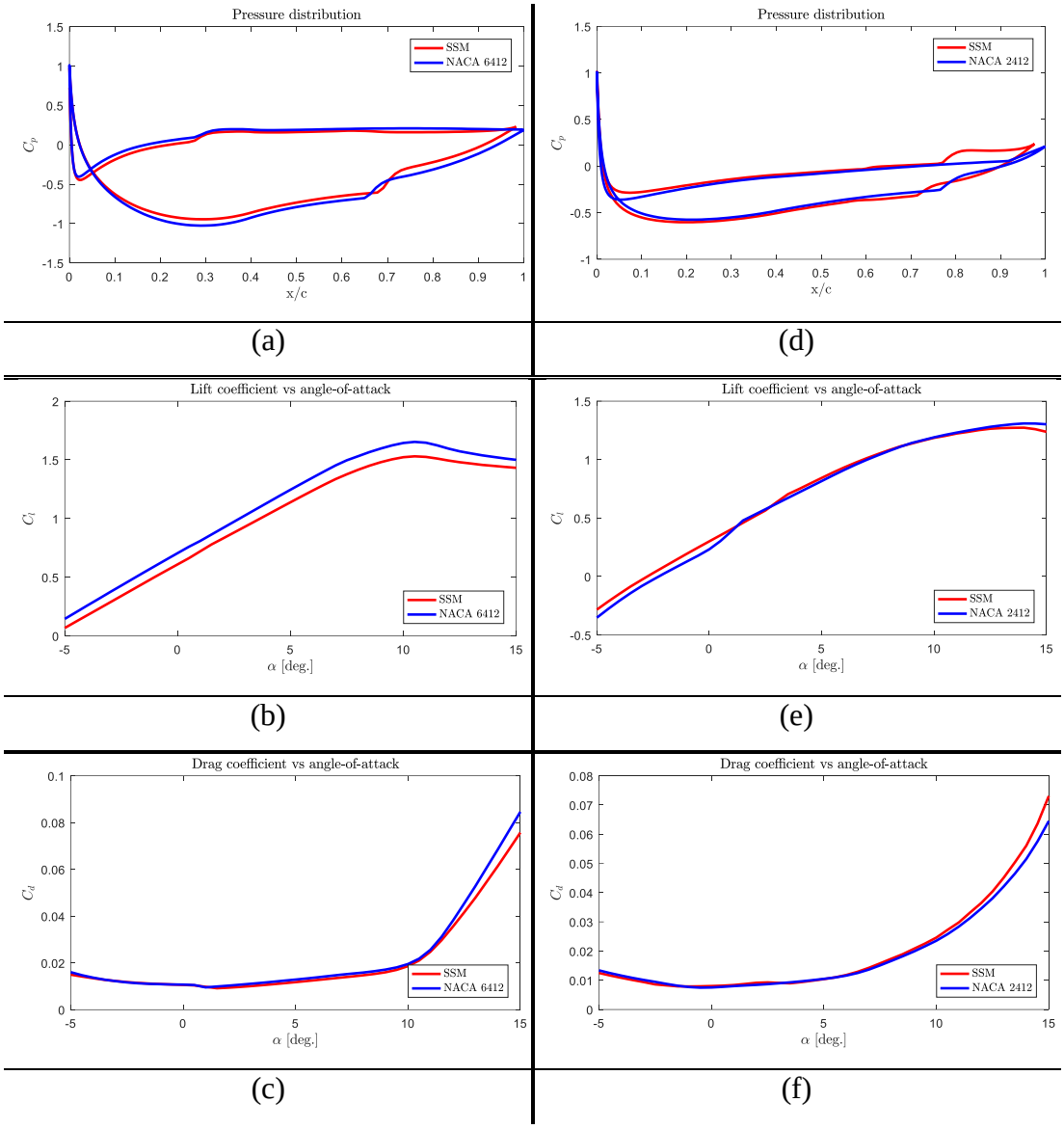

Figure 5.11: Comparison of Aerodynamic Behavior of the Surface Formed by Proposed SSM with $N = 8$ SLEs for NACA 6412 with NACA 6412 Profile: (a) Pressure Distribution, (b) Lift Coefficient vs. AoA, (c) Drag Coefficient vs. AoA and the Surface Formed by Proposed SSM with $N = 8$ SLEs for NACA 2412 with NACA 2412 Profile: (d) Pressure Distribution, (e) Lift Coefficient vs. AoA, (f) Drag Coefficient

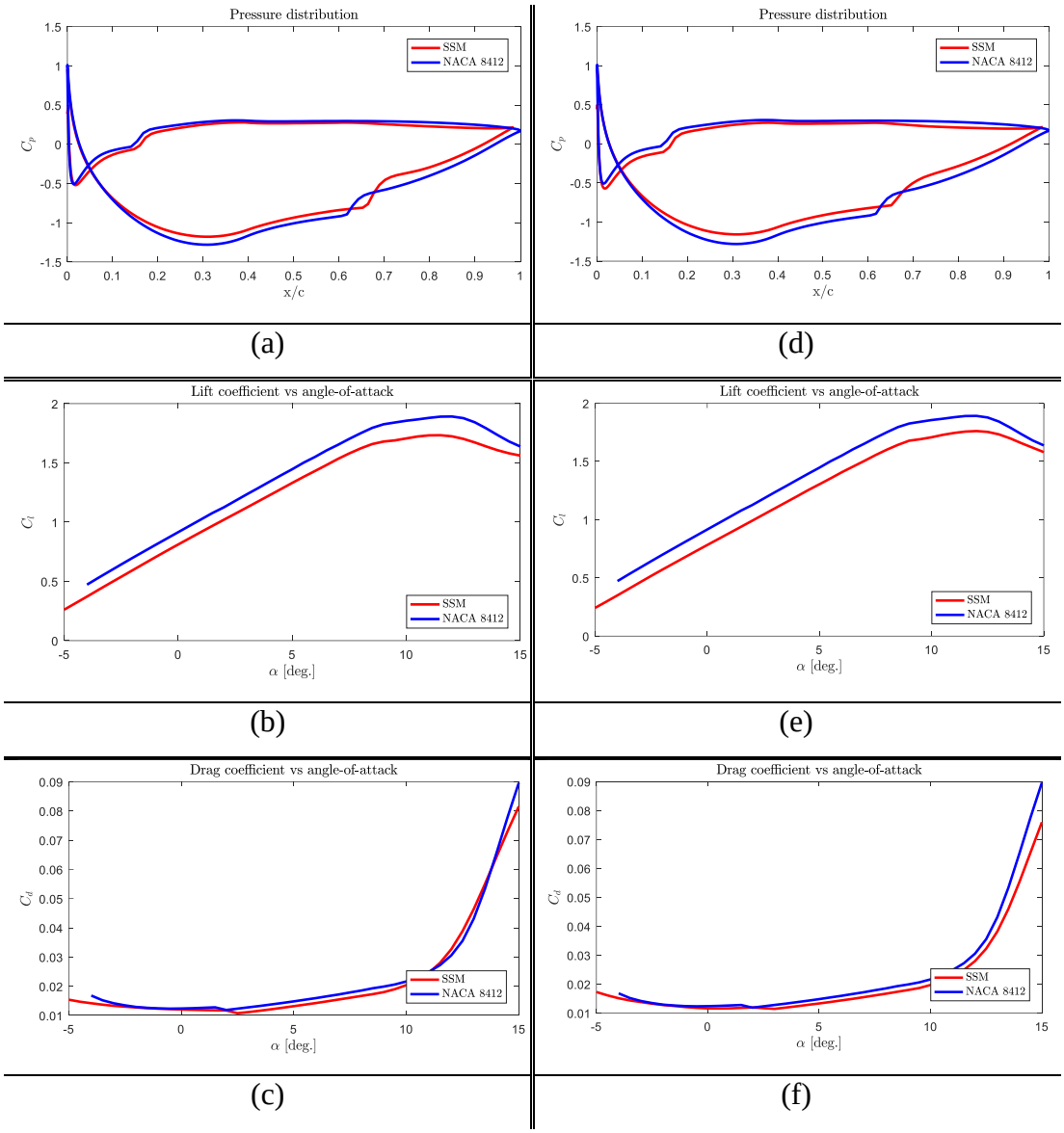

Figure 5.12: Comparison of Aerodynamic Behavior of the Surface Formed by Proposed SSM with $N = 4$ SLEs for NACA 8412 with NACA 8412 Profile: (a) Pressure Distribution, (b) Lift Coefficient vs. AoA, (c) Drag Coefficient vs. AoA and the Surface Formed by Proposed SSM with $N = 6$ SLEs for NACA 8412 with NACA 8412 Profile: (d) Pressure Distribution, (e) Lift Coefficient vs. AoA, (f) Drag Coefficient

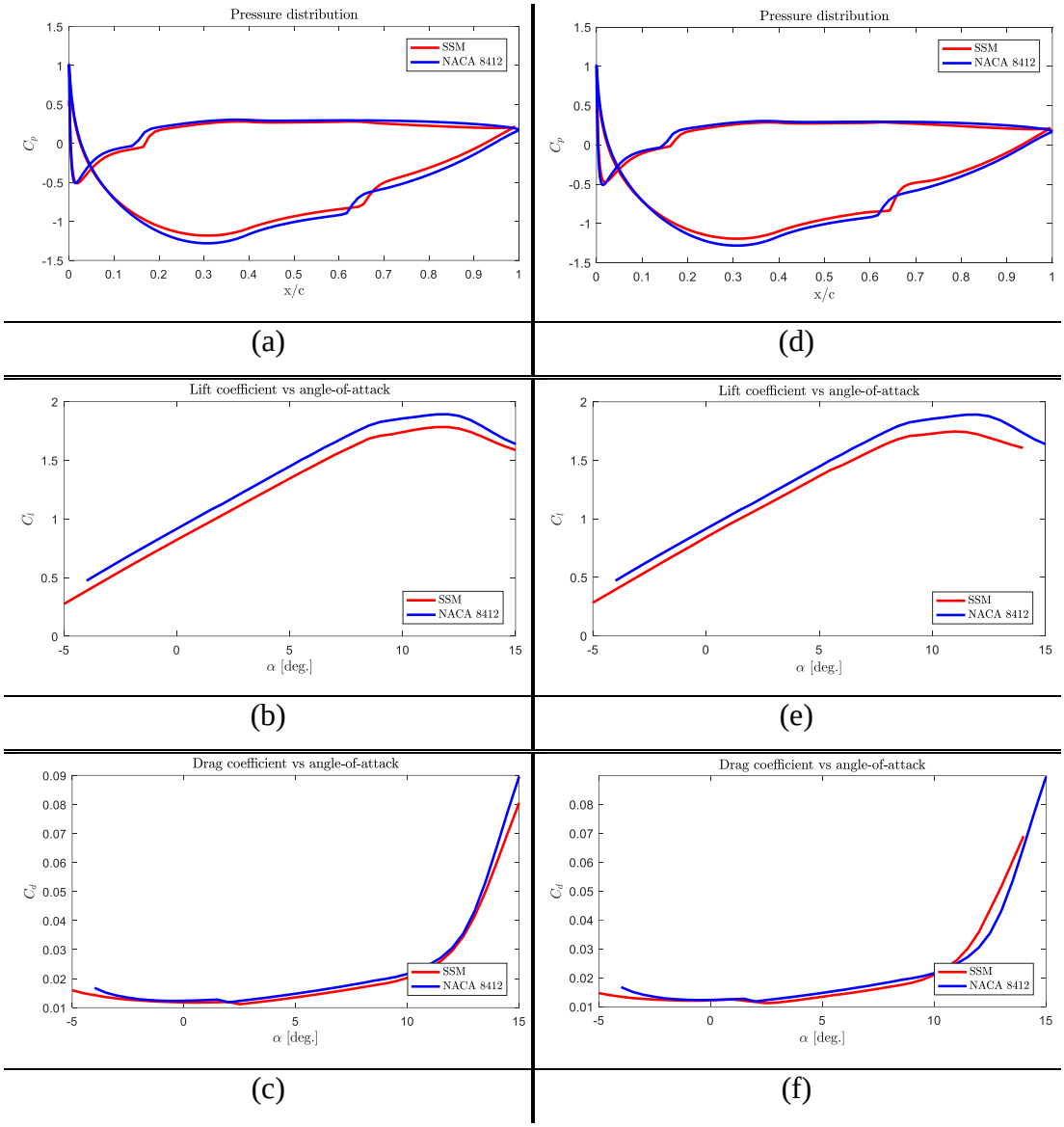

Figure 5.13: Comparison of Aerodynamic Behavior of the Surface Formed by Proposed SSM with $N = 10$ SLEs for NACA 8412 with NACA 8412 Profile: (a) Pressure Distribution, (b) Lift Coefficient vs. AoA, (c) Drag Coefficient vs. AoA and the Surface Formed by Proposed SSM with $N = 12$ SLEs for NACA 8412 with NACA 8412 Profile: (d) Pressure Distribution, (e) Lift Coefficient vs. AoA, (f) Drag Coefficient

5.5 Design of Four-Bar Linkages for Scissor-Structural Mechanisms

Optimum design of SSMs contains the design of the output link of the FB linkage too. Therefore, throughout the results presented above, a FB linkage assumed to be attached which is represented by the output link of the FB linkage. Output link of the FB linkage designed with two parameters which are k_0 and k_γ. These parameters roughly give the answer of how the output link of the attached FB linkage will be. Although there is an option to drive that link directly, due to mobility requirements (since that link rocks in all design results), designing a suitable FB linkage allows to get a full-turn link, which is thought as anchor-link. By using the results, the input parameters can be obtained to design a suitable FB linkage by using the methodology described in Chapter 3.

5.5.1 Design of Function Generators for Scissor-Structural Mechanisms

In order to design a function generator for SSMs presented, one needs output angles and length of one of link of FB linkage to be synthesized. Since the angles and the length of the output link is prescribed, in order to minimize the design error of the SSM, by using the methodology presented in Chapter 3.2.1, function generator for the SSM can be synthesized. In Table 5.3, angles and the lengths of the output link for designed SSMs with various number of SLEs are presented:

Table 5.3: Output Angles and the Output Link Lengths to Synthesize Function Generators for Presented SSMs for Various Number of SLEs

	$\boldsymbol{\phi(t=0)}$	$\boldsymbol{\phi_1}$	$\boldsymbol{\phi_2}$	$\boldsymbol{\phi_3}$	$\boldsymbol{a_4}$ $[\boldsymbol{m}]$
$\boldsymbol{N=4}$	107.8°	101.3°	96.3°	90.8°	0.0223
$\boldsymbol{N=6}$	138.9°	125.9°	117.4°	107.9°	0.0159
$\boldsymbol{N=8}$	142.3°	125.3°	114.3°	102.3°	0.0128
$\boldsymbol{N=10}$	129°	112°	100°	88°	0.0103
$\boldsymbol{N=12}$	110.6°	93.1°	80.1°	67.6°	0.0079

In Table 5.3 rotations $\phi(t=0)$, ϕ_1, ϕ_2, ϕ_3 represent the angles of anchor-link of the SSM, in order to satisfy NACA 2412, 4412, 6412 and 8412 respectively.

If a function generator is designed in order to drive the SSM with $N = 8$ SLEs, the best result which is a Class-I Grashof mechanism and fit into the torque box of the aircraft wing can be seen in the Figure 5.14.

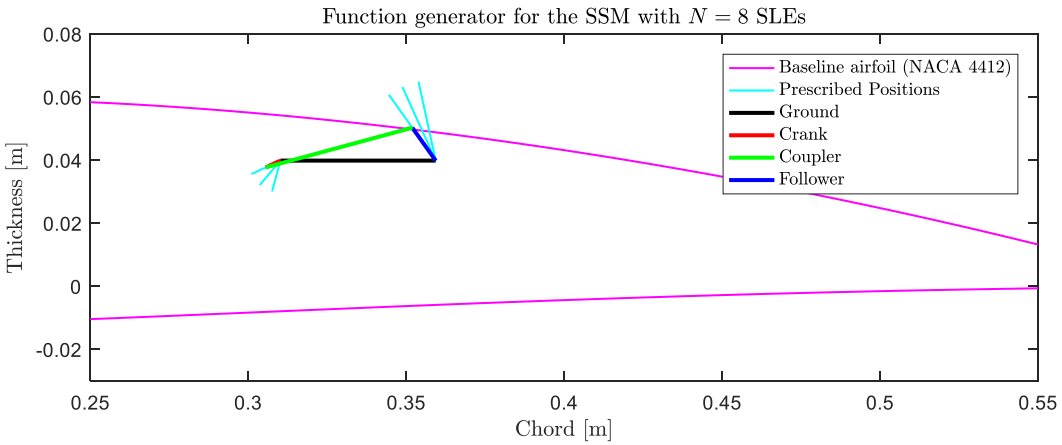

Figure 5.14: Function Generator FB Linkage for the Proposed SSM with $N = 8$ SLEs

As seen from Figure 5.15, synthesized function generator works with feasible transmission angle.

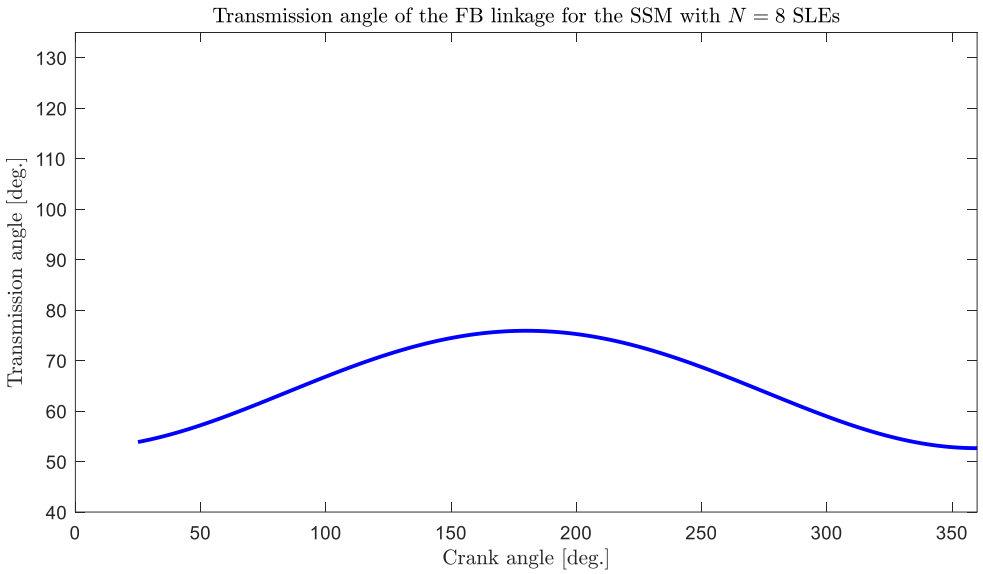

Figure 5.15: Transmission Angle Variation of the Function Generator FB Linkage for the Proposed SSM with $N = 8$ SLEs

5.5.2 Design of Motion Generators for Scissor-Structural Mechanisms

In order to design a motion generator for SSMs presented, one needs prescribed positions of the coupler link of FB linkage to be synthesized. Since the MSPP of the coupler link are prescribed, in order to minimize the design error of the SSM, by using the methodology presented in Chapter 3.2.1, motion generator for the SSM can be synthesized. In Table 5.4 coordinates of the prescribed positions of the coupler link for designed SSMs with various number of SLEs are presented. Similar to Table 5.3, prescribed points represent the locations of end of anchor-link of the SSM, in order to visit NACA 2412, 4412, 6412 and 8412 respectively.

Table 5.4: Multiply Separated Prescribed Positions to Synthesize Motion Generators for Presented SSMs for Various Number of SLEs

	P_1	P_2	P_3	P_4
$N = 4$	0.3433, 0.0498	0.3458, 0.0505	0.3477, 0.0508	0.3498, 0.0509
$N = 6$	0.3438, 0.0480	0.3464, 0.0504	0.3485, 0.0516	0.3509, 0.0526
$N = 8$	0.3456, 0.0476	0.3483, 0.0502	0.3505, 0.0514	0.3530, 0.0522
$N = 10$	0.3487, 0.0483	0.3513, 0.0498	0.3534, 0.0504	0.3555, 0.0506
$N = 12$	0.3527, 0.0489	0.3551, 0.0494	0.3568, 0.0493	0.3585, 0.0488

In Table 5.5 corresponding rotations of the coupler link for designed SSMs with various number of SLEs are presented. These rotations are the differences of the angles presented in the Table 5.3.

In order to drive the SSM with $N = 8$ SLEs, if three MSPP, P_2, P_3, P_4 and $\alpha_2, \alpha_3, \alpha_4$,are selected; the center and circle curves can calculated as seen in Figure 5.16.

Table 5.5: Recommended Coupler Rotations to Synthesize Motion Generators for Presented SSMs for Various Number of SLEs

	$\boldsymbol{\alpha(t=0)}$	$\boldsymbol{\alpha_2}$	$\boldsymbol{\alpha_3}$	$\boldsymbol{\alpha_4}$
$\boldsymbol{N=4}$	107.8°	−6.5°	−5°	−5.5°
$\boldsymbol{N=6}$	138.9°	−13°	−8.5°	−9.5°
$\boldsymbol{N=8}$	142.3°	−17°	−11°	−12°
$\boldsymbol{N=10}$	129°	−17°	−12°	−12°
$\boldsymbol{N=12}$	110.6°	−17.5°	−13°	−12.5°

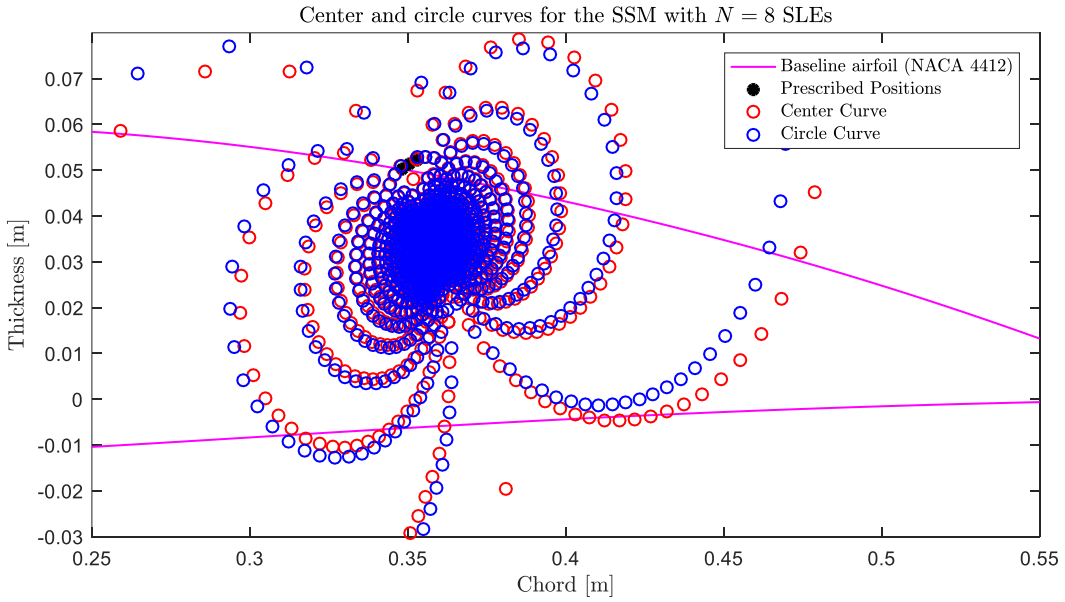

Figure 5.16: Possible Ground and Moving Pivots (Center and Circle Points) in order to Design Motion Generator FB Linkage for the Proposed SSM with $N = 8$ SLEs

If a motion generator is designed by using the results, the best mechanism which is a Class-I Grashof mechanism and fit into the torque box of the aircraft wing can be seen in the Figure 5.17. Moreover, as seen from Figure 5.18, synthesized motion generator works with feasible transmission angle.

Link lengths of the function generator are $49.2, 5.1, 53.5, 12.8$ [mm] whereas link lengths of the motion generator are $12.8, 2.9, 9.8, 6.2$ [mm]. Although motion

generator has the shorter link lengths (less weight), for manufacturing considerations, designing a function generator may be more beneficial.

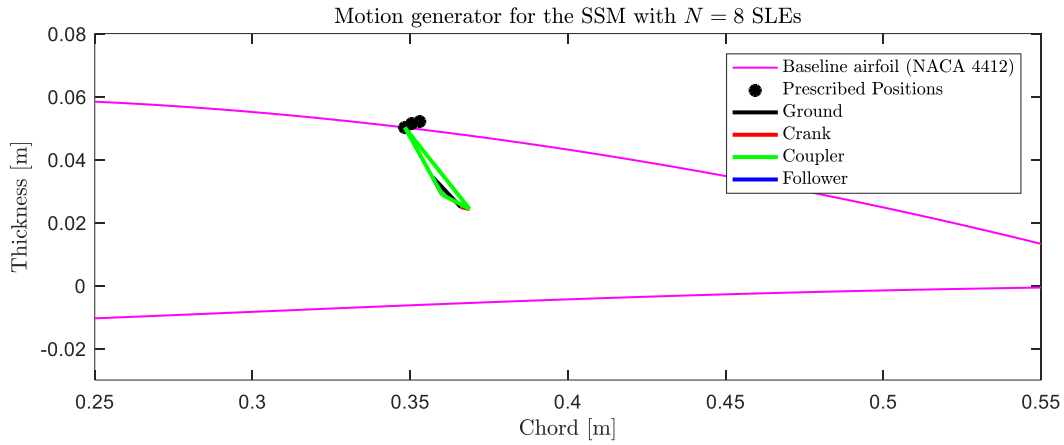

Figure 5.17: Motion Generator FB Linkage for the Proposed SSM with $N = 8$ SLEs

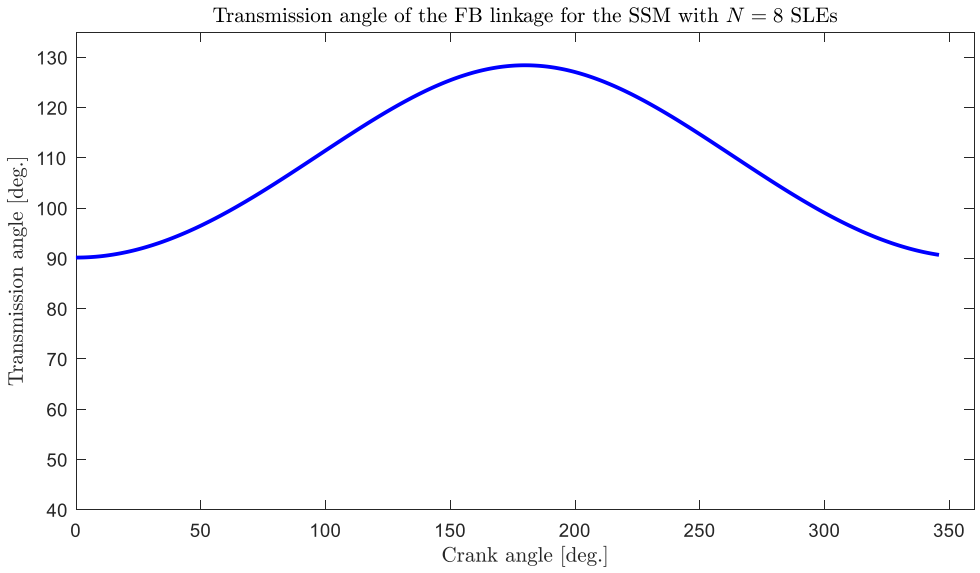

Figure 5.18: Transmission Angle Variation of the Motion Generator FB Linkage for the Proposed SSM with $N = 8$ SLEs

5.6 Kinematic Analysis of Scissor-Structural Mechanisms

In order to calculate inertial forces and moments, kinematic analysis of the SSM should be done. In Figure 5.19, angular velocities and accelerations of selected links of the proposed SSM with $N = 8$ SLEs for NACA 8412 are shown for the constant initial velocity of anchor-link $\dot{\gamma}_0 = 40$ [rpm].

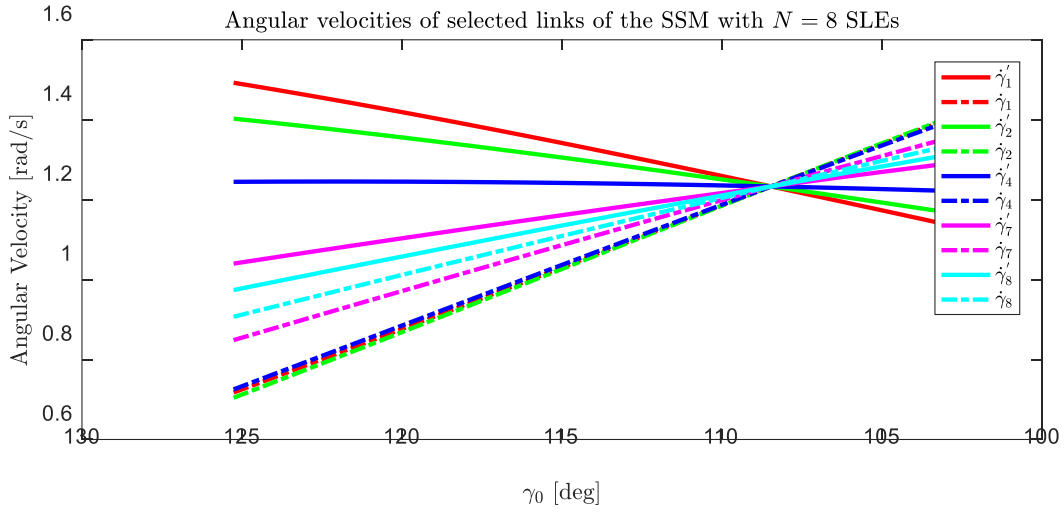

(a)

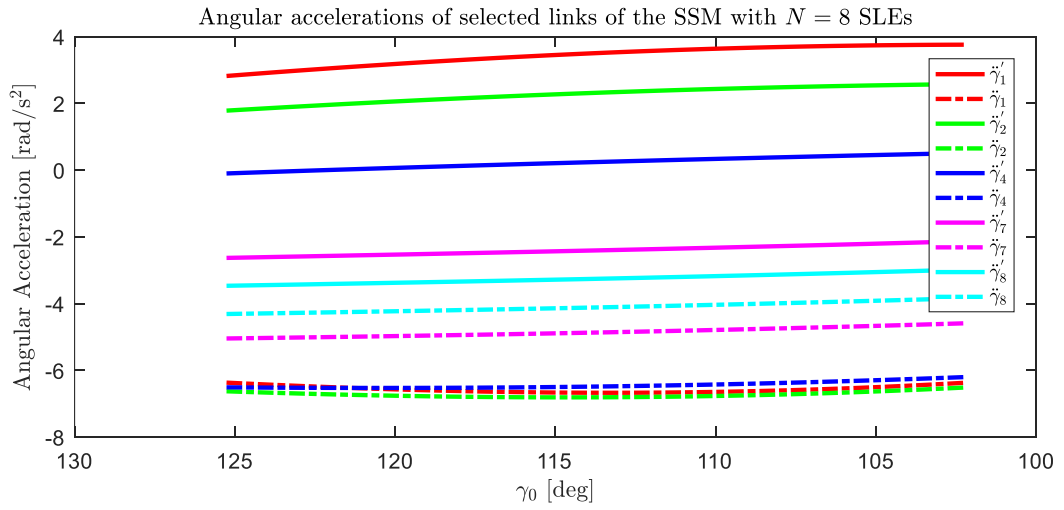

(b)

Figure 5.19: (a) Angular Velocities and (b) Angular Accelerations of the SSM with $N = 8$ SLEs for NACA 8412

Figure 5.20 shows the angular velocities and accelerations of selected links of the same mechanism, while it is turning in counter clock-wise direction in order to satisfy NACA 2412.

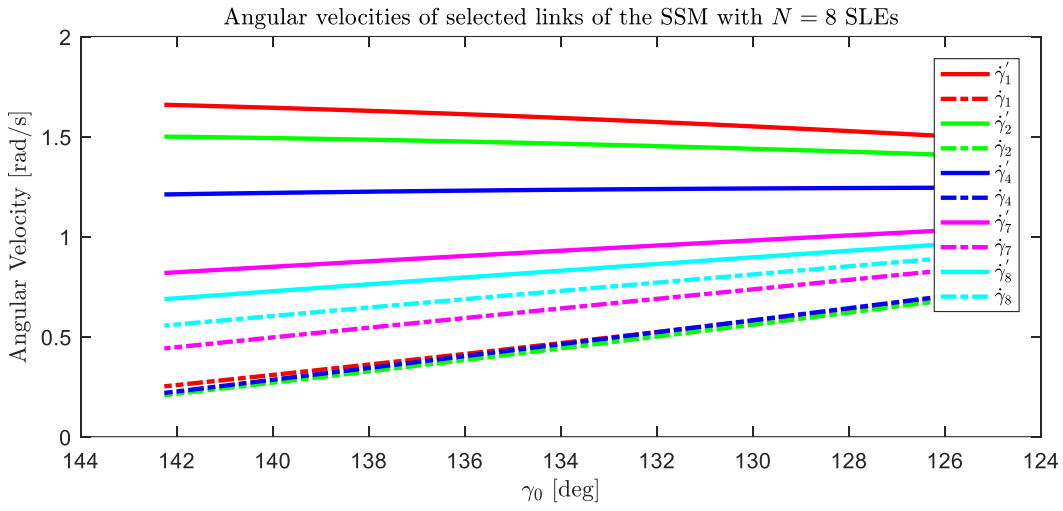

(a)

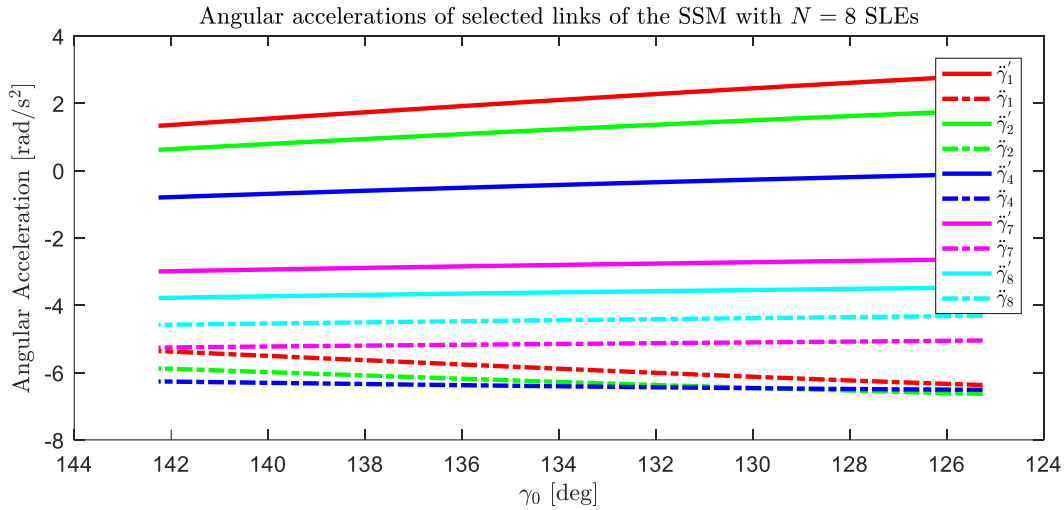

(b)

Figure 5.20: (a) Angular Velocities and (b) Angular Accelerations of the SSM with $N = 8$ SLEs for NACA 2412

Figure 5.21, Figure 5.22, Figure 5.23 and Figure 5.24 show the angular velocities and accelerations of selected links of the SSMs with $N = 4, 6, 10, 12$ SLEs respectively.

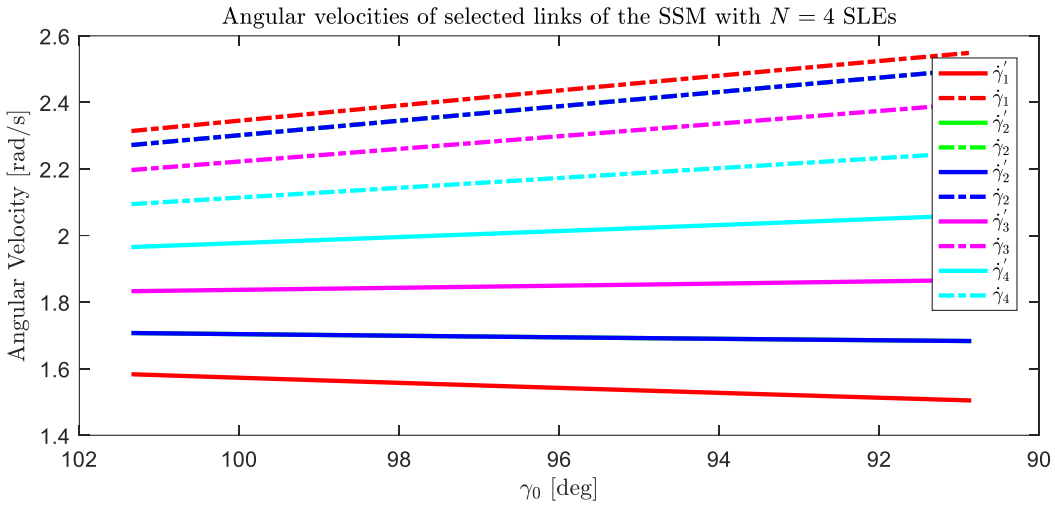

(a)

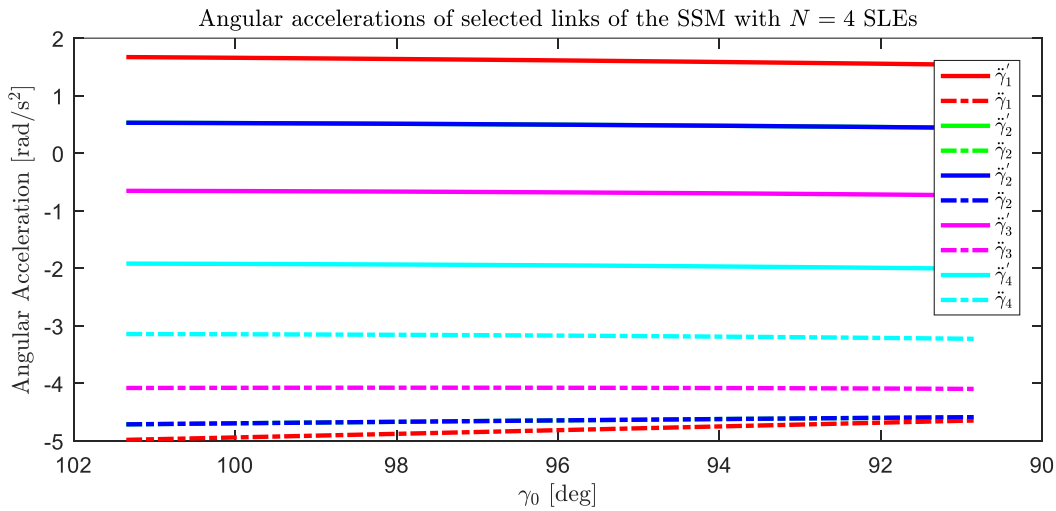

(b)

Figure 5.21: (a) Angular Velocities and (b) Angular Accelerations of the SSM with $N = 4$ SLEs for NACA 8412

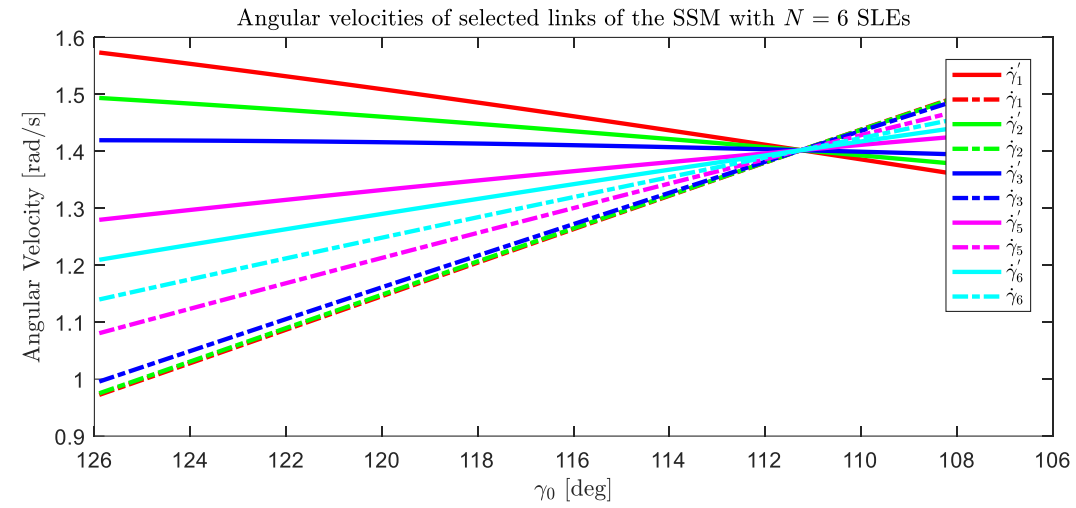

(a)

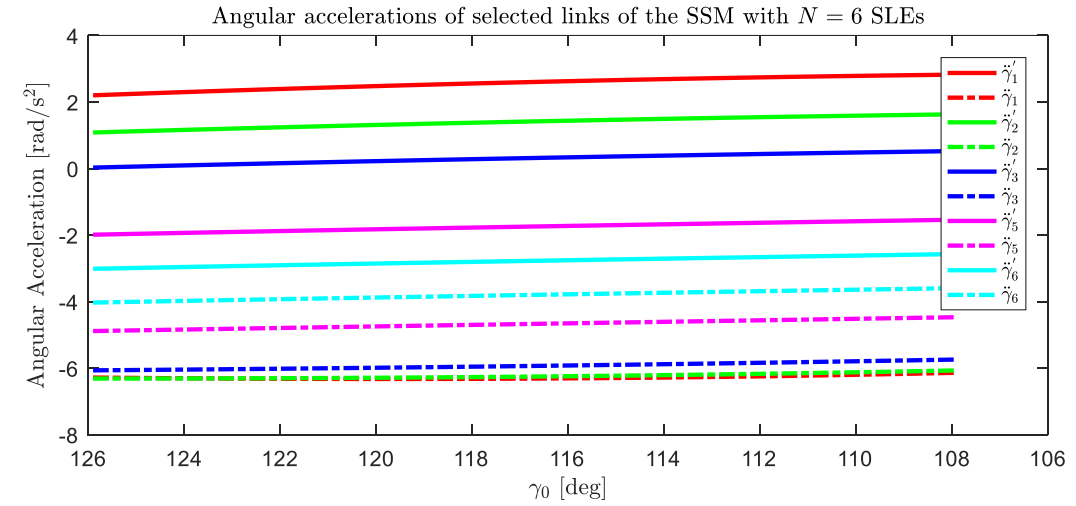

(b)

Figure 5.22: (a) Angular Velocities and (b) Angular Accelerations of the SSM with $N = 6$ SLEs for NACA 8412

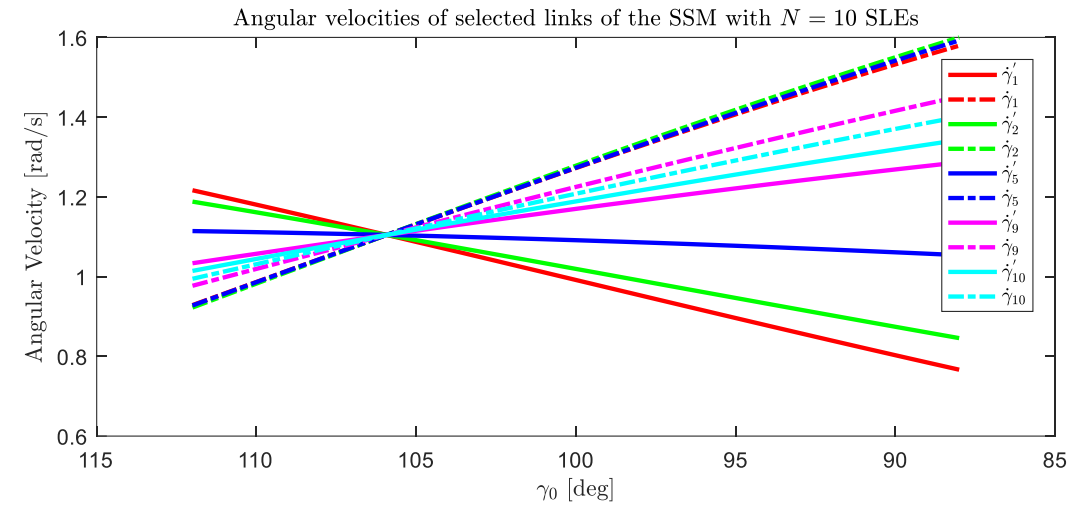

(a)

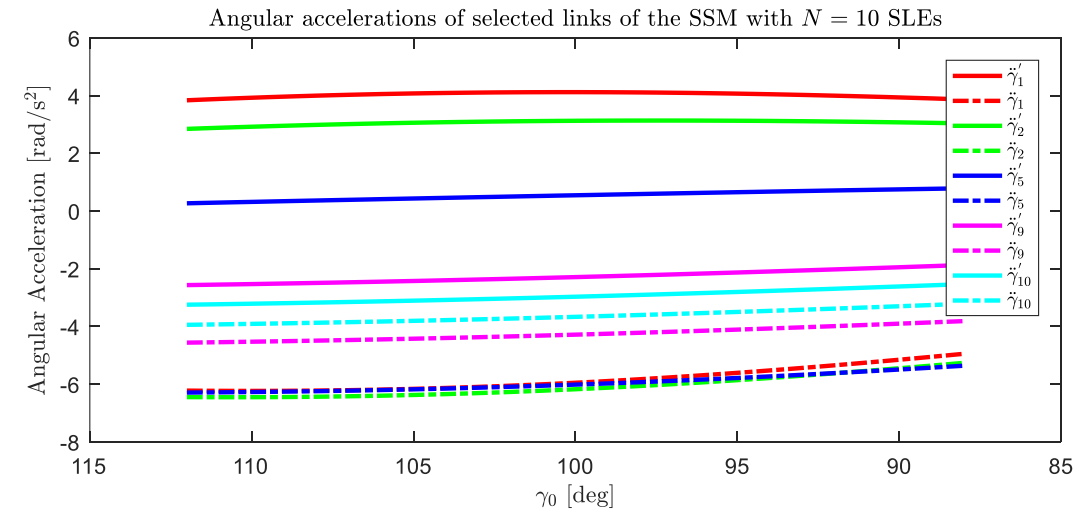

(b)

Figure 5.23: (a) Angular Velocities and (b) Angular Accelerations of the SSM with $N = 10$ SLEs for NACA 8412

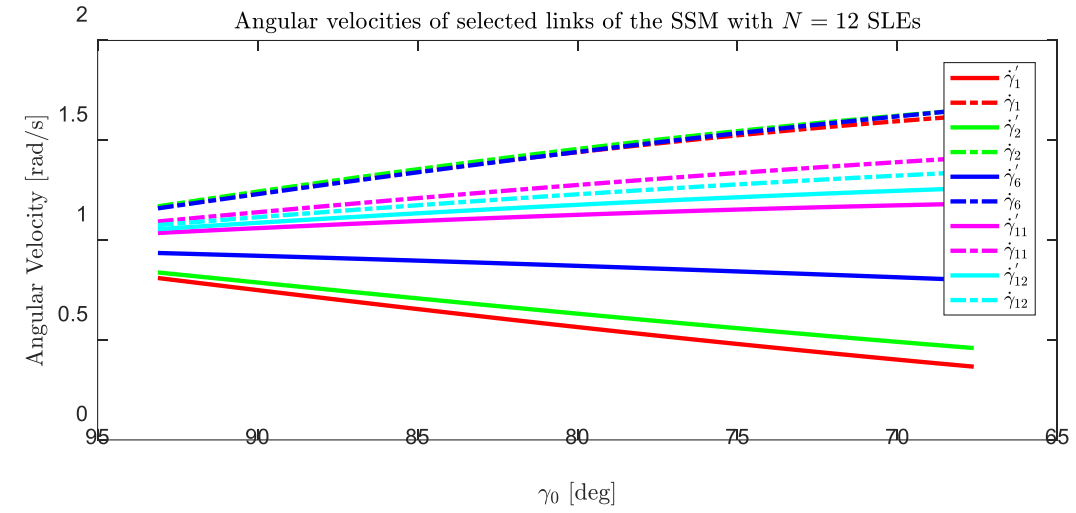

(a)

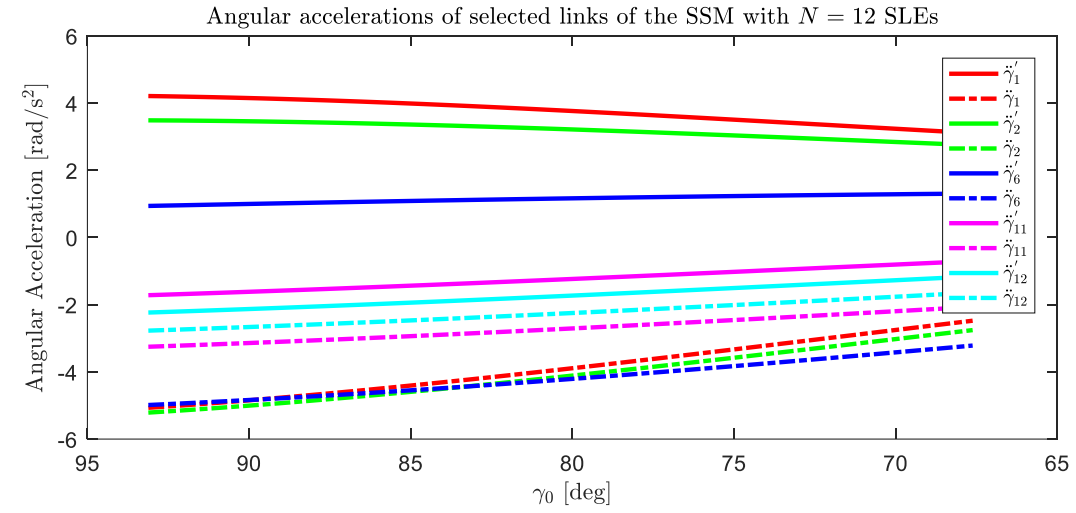

(b)

Figure 5.24: (a) Angular Velocities and (b) Angular Accelerations of the SSM with $N = 12$ SLEs for NACA 8412

In all cases, the links which are on the same side with the anchor-link, get slower while the other links are accelerating. Since the anchor-link has zero acceleration, all links have almost constant acceleration as desired and expected.

5.7 Dynamic Force Analysis of Scissor-Structural Mechanisms

Dynamic force analysis of the mechanism can be performed in two conditions which are “in in-vacuo” and “under aerodynamic loading”.

5.7.1 Dynamic Force Analysis of Scissor-Structural Mechanisms in In-Vacuo Condition

First of all, one should define masses and mass centers. For that purpose the masses of links are calculated by assuming the material of the links: aluminum with $\rho_{Al} = 2700$ $\left[\frac{kg}{m^3}\right]$. The volumes of links and their moment of inertias are calculated assuming that the links are those of rectangular beams with square cross-sections of the. Both sides of each unique element are one of eigth of airfoil thickness. The mass centers of each element are assumed to be located at their geometric centers.

In Figure 5.25, masses of SLEs of the SSM with $N = 8$ SLEs can be seen. By considering these parameters, the weight penalty of the mechanism brought to the wing is 156.5 [gr], where the weight of the aircraft is 25 [kg].

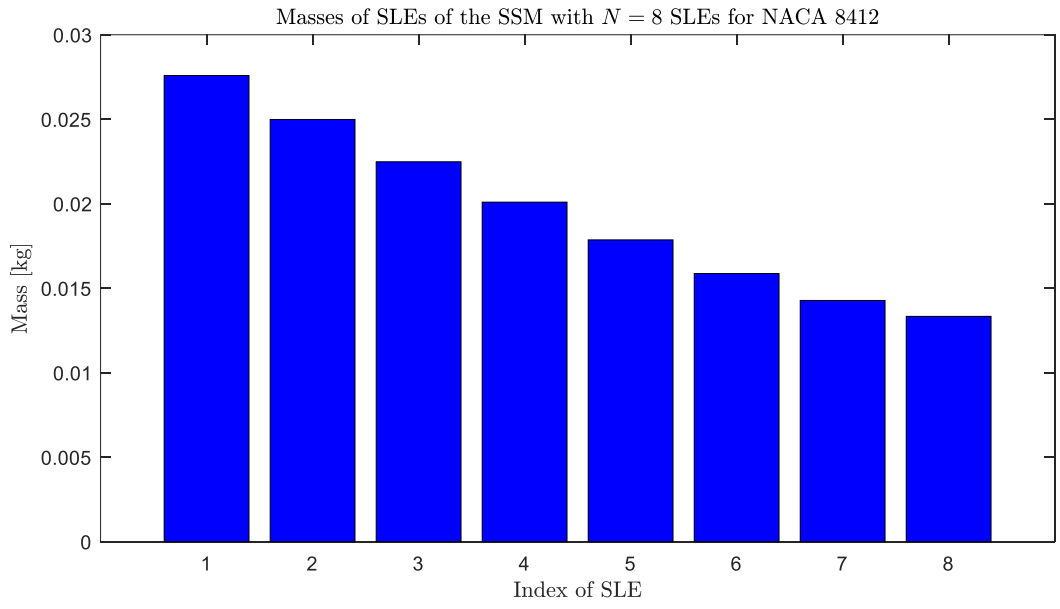

Figure 5.25: Masses of SLEs of the SSM with $N = 8$ SLEs

In Figure 5.26a, magnitudes of internal forces of selected links of the SSM with $N = 8$ SLEs for NACA 8412 are shown.

In Figure 5.26b, magnitude of required torque to drive the SSM with $N = 8$ SLEs for NACA 8412 are shown.

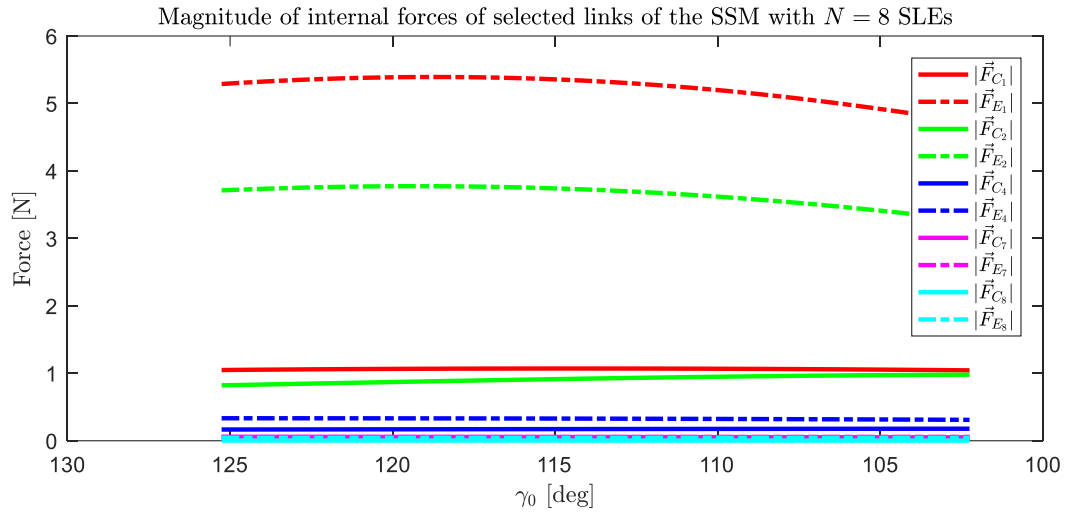

(a)

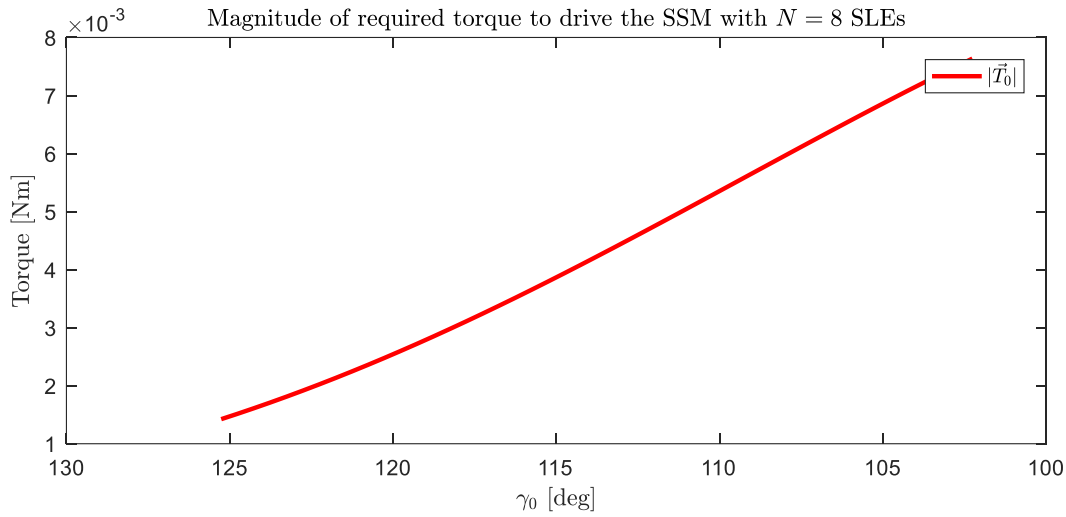

(b)

Figure 5.26: (a) Magnitude of Internal Forces of Selected Links of the SSM and (b) Magnitude of Required Torque to Drive the SSM with $N = 8$ SLEs for NACA 8412

In Figure 5.27, magnitudes of internal forces of selected links and the magnitude of required torque of the SSM with $N = 8$ SLEs for NACA 2412 are shown respectively. As seen from the figure, the mechanism requires less torque while it is adding decamber capability to the aircraft wing. This fact is true also for other SSMs. Therefore, analyzing the designed mechanisms only while they are cambering is sufficient to determine the maximum required torque value.

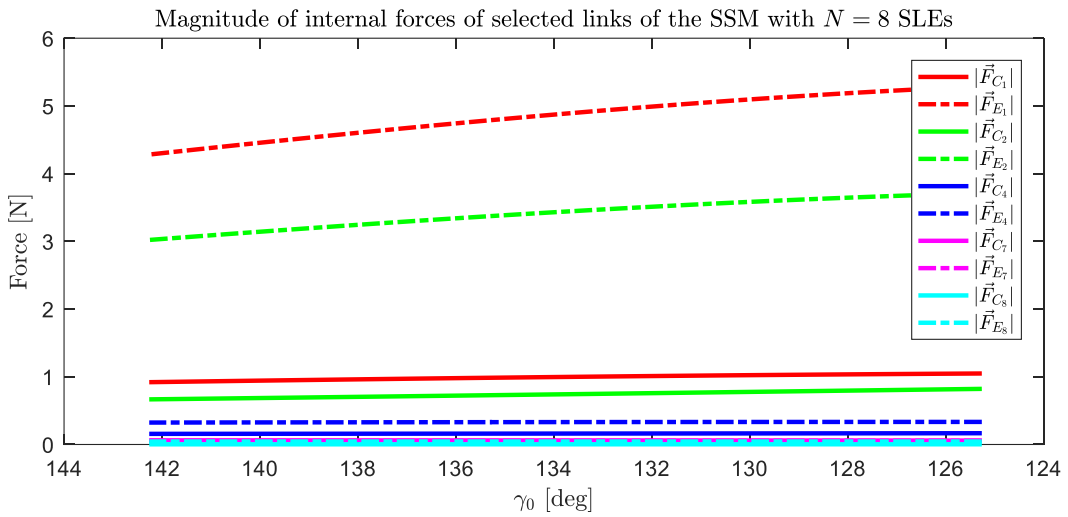

(a)

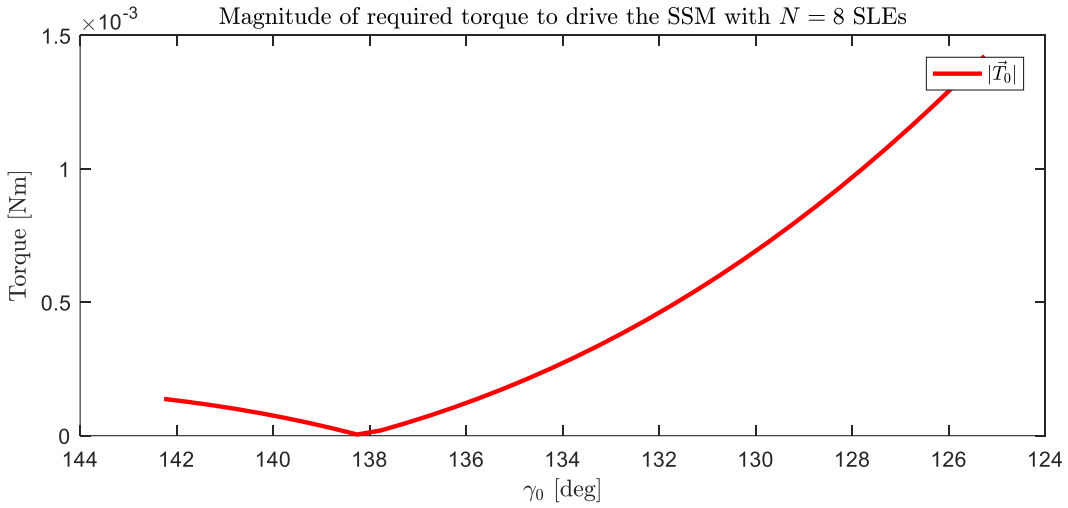

(b)

Figure 5.27: (a) Magnitude of Internal Forces of Selected Links of the SSM and (b) Magnitude of Required Torque to Drive the SSM with $N = 8$ SLEs for NACA 2412

It can be seen from figures that only the links close to the torque application have some internal forces due to the applied torque, whereas the other links carry almost zero internal forces. The main characteristics of these type of structural-mechanisms is their being of stress-strain free state. The computed very low internal forces and moments verify this. Moreover, result gives a torque value which is very low since the SSM is too light and aerodynamic loading is ignored.

In order to observe the effect of total number of used SLEs on the torque value, other SSMs have also been analyzed.

In Figure 5.28, masses of SLEs of the SSMs with $N = 4,6,10,12$ SLEs can be seen. By considering these parameters, the weight penalty of the mechanisms brought to the wing are 120.8 [gr], 137.5 [gr], 176.3 [gr], 196.6 [gr] respectively. As expected, increase in total number of used SLEs increases the weigth of the wing.

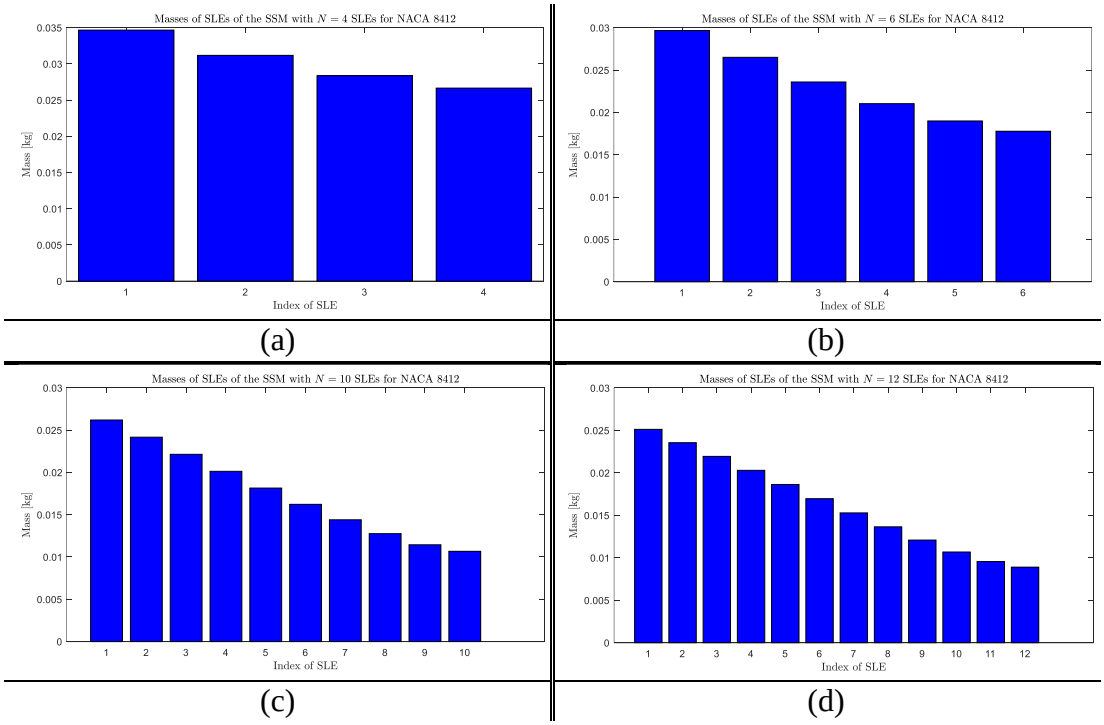

Figure 5.28: Masses of SLEs of the SSM with (a) $N = 4$ SLEs, (b) $N = 6$ SLEs, (c) $N = 10$ SLEs, (d) $N = 12$ SLEs

Figure 5.29, Figure 5.30, Figure 5.31 and Figure 5.32 show magnitudes of internal forces of selected links and the magnitude of required torque of the SSMs with $N =$ 4,6,10,12 SLEs in in-vacuo condition respectively.

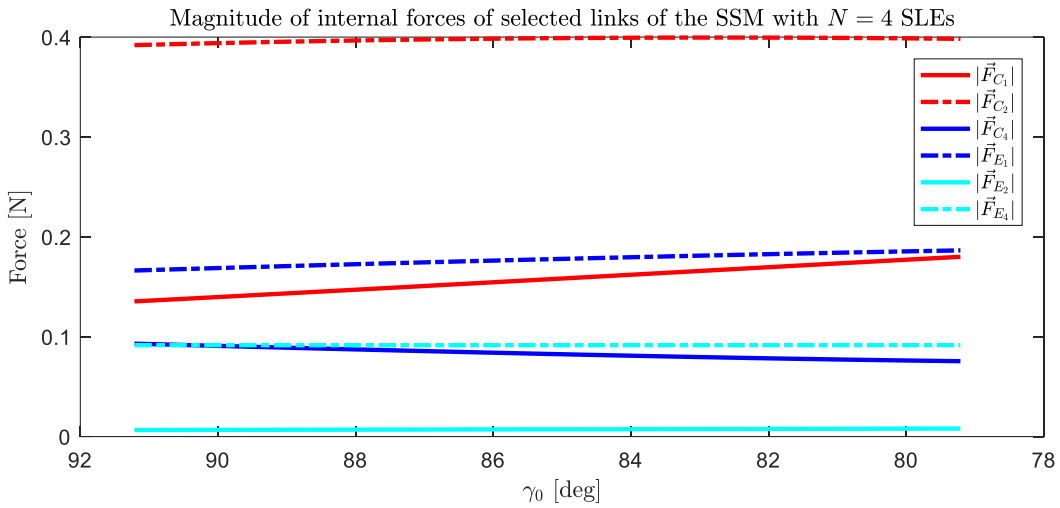

(a)

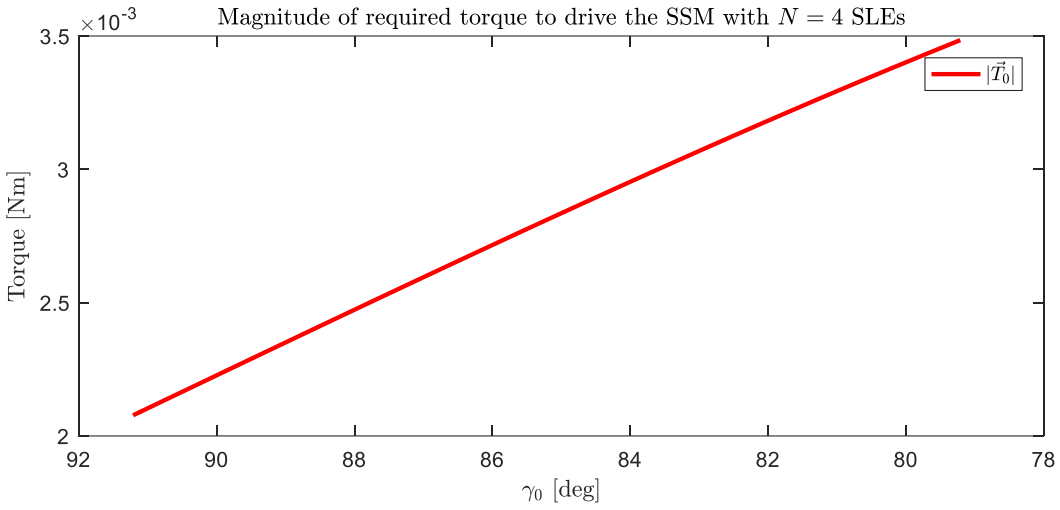

(b)

Figure 5.29: (a) Magnitude of Internal Forces of Selected Links of the SSM and (b) Magnitude of Required Torque to Drive the SSM with $N = 4$ SLEs for NACA 8412

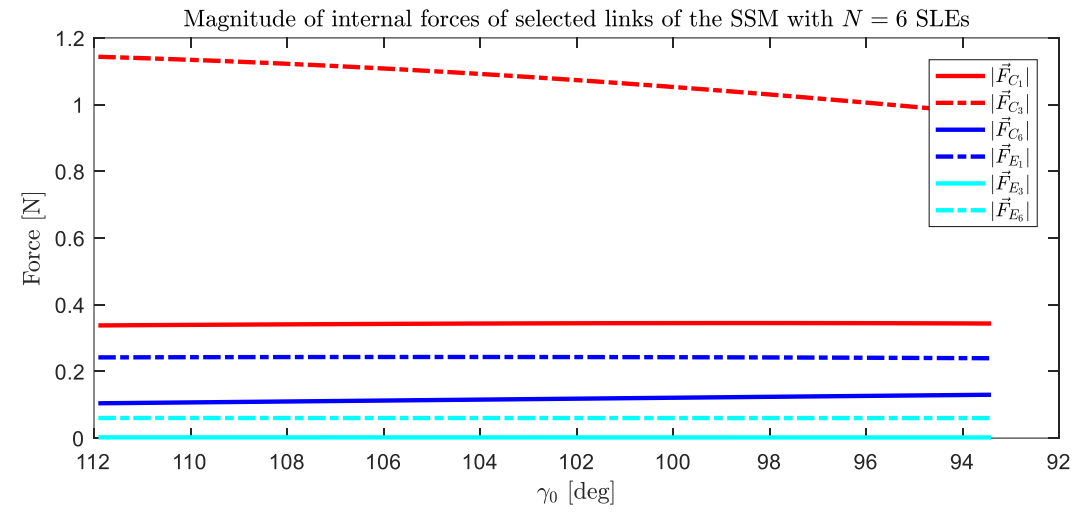

(a)

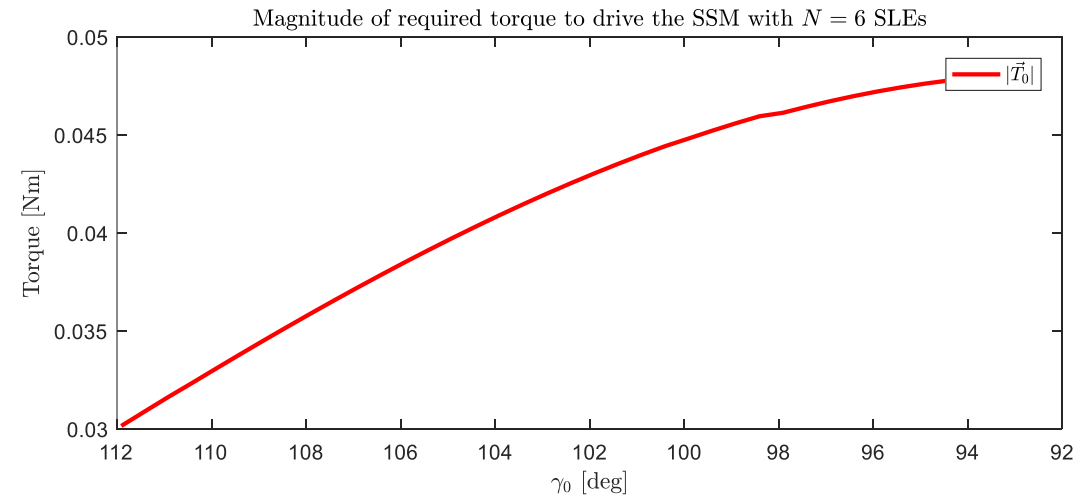

(b)

Figure 5.30: (a) Magnitude of Internal Forces of Selected Links of the SSM and (b) Magnitude of Required Torque to Drive the SSM with $N = 6$ SLEs for NACA 8412

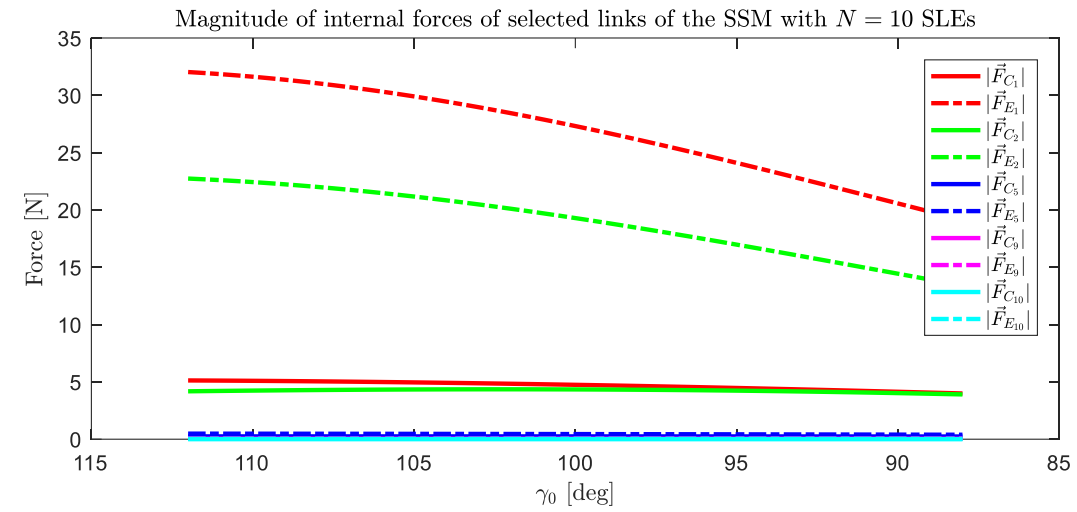

(a)

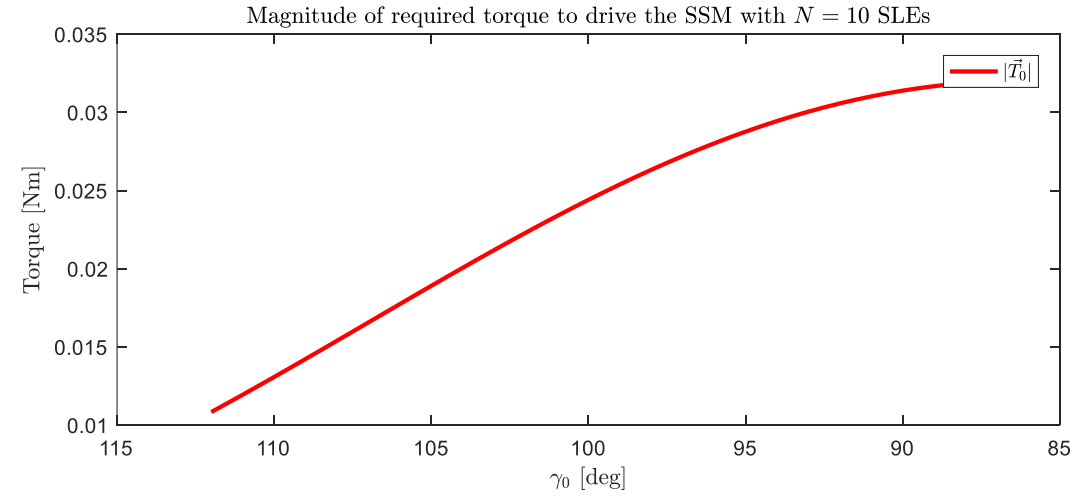

(b)

Figure 5.31: (a) Magnitude of Internal Forces of Selected Links of the SSM and (b) Magnitude of Required Torque to Drive the SSM with $N = 10$ SLEs for NACA 8412

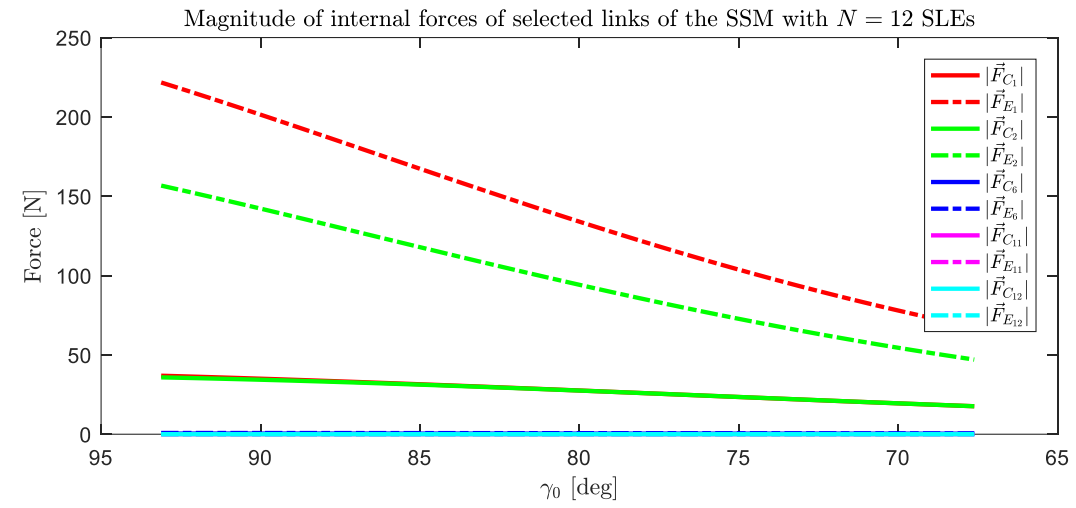

(a)

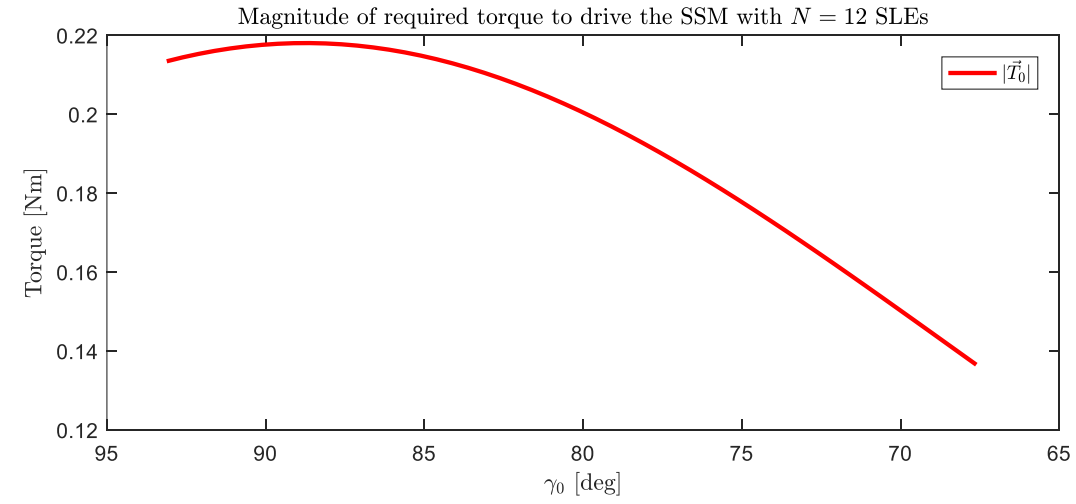

(b)

Figure 5.32: (a) Magnitude of Internal Forces of Selected Links of the SSM and (b) Magnitude of Required Torque to Drive the SSM with $N = 12$ SLEs for NACA 8412

As the total number of used SLEs is increasing, the required torque values increases, but for the case $N = 12$ the torque values decreased a bit. That's why the total weight of the SSM, which helps to the motion of the mechanism while cambering. From all figures, one can conclude that all required torque values are below 0.35 [Nm]. This value found to be lower than /he torque value of compared design of the project CHANGE (0.4 [Nm]) [102], and further verifies the results of the study.

5.7.2 Dynamic Force Analysis of Scissor-Structural Mechanisms Under Aerodynamic Loading

Calculated pressure coefficient distribution of the surface formed by the SSM can be used to estimate required torque to drive the SSM under aerodynamic loading. In order to convert the C_p into nodal forces on the upper and lower surface hinge locations of the SSM, sea level properties of the air are used. Air velocity is assumed as 0.2 Mach. For the simplicity of the problem, a single C_p distribution is used for all poses of the SSM.

In Figure 5.33, magnitudes of internal forces of selected links and the magnitude of required torque of the SSM with $N = 8$ SLEs for NACA 8412 are shown respectively. As seen from the figure, the mechanism requires much more torque when the pressure distribution over the wing is considered.

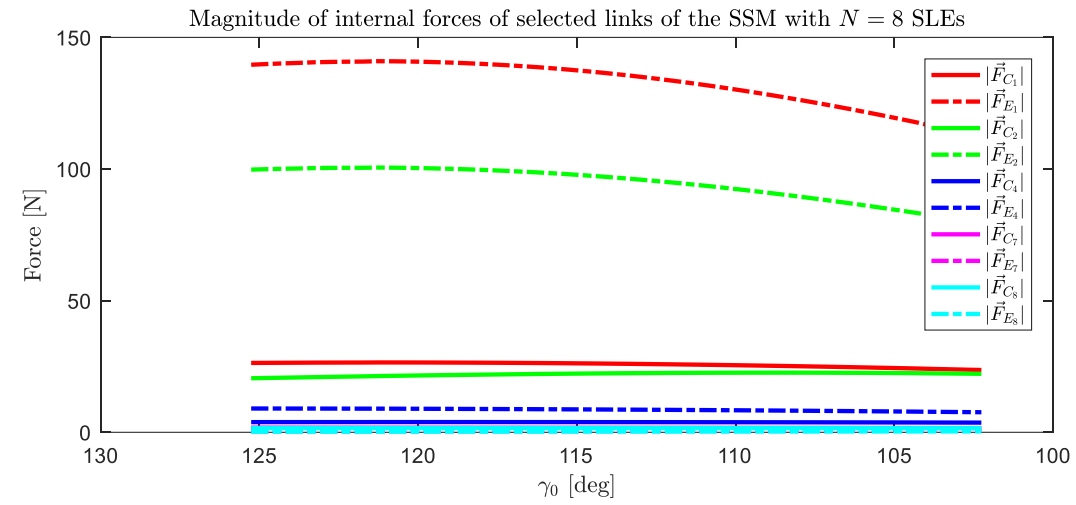

(a)

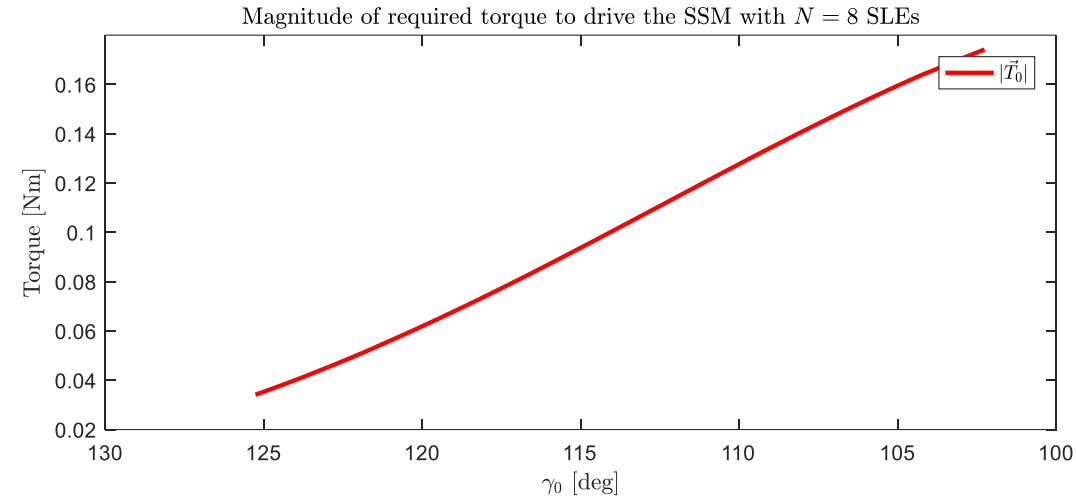

(b)

Figure 5.33: (a) Magnitude of Internal Forces of Selected Links of the SSM and (b) Magnitude of Required Torque to Drive the SSM with $N = 8$ SLEs for NACA 8412

Figure 5.34, Figure 5.35, Figure 5.36 and Figure 5.37 show magnitudes of internal forces of selected links and the magnitude of required torque of the SSMs with $N =$ 4,6,10,12 SLEs under aerodynamic loading respectively.

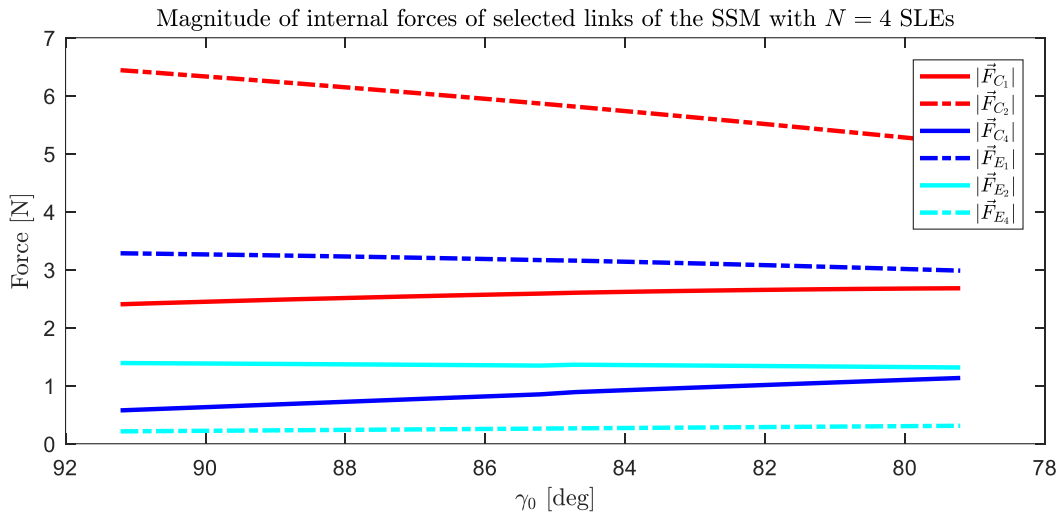

(a)

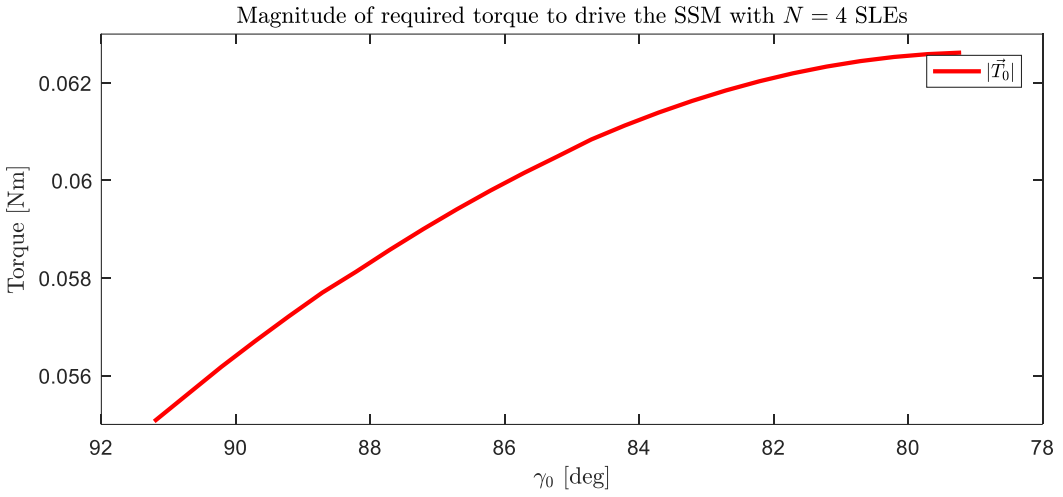

(b)

Figure 5.34: (a) Magnitude of Internal Forces of Selected Links of the SSM and (b) Magnitude of Required Torque to Drive the SSM with $N = 4$ SLEs for NACA 8412

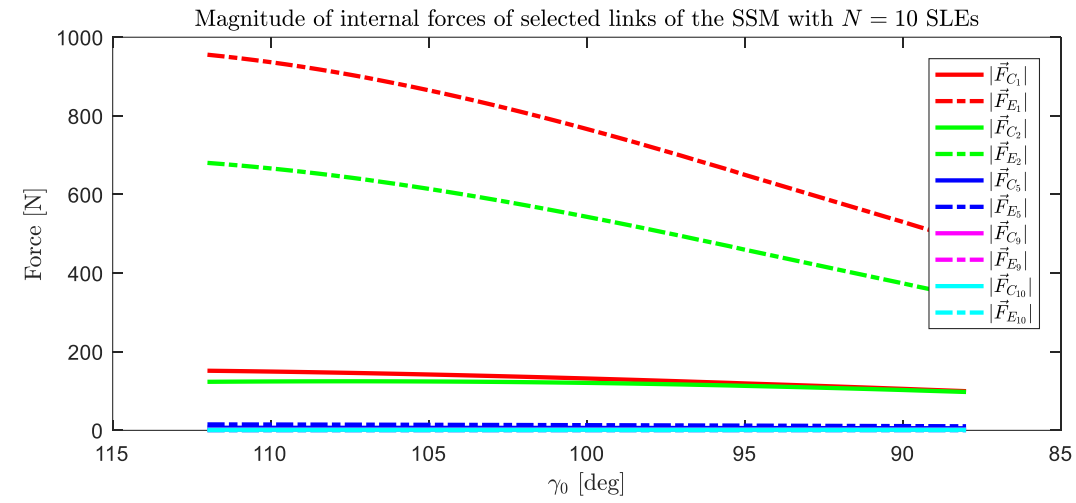

(a)

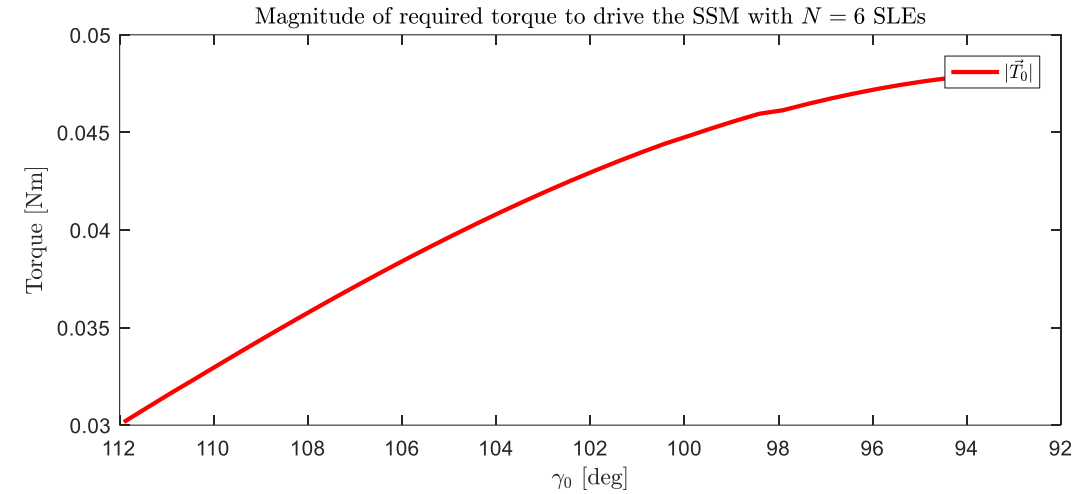

(b)

Figure 5.35: (a) Magnitude of Internal Forces of Selected Links of the SSM and (b) Magnitude of Required Torque to Drive the SSM with $N = 6$ SLEs for NACA 8412

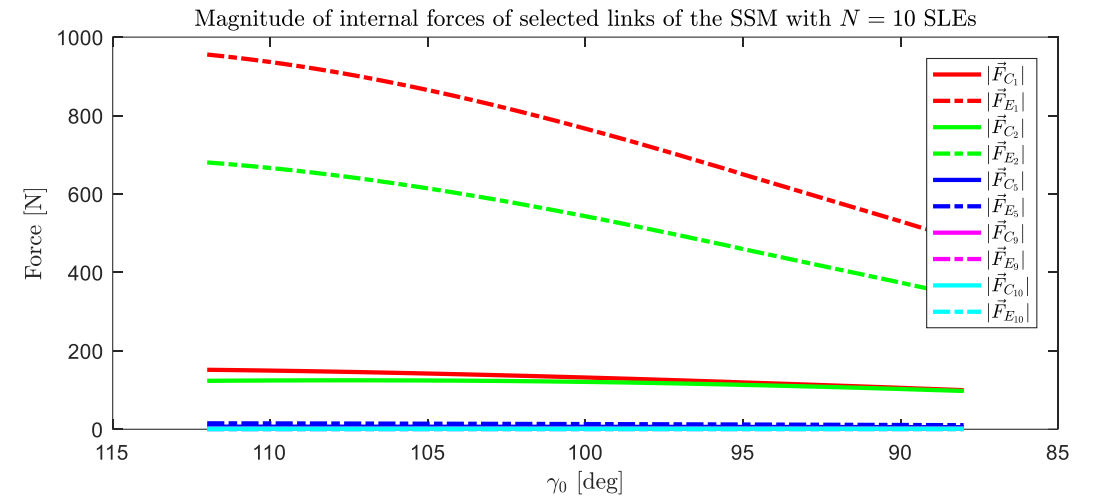

(a)

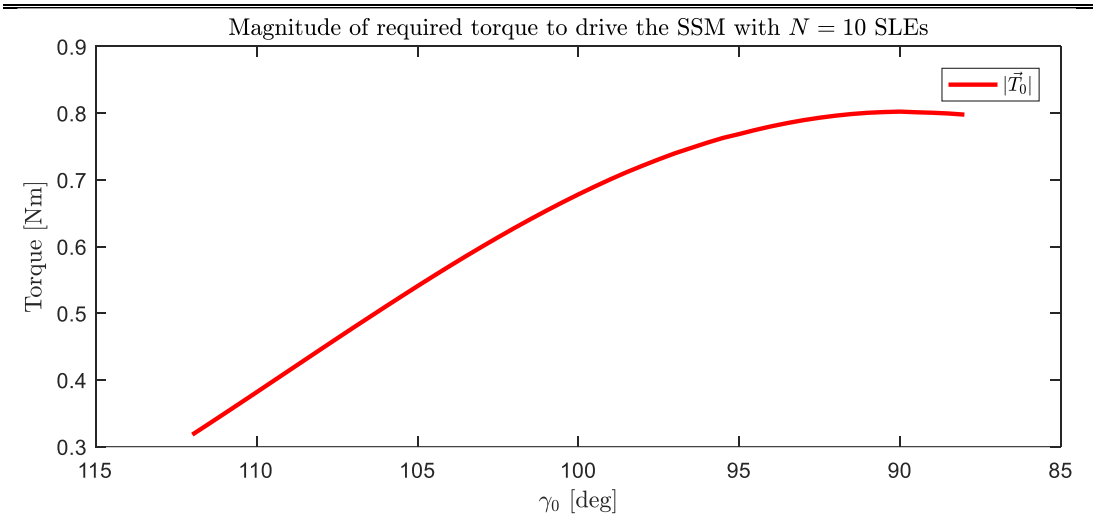

(b)

Figure 5.36: (a) Magnitude of Internal Forces of Selected Links of the SSM and (b) Magnitude of Required Torque to Drive the SSM with $N = 10$ SLEs for NACA 8412

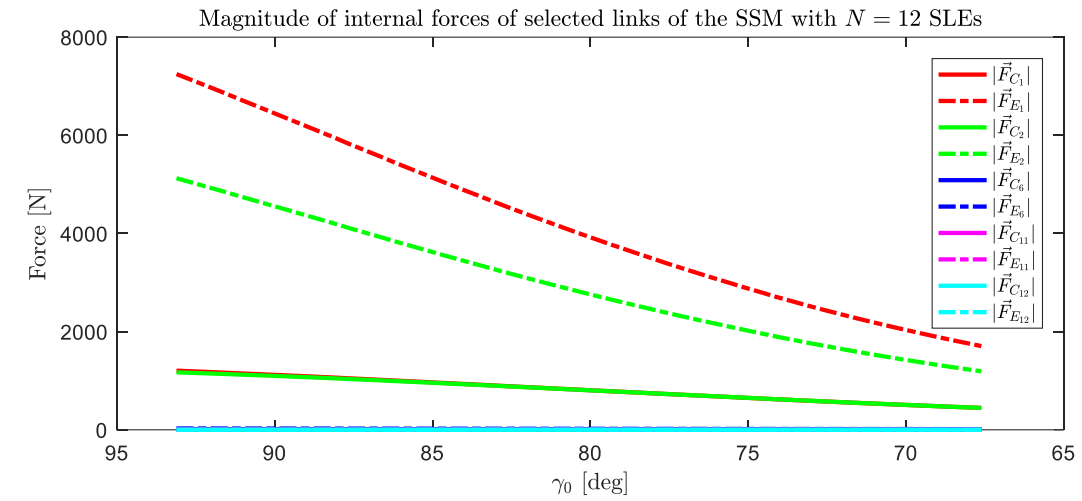

(a)

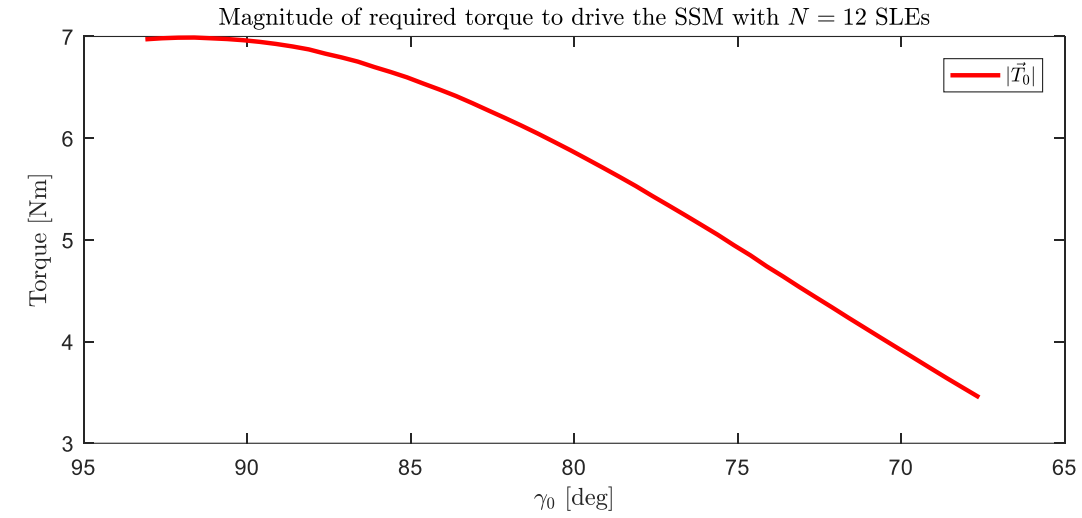

(b)

Figure 5.37: (a) Magnitude of Internal Forces of Selected Links of the SSM and (b) Magnitude of Required Torque to Drive the SSM with $N = 12$ SLEs for NACA 8412

From all figures, one can conclude that all required torque values increase dramatically when the pressure distribution is included into the analyses. Similarly, as the total number of used SLEs is increasing, the required torque values increases.

5.8 Discussion and Conclusion

In Chapter 5, the results obtained from the developed computer-routine are presented. Elapsed time of the computer-routine for a single result around 1 minute. Therefore, any optimization, if it is included, may be expensive in terms of time. This chapter also summarizes the results of SSMs' effects on wing skin and aerodynamic performances. Kinematic analysis of the SSMs have also been presented in this chapter in order to predict inertial forces and moments. This chapter ends with dynamic force analysis of the proposed SSMs in order to predict required torque to drive the SSM, both in in-vacuo conditions and under aerodynamic loading.

CHAPTER 6

CONCLUSION

6.1 General Conclusions

In this thesis, synthesis, analysis and design of a special type of deployable mechanism, which is scissor-structural mechanism (SSM), for morphing of the trailing edge of an aircraft wing is presented. Assuming that the wing skin is fully compliant, a novel mechanism for the morphing of trailing edge of an aircraft wing is synthesized. In order to satisfy the mobility requirements, a FB linkage mechanism is assumed to be attached to the designed SSM which is represented in the results by only anchor-link.

First of all, a computer-routine, which synthesizes, analyzes and design a SSM in order to morph two different 2D curves into another shape, is developed. This computer-routine does not include any optimization; however, user is free to specify many input parameters in order to get a good result.

In this thesis, those 2D curves are selected from 4-digit NACA airfoils. With developed computer-routine, those NACA airfoils are morphed into another NACA airfoils which have different camber rates and chord lengths. Although, the results are not optimized, desired NACA airfoils are satisfied with designed SSMs with less than 0.25% mean design errors.

SSMs effect the wing skin by stretching or shrinking the skin. In order to avoid any slack of the wing skin, wing skin should be in tension. However, two of five SSMs shrink the wing skin, because the SSMs are designed to satisfy the airfoils having almost the same chord length. The results show that in order to avoid slack of the wing

skin, chord length of the wing skin should also be morphed and developed computer-routine allows this.

Since designed SSMs afford the target profiles with little mean design errors, in order to ensure the aerodynamic performance of the surface formed by SSMs, the profiles obtained from proposed mechanisms are modelled and analyzed aerodynamically with the XFOIL. The obtained results are compared with NACA airfoils. The results show that surfaces formed by SSMs for each case nearly produce the same pressure distribution and drag with target airfoil profiles, except the location where the anchor-link is attached to the SSMs. This exception causes little lift penalty and result in 10% less lift. This fact is a drawback but the proposed SSMs have the capability to obtain high camber rates, so they can also generate higher lifts than NACA airfoils.

Furthermore, kinematic analysis, including velocity and acceleration analyses, have been undertaken in order to determine the inertial forces and moments. If the SSM is driven with constant angular velocity, the whole mechanism deploys with almost constant acceleration as expected. For less fluctuation in inertial forces and moments, the SSM should be driven with constant and low RPMs.

The dynamic force analysis of the designed SSM have also been performed in order to compute the required torque value necessary for driving the whole SSM. Aerodynamic loading increases the torque requirement tenfold. Moreover, computations show that using large number of SLEs causes extra weight and leads to more torque requirements. Hence, using $N = 6, 8, 10$ SLEs are more appropriate, which is another outcome of the thesis.

6.2 Recommendations for Future Work

This study focuses on synthesis, analysis and design of scissor-structural mechanisms for morphing of the trailing edge of an aircraft wing. For that purpose, a computer-routine that synthesize a SSM and FB linkage is developed, in order to help designers in the conceptual design phase.

Since this thesis presents a novel method in order to morph 2D shapes, this method can be enriched by implementing an optimization tool, a structural-dynamics tool, a

2D FEM tool in order to predict more reasonable solutions. Optimization tool can help users to determine the best mechanism in terms of mean design error, effect on wing skin, aerodynamic performance and required torque. Since all parts of the mechanism are considered as rigid, a module for the structural dynamics of the mechanism can also be helpful, whereas a 2D FEM tool helps to predict equivalent stresses and reasonably design of mechanism links.

Since complete design of aircraft wing is not considered, performance of the SSM with the whole wing can be researched. Therefore, a detailed design of the trailing edge of an aircraft wing, including the necessary electrical equipment of servo actuators such as cabling, battery selection and placement of these equipment can also be considered.

SSMs can also be used to morph the leading edge of the aircraft wing, wing twist and span morphing. Therefore, morphing via SSMs can be a can be a strong alternative to conventional aircraft wings.

REFERENCES

[1] S. Barbarino, O. Bilgen, R. M. Ajaj, M. I. Friswell, and D. J. Inman, "A Review of Morphing Aircraft," *J. Intell. Mater. Syst. Struct.*, vol. 22, no. 9, pp. 823–877, 2011.

[2] "Info NIAC," 2009. [Online]. Available: http://www.infoniac.com/science/researchers-analyze-birds-to-develop-wing-flapping-robotic-aircraft.html. [Accessed: 13-Jun-2018].

[3] "Animals Mix," 2018. [Online]. Available: https://www.animalsmix.com/animals/gliding-bird-animals-43ecce.html. [Accessed: 13-Jun-2018].

[4] "Dreams Metroeve," 2017. [Online]. Available: http://www.dreams.metroeve.com/kingfisher/#.WyF2o0iFN3g. [Accessed: 13-Jun-2018].

[5] K. McDonald, "UC San Diego News CEnter," 2016. [Online]. Available: https://ucsdnews.ucsd.edu/pressrelease/scientists_determine_how_birds_soar_to_great_heights. [Accessed: 13-Jun-2018].

[6] J. H. S. Fincham, R. M. Ajaj, and M. I. Friswell, "Aerodynamic performance of corrugated skins for spanwise wing morphing," in *14th AIAA Aviation Technology, Integration, and Operations Conference*, 2014, no. June, pp. 1–14.

[7] B. Woods, J. H. S. Fincham, and M. I. Friswell, "Aerodynamic Modelling of the Fish Bone Active Camber Morphing Concept Aerodynamic Modelling of the Fish Bone Active Camber Morphing Concept," in *RAeS Applied Aerodynamics Conference*, 2014, no. July.

[8] "Cambridge Dictionary," 2018. [Online]. Available: https://dictionary.cambridge.org/tr/sözlük/ingilizce/morph?q=morphing. [Accessed: 23-Jul-2018].

[9] J. H. S. Fincham and M. I. Friswell, "Aerodynamic optimisation of a camber morphing aerofoil," *Aerosp. Sci. Technol.*, vol. 43, pp. 245–255, 2015.

[10] K. R. Olympio and F. Gandhi, "Flexible skins for morphing aircraft using cellular honeycomb cores," *J. Intell. Mater. Syst. Struct.*, vol. 21, no. 17, pp. 1719–1735, 2010.

[11] A. Y. N. Sofla, S. A. Meguid, K. T. Tan, and W. K. Yeo, "Shape morphing of aircraft wing: Status and challenges," *Mater. Des.*, vol. 31, no. 3, pp. 1284–1292, 2010.

[12] I. H. Abbott and A. E. Von Doenhoff, "Theory of Wing Sections: Including a Summary of Airfoil data," *Press*, 1959.

[13] D. P. Raymer, *Aircraft Design: A Conceptual Approach Fourth Edition*. 2006.

[14] S. Murugan, B. K. S. Woods, and M. I. Friswell, "Hierarchical modeling and optimization of camber morphing airfoil," *Aerosp. Sci. Technol.*, vol. 42, pp. 31–38, 2015.

[15] V. Giurgiutiu, Z. Chaudhry, and C. Rogers, "Active control of helicopter rotor blades with induced strain actuators," in *Adaptive Structures Forum*, American Institute of Aeronautics and Astronautics, 1994.

[16] J. D. Anderson, "Introduction to Flight." p. 814, 2005.

[17] F. E. C. Culick, “The Wright Brothers: First Aeronautical Engineers and Test Pilots,” *AIAA J.*, 2003.
[18] H. F. Parker, “Variable-Camber Rib for Aeroplane-Wings,” 1,341,758, 1920.
[19] E. V. Crowell and W. Hawkins, “Aeroplane-Wing Construction,” 1,412,455, 1922.
[20] L. W. Bonney, “Aeroplane Control,” 1,710,672, 1929.
[21] L. W. Bonney, “Aeroplane Wing or Aerofoil Structure,” 1,710,673, 1929.
[22] J. F. Cook, “Aerofoil,” 1,766,107, 1930.
[23] R. C. Stroop, “Airplane Appliance,” 1,823,069, 1931.
[24] U. Antoni, “Construction of Flexible Aeroplane Wings Having a Variable Profile,” 1,886,362, 1932.
[25] C. H. Grant, “Airfoil,” 2,022,806, 1935.
[26] J. Fresco, “Variable Camber Wing,” 2,410,056, 1946.
[27] G. D. Bryant and A. W. Stewart, “Variable-Camber Airfoil,” 3,109,613, 1963.
[28] E. M. Wright, “Variable Camber Airfoil,” 3,332,383, 1967.
[29] J. B. Cole, “Variable Camber Airfoil,” 4,053,124, 1977.
[30] E. J. Zapel, “Variable Camber Trailing Edge for Airfoil,” 4,131,253, 1978.
[31] P. L. Bishay, “2016-17 CSUN’s Smart Morphing Wing Senior Design Project,” 2018. [Online]. Available: http://www.csun.edu/~pbishay/projects.php. [Accessed: 17-Aug-2018].
[32] H. Takahashi, T. Yokozeki, and Y. Hirano, “Development of variable camber wing with morphing leading and trailing sections using corrugated structures,” *J. Intell. Mater. Syst. Struct.*, vol. 27, no. 20, pp. 2827–2836, Apr. 2016.
[33] D. Kumar, S. F. Ali, and A. Arockiarajan, “Structural and Aerodynamics Studies on Various Wing Configurations for Morphing,” *IFAC-PapersOnLine*, vol. 51, no. 1, pp. 498–503, 2018.
[34] “FlexFoil™ Compliant Control Surfaces.” [Online]. Available: https://www.flxsys.com/flexfoil. [Accessed: 17-Aug-2018].
[35] B. K. Woods and M. I. Friswell, “Structural Characterization of the Fish Bone Active Camber Morphing Airfoil,” in *22nd AIAA/ASME/AHS Adaptive Structures Conference*, 2014.
[36] R. Pecora, F. Amoroso, and M. Magnifico, “Toward the bi-modal camber morphing of large aircraft wing flaps: the CleanSky experience,” in *Industrial and Commercial Applications of Smart Structures Technologies 2016*, 2016, vol. 9801, pp. 980106–980112.
[37] L. F. Campanile and S. Anders, “Aerodynamic and aeroelastic amplification in adaptive belt-rib airfoils,” *Aerosp. Sci. Technol.*, vol. 9, no. 1, pp. 55–63, 2005.
[38] K. Zhao, J. P. Schmiedeler, and A. P. Murray, “Design of Planar, Shape-Changing Rigid-Body Mechanisms for Morphing Aircraft Wings,” *J. Mech. Robot.*, vol. 4, no. 4, pp. 41007–41010, Sep. 2012.
[39] J. D. Bartley-Cho, D. P. Wang, C. A. Martin, J. N. Kudva, and M. N. West, “Development of High-rate, Adaptive Trailing Edge Control Surface for the Smart Wing Phase 2 Wind Tunnel Model,” *J. Intell. Mater. Syst. Struct.*, vol. 15, no. 4, pp. 279–291, Apr. 2004.
[40] S. Ricci, “Advanced course on morphing aircraft, Lisbon, Portugal,” 2008. [Online]. Available: https://cordis.europa.eu/event/rcn/29940_en.html.

[Accessed: 17-Aug-2018].
[41] R. Wu, C. Soutis, S. Zhong, and A. Filippone, “A morphing aerofoil with highly controllable aerodynamic performance,” *Aeronaut. J.*, vol. 121, no. 1235, pp. 54–72, 2017.
[42] S. Vasista, L. Tong, and K. C. Wong, “Realization of Morphing Wings: A Multidisciplinary Challenge,” *J. Aircr.*, vol. 49, no. 1, pp. 11–28, 2012.
[43] B. A. Grohmann *et al.*, “Multidisciplinary Design and Optimization of Active Trailing Edge for Smart Helicopter Rotor Blade,” *Mech. Adv. Mater. Struct.*, vol. 15, no. 3–4, pp. 307–324, Apr. 2008.
[44] K. K. Maute and G. W. Reich, “Integrated Multidisciplinary Topology Optimization Approach to Adaptive Wing Design,” *J. Aircr.*, vol. 43, no. 1, pp. 253–263, Jan. 2006.
[45] G. Molinari, A. F. Arrieta, M. Guillaume, and P. Ermanni, “Aerostructural Performance of Distributed Compliance Morphing Wings: Wind Tunnel and Flight Testing,” *AIAA J.*, vol. 54, no. 12, pp. 0–0, 2016.
[46] J.-S. Bae, N.-H. Kyong, T. M. Seigler, and D. J. Inman, “Aeroelastic Considerations on Shape Control of an Adaptive Wing,” *J. Intell. Mater. Syst. Struct.*, vol. 16, no. 11–12, pp. 1051–1056, Dec. 2005.
[47] J. N. Kudva, “Overview of the DARPA Smart Wing Project,” *J. Intell. Mater. Syst. Struct.*, vol. 15, no. 4, pp. 261–267, Apr. 2004.
[48] S. . Thornton, “Reduction of Structural Loads Using Maneuver Load Control on the Advanced Fighter Technology Integration (AFTI)/F-111 Mission Adaptive Wing,” 1993.
[49] J. SZODRUCH, “The influence of camber variation on the aerodynamics of civil transport aircraft,” in *23rd Aerospace Sciences Meeting*, American Institute of Aeronautics and Astronautics, 1985.
[50] S. B. Smith and D. W. Nelson, “Determination of the aerodynamic characteristics of the mission adaptive wing,” *J. Aircr.*, vol. 27, no. 11, pp. 950–958, Nov. 1990.
[51] A. L. Martins and F. M. Catalano, “Drag optimization for transport aircraft Mission Adaptive Wing ,” *Journal of the Brazilian Society of Mechanical Sciences and Engineering* , vol. 25. scielo , pp. 1–8, 2003.
[52] M. Siclari, W. Van Nostrand, and F. Austin, “The design of transonic airfoil sections for an adaptive wing concept using a stochastic optimization method,” in *34th Aerospace Sciences Meeting and Exhibit*, American Institute of Aeronautics and Astronautics, 1996.
[53] K. Smith, J. Butt, M. von Spakovsky, and D. Moorhouse, “A Study of the Benefits of Using Morphing Wing Technology in Fighter Aircraft Systems,” in *39th AIAA Thermophysics Conference*, American Institute of Aeronautics and Astronautics, 2007.
[54] J. J. Dicker Jr., G. R. Pennock, and J. E. Shigley, *Theory of Machines and Mechanisms*, Third Edit. New York: Oxford University Press, Inc., 2003.
[55] D. H. Myszka, *Machines & Mechanisms: Applied Kinematic Analysis*, 4th ed. Pearson Higher Ed USA, 2010.
[56] K. Russell, Q. Shen, and R. S. Sodhi, *Mechanism Design: Visual and Programmable Approaches*. Boca Raton, FL, USA: CRC Press, Inc., 2013.

[57] A. G. Erdman, G. N. Sandor, and S. Kota, *Mechanism Design: Analysis and Synthesis (4th Edition)*. 2001.
[58] R. L. Norton, *Design of Machinery*. 2003.
[59] J. S. Rao, *Mechanism and Machine Theory*, 2nd ed. newagepublishers, 1992.
[60] P. A. Simionescu and D. Beale, "Optimum synthesis of the four-bar function generator in its symmetric embodiment: the Ackermann steering linkage," *Mech. Mach. Theory*, vol. 37, no. 12, pp. 1487–1504, 2002.
[61] B. F. Freudenstein and N. York, "Approximate Synthesis of Four-Bar Linkages *[1 , 2]," vol. 77, no. August 2010, pp. 853–861.
[62] W. Sun, "Optimum design method for four-bar function generators," *J. Optim. Theory Appl.*, vol. 38, no. 2, pp. 287–293, 1982.
[63] A. C. Rao, "Kinematic design of four-bar function-generators with optimum sensitivity," *Mech. Mach. Theory*, vol. 10, no. 6, pp. 531–535, 1975.
[64] Z. Liu and J. Angeles, "Least-Square Optimization of Planar and Spherical Four-Bar Function Generator Under Mobility Constraints," *J. Mech. Des.*, vol. 114, no. 4, pp. 569–573, Dec. 1992.
[65] S. O. Tinubu and K. C. Gupta, "Optimal Synthesis of Function Generators Without the Branch Defect," *J. Mech. Transm. Autom. Des.*, vol. 106, no. 3, pp. 348–354, Sep. 1984.
[66] L. Burmester, *Lehrbuch der Kinematik*. 1888.
[67] D. Tesar and P. W. Eschenbach, "Four Multiply Separated Positions in Coplanar Motion," *J. Eng. Ind.*, vol. 89, no. 2, pp. 231–234, May 1967.
[68] D. Tesar, "The generalized concept of three multiply separated positions in coplanar motion," *J. Mech.*, vol. 2, no. 4, pp. 461–474, 1967.
[69] D. Tesar, "The generalized concept of four multiply separated positions in coplanar motion," *J. Mech.*, vol. 3, no. 1, pp. 11–23, 1968.
[70] M. Polat, "Computer Aided Synthesis of Planar Mechanisms," METU, 1985.
[71] E. Demir, "Kinematic Design of Mechanisms in a Computer Aided Design Environment," METU, 2005.
[72] J. Martin, Peter, "Burmester Curve and Numerical Motion Generation of Grashof Mechanisms with Perimeter and Transmission Angle Optimization in MATHCAD," New Jersey Institute of Technology, 2007.
[73] K. Erener, "Developing a Four Bar Mechanism Synthesis Program in CAD Environment," METU, 2011.
[74] Q. Shen, W.-T. Lee, and K. Russell, "On Adjustable Planar Four-Bar Motion Generation With Order, Branch and Circuit Defect Rectification," *J. Mech. Robot.*, vol. 7, no. 3, pp. 34501–34505, Aug. 2015.
[75] E. Söylemez, *Mechanisms*. Ankara: Middle East Technical university, 1979.
[76] S. Bai and J. Angeles, "A unified input–output analysis of four-bar linkages," *Mech. Mach. Theory*, vol. 43, no. 2, pp. 240–251, Feb. 2008.
[77] G. E. Forsythe, "Pitfalls in Computation , or why a Math Book isn't Enough," *Am. Math. Mon.*, 2008.
[78] Y. Akgün, C. J. Gantes, W. Sobek, K. Korkmaz, and K. Kalochairetis, "A novel adaptive spatial scissor-hinge structural mechanism for convertible roofs," *Eng. Struct.*, vol. 33, no. 4, pp. 1365–1376, 2011.
[79] Y. Chen, "Design of Structural Mechanisms," University of Oxford, 2003.

[80] H. L. Şahin and Y. Yaman, “Design and Analysis of a Mechanism for the Chord and Camber Morphing of an Aircraft Wing,” in *7th EASN International Conference on Innovation in European Aeronautics Research*, 2017.
[81] F. Escrig and J. P. Valcarcel, “Geometry of Expandable Space Structures,” *Int. J. Sp. Struct.*, vol. 8, no. 1–2, pp. 71–84, Apr. 1993.
[82] J. S. Zhao, F. Chu, and Z. J. Feng, “The mechanism theory and application of deployable structures based on SLE,” *Mech. Mach. Theory*, vol. 44, no. 2, pp. 324–335, 2009.
[83] C. Wu-jun, L. Yao-zhi, F. Gong-yi, G. Jing-hai, and D. Shi-lin, “A Study on Space Masts Based on Octahedral T russ Family,” *Int. J. Sp. Struct.*, vol. 16, pp. 75–82, 2001.
[84] Y. Rosenfeld and R. D. Logcher, “New Concepts for Deployable-Collapsable Structures,” *Int. J. Sp. Struct.*, vol. 3, no. 1, pp. 20–32, Mar. 1988.
[85] F. Escrig, J. Perez Valcarcel, and J. Sanchez, “Deployable cover on a swimming pool in Seville,” *Journal of the International Association for Shell and Spatial Structures (J. IASS)*. 1996.
[86] A. P. Thrall, S. Adriaenssens, I. Paya-Zaforteza, and T. P. Zoli, “Linkage-based movable bridges: Design methodology and three novel forms,” *Eng. Struct.*, 2012.
[87] Z. You and S. Pellegrino, “Foldable bar structures,” *Int. J. Solids Struct.*, vol. 34, no. 15, pp. 1825–1847, 1997.
[88] Hanaor and Levy, “Evaluation of Deployable Structures for Space Enclosures,” *Int. J. Sp. Struct.*, vol. 16, no. 4, pp. 211–229, 2001.
[89] M. B. Sala and R. Sastre, “Mobility and transformability in architectural structures . Proposal of a transformable system of telescopic and x-articulated bars : cinematic , geometric , and structural analysis,” in *Proceedings of the First Conference Transformables 2013*, 2013, no. September, pp. 47–52.
[90] H. L. Şahin and Y. Yaman, “Design and Analysis of a Novel Mechanism for the Morphing of Trailing Edge of an Aircraft Wing,” *MATEC Web Conf.*, vol. 188, 2018.
[91] Y. Akgün, “A novel transformation model for deployable scissor-hinge structures,” İzmir Institute of Technology, 2010.
[92] T. Langbecker, “Kinematic Analysis of Deployable Scissor Structures,” *Int. J. Sp. Struct.*, vol. 14, no. 1, pp. 1–15, 1999.
[93] K. Roovers and N. De Temmerman, “Deployable scissor grids consisting of translational units,” *Int. J. Solids Struct.*, vol. 121, pp. 45–61, 2017.
[94] J. Cai, Y. Xu, and J. Feng, “Kinematic analysis of Hoberman’s Linkages with the screw theory,” *Mech. Mach. Theory*, vol. 63, pp. 28–34, 2013.
[95] F. Maden, K. Korkmaz, and Y. Akgün, “A review of planar scissor structural mechanisms : geometric principles and design methods,” *Archit. Sci. Rev.*, vol. 54, no. 3, pp. 246–257, 2011.
[96] G. Gogu, “Chebychev-Grübler-Kutzbach’s criterion for mobility calculation of multi-loop mechanisms revisited via theory of linear transformations,” *Eur. J. Mech. A/Solids*, vol. 24, no. 3, pp. 427–441, 2005.
[97] J. Zhao, Z. Feng, N. Ma, and F. Chu, *Design of Special Planar Linkages*, Springer T. Springer-Verlag Berlin Heidelberg, 2014.

[98] S. A. Shamsudin, A. P. Murray, D. H. Myszka, and J. P. Schmiedeler, "Kinematic synthesis of planar, shape-changing, rigid body mechanisms for design profiles with significant differences in arc length," *Mech. Mach. Theory*, vol. 70, pp. 425–440, 2013.
[99] "MATLAB®," 2018. [Online]. Available: https://www.mathworks.com/products/matlab.html. [Accessed: 19-Aug-2018].
[100] I. H. Abbott and A. E. Von Doenhoff, "Theory of Wing Sections: Including a Summary of Airfoil data," *Press*, vol. 11, p. 693, 1959.
[101] L. Ünlüsoy, "Effects of Morphing on Aeroelastic Behaviour of Unmanned Aerial Vehicle," METU, 2014.
[102] G. B. Spirlet, "Design of Morphing Leading and Trailing Edge Surfaces for Camber and Twist Control," Delft University of Technology, 2015.
[103] D. Bertetta, S. Brizzolara, S. Gaggero, M. Viviani, and L. Savio, "Numerical and experimental optimization of a CP propeller at different pitch settings," in *Sustainable Maritime Transportation and Exploitation of Sea Resources - Proceedings of the 14th International Congress of the International Maritime Association of the Mediterranean, IMAM 2011*, 2012, vol. 1.
[104] H. L. Şahin, B. O. Çakır, and Y. Yaman, "Aerodynamic Modelling and Analysis of a Novel Mechanism for Chord and Camber Morphing Wing," *MATEC Web Conf.*, vol. 188, 2018.
[105] M. Drela, "XFOIL: An analysis and design system for low Reynolds number airfoils," in *Low Reynolds number aerodynamics: Proceedings of the Conference Notre Dame, Indiana, USA, 5–7 June 1989*, 1989, pp. 1–12.
[106] T. J. R. Hughes, "The Finite Element Method: Linear Static and Dynamic Finite Element Analysis," *Computer Methods in Applied Mechanics and Engineering*, vol. 65, no. 2. 2000.
[107] C. G. Davila, P. P. Camanho, and C. A. Rose, "Failure Criteria for FRP Laminates," *J. Compos. Mater.*, vol. 39, no. 4, pp. 323–345, 2005.
[108] H. Liu, "Linear Strength Vortex Panel Method for NACA Linear Strength Vortex Panel Method for NACA 4412 Airfoil," 2018.
[109] "xflr5," 2018. [Online]. Available: http://www.xflr5.com/xflr5.htm. [Accessed: 19-Aug-2018].

APPENDIX A

FLOWCHART OF THE COMPUTER-ROUTINE

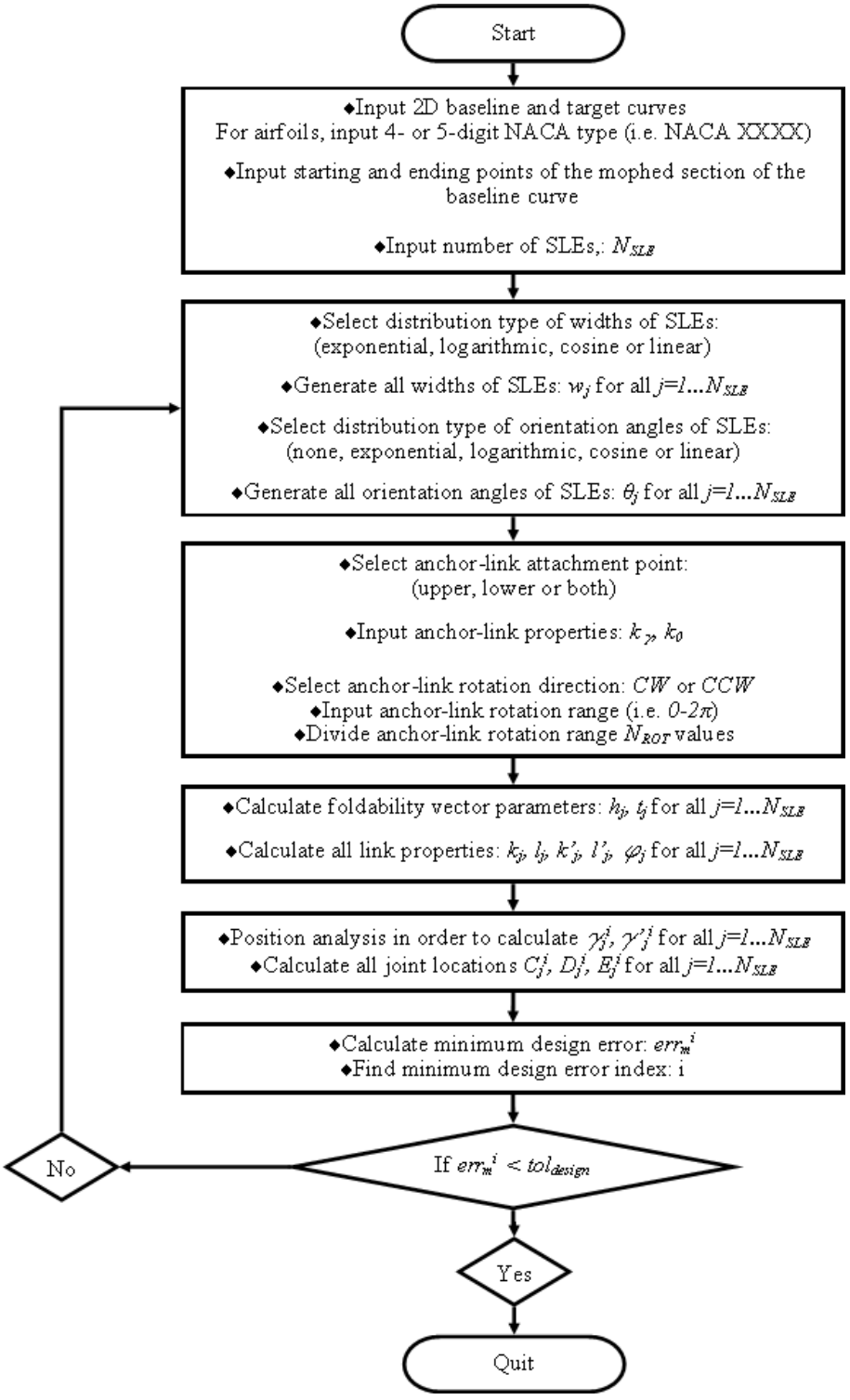

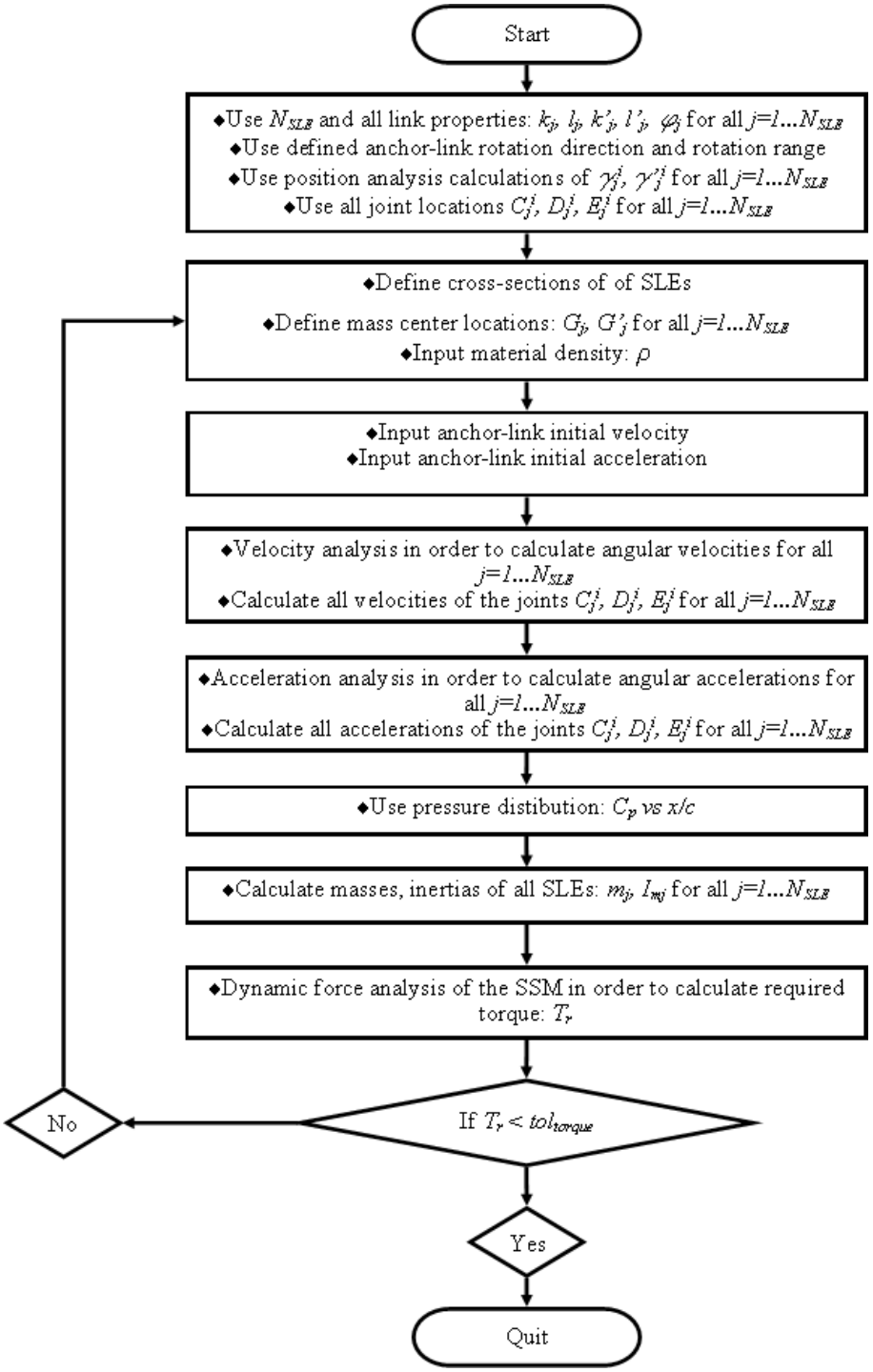
Start
♦Use N_{SLB} and all link properties: k_j, l_j, k'_j, l'_j, φ_j for all $j=1...N_{SLB}$
♦Use defined anchor-link rotation direction and rotation range
♦Use position analysis calculations of γ_j^i, γ'^i_j for all $j=1...N_{SLB}$
♦Use all joint locations C_j^i, D_j^i, E_j^i for all $j=1...N_{SLB}$
♦Define cross-sections of of SLEs
♦Define mass center locations: G_j, G'_j for all $j=1...N_{SLB}$
♦Input material density: ρ
♦Input anchor-link initial velocity
♦Input anchor-link initial acceleration
♦Velocity analysis in order to calculate angular velocities for all $j=1...N_{SLB}$
♦Calculate all velocities of the joints C_j^i, D_j^i, E_j^i for all $j=1...N_{SLB}$
♦Acceleration analysis in order to calculate angular accelerations for all $j=1...N_{SLB}$
♦Calculate all accelerations of the joints C_j^i, D_j^i, E_j^i for all $j=1...N_{SLB}$
♦Use pressure distibution: C_p vs x/c
♦Calculate masses, inertias of all SLEs: m_j, I_{mj} for all $j=1...N_{SLB}$
♦Dynamic force analysis of the SSM in order to calculate required torque: T_r
If $T_r < tol_{torque}$
No
Yes
Quit